# UNIVERSITA' DEGLI STUDI DI PADOVA

FACOLTÀ DI SCIENZE MM.FF.NN.

DIPARTIMENTO DI SCIENZE CHIMICHE

SCUOLA DI DOTTORATO DI RICERCA IN SCIENZE MOLECOLARI
INDIRIZZO SCIENZE CHIMICHE
CICLO XXIII


## DITHIOLENE AND THIOLATE TRANSITION METAL COMPLEXES:TOWARDS AN EXPLORATION OF THEIR MULTI-FUNCTIONAL PROPERTIES


DIRETTORE DELLA SCUOLA: CHIAR.MO PROF. MAURIZIO CASARIN
SUPERVISORE: CHIAR.MO PROF. EUGENIO TONDELLO

DOTTORANDO: ALESSIA FAMENGO

## Abstract

This work has dealt with the synthesis and characterization of transition metal complexes with two types of sulphur based ligands: 1,2 dithiolato ligands and thiol-carboxylate ligands.

The electronic features related to the metal-sulphur interaction, such as the rich redox behaviour associated to the interplay between the sulphur and a redox active metal, the better overlap between sulphur and metal orbitals, the ability of forming coordination compounds in different topologies, from discrete complexes to extended 1-D network, make sulphur-based coordination compounds. We have explored these features starting from non *redox innocent* metal bis-dithiolene complexes as possible molecular precursors in the field of molecular magnetism, as paramagnetic centers able to organize in more complex coordination compounds.

In the first part of this work, "classical" metal bis-dithiolene complexes have been investigated as metallo-ligands towards the coordination of "acceptor" metal complexes, in order to build up coordination compounds of higher nuclearities with paramagnetic centers. Particularly, the investigated dithiolenes were $[Cu(mnt)_2]^{2-}$ ,$[Cu(tfadt)_2]^{2-}$and $[Ni(dmid)_2]^{-}$ while the "acceptor" metal complexes are Mn(III) porphinato ,Mn(III) salen-like complexes and finally a mixed valence Mn(II)Mn(III) complex.

We have observed that the reactivity in solution of metal-bis –dithiolene together with the Mn-based complexes employed has lead to co-crystallization salts where the coordinating group of the dithiolene does not coordinate the Mn center.

From these observation, we have decided to synthesize a series of new 1,2 dithiolato ligands bearing a potential coordinating functional group. We have choosen to functionalize them with crown-ether macrocycles with different sizes, in order modulate their selectivity for transition metal ions or lanthanide ions. The corresponding radical nickel(dithiolene) complexes have been synthesized and polymetallic Ni-Na and Ni-Ni chains have been obtained as well as a bimetallic Ni-Ni discrete complex. We have provided their physico-chemical characterizations in order to understand their rich redox behaviour and their magnetic properties. The investigation on these new 1,2 dithiolato

ligands is still in progress in order to build up polymetallic assemblies also with lanthanide ions.

We have then switched to another class of sulphur-based ligands, the thiol-carboxylate ligands. 2-mercaptonicotinic acid has been considered as versatile ligand towards the synthesis of sulphur-based metal complexes. This polyfunctional ligand can coordinate with N, O or S donor atoms. Under hydrothermal conditions, Zn(II) and 2-mercaptonicotinic acid afforded a coordination polymer where 2-mercaptonicotinic acid is S,O chelating. The electronic properties were studied by means of theoretical calculations and experimental measurments.

Under the same reaction conditions, Ni(II) did not led to any crystalline material. By switching the reaction conditions, it has been observed a mononuclear S,O chelated Ni bis(mercaptonicotinate).

Questo lavoro di dottorato ha riguardato la sintesi e la caratterizzazione di complessi di metalli di transizione con leganti donatori allo zolfo.

In particolare sono stati considerati i leganti 1,2 ditiolato e un legante tipo tiol-carbossilato, l'acido 2-mercaptonicotinico.

Lo zolfo presenta una variabilità maggiore di stati di ossidazione rispetto all'ossigeno e a questo si riconduce il particolare comportamento redox dei complessi con legami M-S. Per questo motivo la sintesi di complessi implicanti il legame metallo-zolfo è un'area di ricerca attiva soprattutto per quanto riguarda la progettazione di materiali con proprietà di conduzione, ottiche o magnetiche.

In questo contesto sono stati considerati i complessi dei metalli di transizione con i leganti 1,2 ditiolato, altresi detti metallo bis-ditioleni.

Nei metallo bis-ditioleni la variabilità degli stati di ossidazione del complesso senza grandi variazioni della geometria di coordinazione li rende adatti per la sintesi di materiali molecolari. In particolare, una via sintetica per l'ottenimento di tali materiali consiste nell'organizzare questi complessi via coordinazione ad un altro centro metallico, in maniera da ottenere composti a più alta nuclearità. Soprattutto per quanto riguarda il magnetismo molecolare, vi è la necessita di organizzare nella stessa molecola più centri paramagnetici.

In questo lavoro di tesi, inizialmente dithioleni paramagnetici "classici" come $[Cu(mnt)_2]^{2-}$ ,$[Cu(tfadt)_2]^{2-}$and $[Ni(dmid)_2]^{\cdot -}$, contenenti gruppi funzionali potenzialmente coordinanti sono stati impiegati come metallo-leganti verso complessi paramagnetici di Mn(III) o a valenza mista Mn(II)/Mn(III). Durante gli esperimenti condotti, è risaltata la reattività in soluzione dei metallo bis-ditioleni verso lo scambio di leganti che non ha condotto alla formazione del complesso polunucleare sperato, sebbene siano stati isolati composti potenzialmente interessanti.

Alla luce di tutto cio, è stata intrapresa la sintesi di nuovi leganti 1,2 ditiolato opportunamente funzionalizzati con gruppi coordinanti quali gli eteri corona.

La versatilità dei ditioleni verso la funzionalizzazione ha permesso di realizzare una serie di leganti con diverse dimensioni del macrociclo, in modo da poter modulare la selettività verso metalli di transizione ma anche verso ioni di lantanidi trivalenti.

Sono stati sintetizzati a partire da questi leganti i complessi ditioleni di nickel, isolandoli in forma di anioni e aventi spin S=1/2. Sono state ottenuti complessi polimetallici Ni-Ni e Ni-Na. Inoltre è stato ottenuto un complesso bimetallico Ni-Ni.

Tutti i complessi sono stati caratterizzati chimicamente. Inoltre, le proprietà magnetiche sono state indagate tramite misure di suscettività magnetica in funzione della temperatura, rivelando per il complesso polimetallico Ni-Ni una forte interazione fra le unità ditiolene costituenti il complesso.

Il legante tiol-carbossilato acido 2- mercaptonicotinico è stato considerato per la sua versatilità alla coordinazione. In condizioni idrotermali e in presenza di Zn(II) e acido 2-mercaptonicotinico, è stato ottenuto un polimero di coordinazione dove il legante mercaptonicotinato funge da chelante S,O e lega a ponte monoatomico i vicini centri metallici. La stessa topologia non è stata ottenuta con il Ni(II). Cambiando le condizioni di reazione, finora solo il complesso monometallico Ni(II) bis-mercaptonicotinato è stato ottenuto.

Le proprietà elettroniche correlate alla situazione di coordinazione S-Zn-O del polimero di coordinazione di Zn(II) sono state investigate per mezzo di calcoli teorici e misure sperimentali.

# Contents

# Aim of the work

In this work the chemistry of sulphur based- thiolate- and dithiolene ligands has been explored in order to design, synthesize and characterize metal complexes suitable for the design of molecular based materials.

The research of new synthesis procedures that leads to the formation of polymetallic complexes represents a still open topic in the field of coordination chemistry, even if a lot of work has been devoted and several new compounds with different metals and ligands has been reported [Stiefel, 1996; Stiefel, 2004]. Due to peculiar features of sulphur-based ligands, such as high polarizability, large negative charge, coordination versatility and manifold apticity, we have decided to investigate transition metal complexes with such ligands. This species often present a "chameleonic" [Maratini, 2011; Stiefel, 2004; Stiefel, 1996] behaviour with respect to their chemical, redox, electronic properties as well as to their coordination behaviour.

In particular, we have investigated the monoanionic radical dithiolene complex $[Ni(dmid)_2]^{\bullet-}$ (4,5 dimercato 1,3 dithiol-2 one) with spin S=1/2 together with the cationic paramagnetic complex with S=2 $[Mn(TPP)]^+$ (TPP= tetraphenylporphirinato) in order to obtain bimetallic complexes with higher nuclearity for application in the field of molecular magnetism through the C=O···Mn(III) interaction.

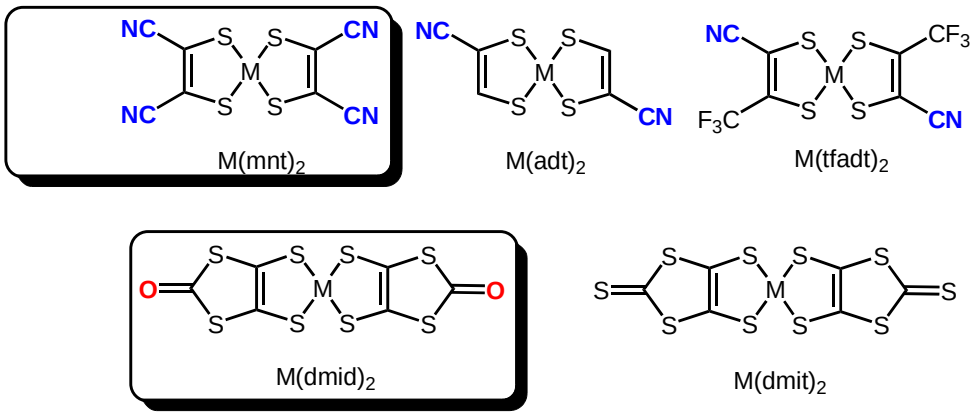


**Fig 1** Formula and acronyms of various dithiolene complexes.

We have then extended our investigation on the paramagnetic S=1/2 $[Cu(mnt)_2]^{2-}$ (mnt= maleonitrilethylendithiolato) dithiolene complex with Mn(III) salen type complexes (salen= salicylaldeide-imminate, spin S=2). $[Cu(mnt)_2]^{2-}$ bears a potentially coordinative –CN group, in principle able to coordinate to a Mn(III) metal centre.

Another Mn based metal complex was considered together with $[Cu(mnt)_2]^{2-}$, the tetranuclear- mixed valence $Mn^{II}/Mn^{III}$ $[Mn_4(hmp)_6]^{4+}$ (Mn(II) S=5/2 and Mn(III) S=1/2; hmp= hydroxymethylpyridine). Finally, a new series of 1,2 dithiolate ligands functionalized with crown-ether macrocycles as possible coordinating groups was synthethized. The corresponding radical monoanionic Ni complexes were synthesized and explored as possible metallo ligands towards paramagnetic 3d metal and lanthanides ions.

In the last part of this work, thiole-based ligand 2-mercaptonicotinic acid has been investigated toward the formation of metal complexes with Zn(II) and Ni(II). The electronic features related to the Zn(II) coordination compound were studied by means of a combined spectroscopic and theoretical approach.

Stiefel, E. I.; Matsumoto, K. *Transition Metal Sulfur Chemistry: Biological and Industrial Significance (ACS Symp. Ser.* 653), (Eds.) **1996**

Stiefel, E. I. *Progr. Inorganic Chemistry* **2004**, 52 Wiley

# Chapter 1

# Introduction

## 1.1.Transition complexes with sulphur based ligands

Metal coordination compounds can be designed to have the desired functional properties acting on the chemical nature and structure of the ligands and metals involved and, consequently, on their electronic characteristics.

A wide class of coordination compounds is represented by transition metal complexes with sulphur based ligands. Research in this field is a challenging topic for what concerns the synthesis of molecular based materials and it has been thoroughly explored by several authors. In particular, the peculiar electronic structure characterising M-S bonds has been the topic of few reviews [Joergensen, 1968; Benedix, 1988; Hadad, 1998; Furlani, 1973]

Metal-sulphur based compounds find their application in different fields, such as catalysis, photovoltaic materials, semiconductor technology, energy storage devices [Stiefel, 1996].

Metal-sulphur complexes constitute also an exciting research area because of the properties of the solid state devices deriving from the formation of M-S bridges and of extended M-S network, leading to electronic collective properties such as conduction and superconduction [Stiefel, 2004].

In this class of coordination compounds, very interesting ligands are thiolates [Humphrey, 2005].

Thiols belong to the class of the organo-sulphides compounds and they contain the functionality R-SH, where S atom is formally in a -2 oxidation state. They are structurally similar to the alcohol group but the chemical properties are different. Thiols can be easily deprotonated and the corresponding thiolates can be regarded as ligands toward coordination of transition metals.

The 1,2 ethylen dithiolato ligand and its derivatives are sulphur chelating ligands and their peculiarity consists on the variable oxidation states that sulphur atom can assume upon coordination with a transition metal center [Stiefel, 2004]. Such ligands have been classified as *non innocent* [Gray, 1964; Stiefel, 2004] because, in the corresponding complexes with transition metals the oxidation state of the metal and of the ligand, can not be easily determined.

Unlike saturated 1,2 dithiolate ligands, dithiolenes ligands in complexes form rigid and planar or quasi planar five membered $C_2S_2M$ rings with considerable electronic flexibility (Fig. 1.1). The higher delocalization of the charge in the $C_2S_2M$ rings, together with the rigidity of the system, allows obtaining metal complexes in different oxidation states without relevant changes of the coordination geometry.

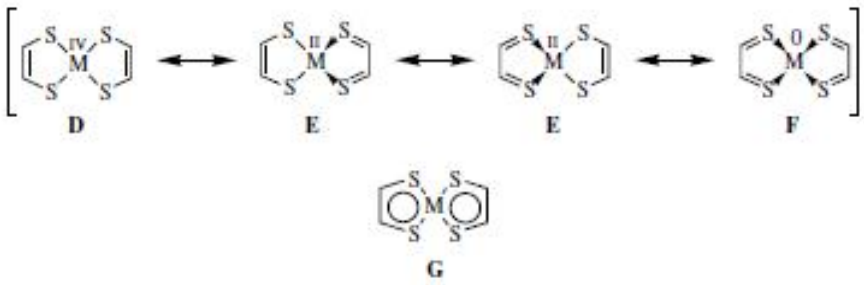


**Fig 1.1** Complex oxidation states with 1,2 ethylen dithiolate ligand.

The outstanding functional properties of metal dithiolene complexes are based on the delocalization of electron density *extended* not only to the $MS_2$ core but also to the whole ligand within the $R_2C_2S_2M$ ring, depending also on the R functional group.

The synthetic organization of metal centers into self-assembling architectures can lead to cooperative properties improving the development of the functional properties of these molecular materials [Andruh, 2007].

In this framework our approach has considered the design and the synthesis of polyfunctional ligand able to coordinate more than one metal center.

With this purpose, several new 1,2 dithiolate ligands bearing coordinative functional groups have been synthesized together with the corresponding nickel complexes,

demonstrating the rich chemistry associated with 1,2 dithiolate ligands and their versatility toward the functionalization with different donor substituents. In this framework, metal bis dithiolene complexes with coordinating functional groups were used as "metallo-ligands" toward transition metals.

Concerning "classical" thiolate chemistry, the thiol based ligand 2-mercaptonicotinic acid has been investigated toward the formation of complexes with Zn(II) and Ni(II), exploiting the versatility of this ligand characterized by three different donor atoms: nitrogen, oxygen and sulphur.

## 1.2 Synthethic strategies for metal assembly

As mentioned, metal complexes can act as metallo-ligands when coordinative substituent are present on the complex. Another strategy consists of linking different metal centers or different metal complexes with a suitable polyfunctional ligand as depicted in Scheme 1.1.

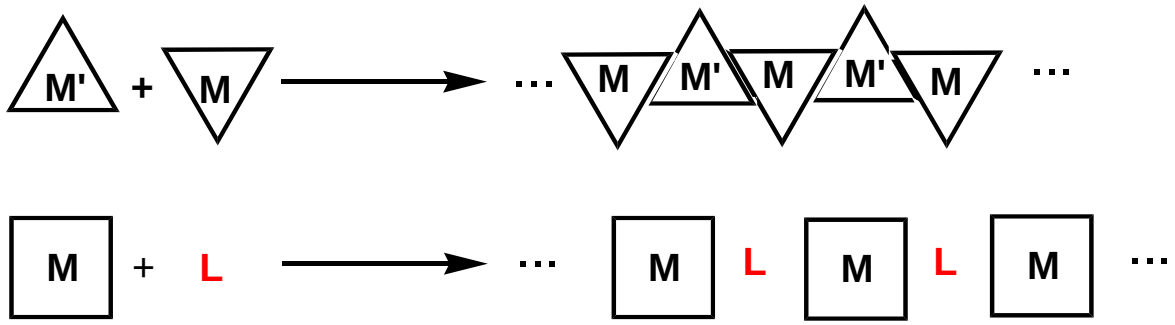


**Scheme 1.1** Metal complexes as metallo-ligands and ligands as linkers, two ways of building up polymetallic complexes.

In paragraph 1.1 we have introduced metal dithiolene complexes as possible metallo-ligands. The anionic nature of the $[Cu(dt)_2]^{2-}$and $[Ni(dt)_2]^{-}$ complexes (dt= dithiolene) makes them particularly adapted for the coordination of cationic centers.

In Fig. 1.3 some examples of metal bis-dithiolene with oxygen and nitrogen donor functional groups are given.

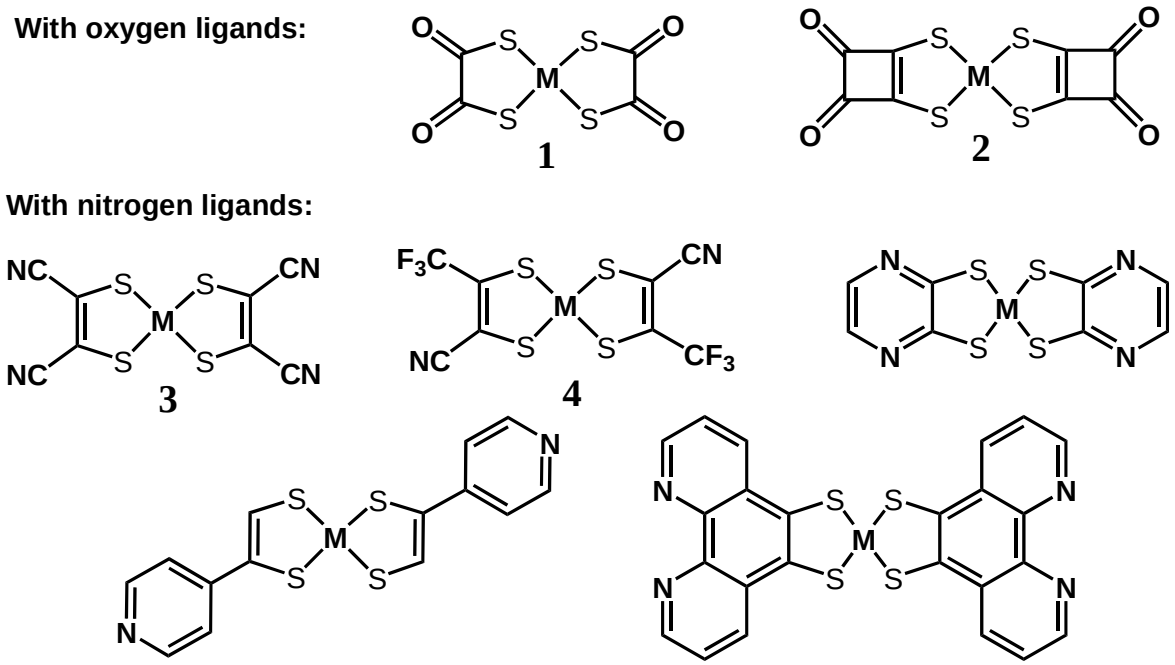


**Fig 1.2** Metal bis-dithiolene complexes with oxygen and nitrogen donor functional groups.

Metal dithiosquarate (**2** in Fig. 1.2) and metal dithiooxalate (**1** in Fig. 1.2) have oxygen donor atoms and they were used for the first time as metallo-ligands by Coucouvanis [Coucouvanis, 1970].

The example shown in Fig. 1.3 is the discrete trimetallic complex [K(18-crown-6)Cu(dto)$_2$K(18-crown-6)] where copper(II) dithioxalate acts as metallo-ligand [Coucouvanis 1985] towards macrocycle complexed-alkali metals. The charge 2- of $[Cu(dto)]^{2-}$ is balanced by two $[K(18crown6)]^{+}$ leading to a neutral trimetallic complex. The charge-balance can favour the formation of such complexes, even if in most cases simple salts can be obtained by simple co-crystallization of the metallo-ligand and its associated complex.

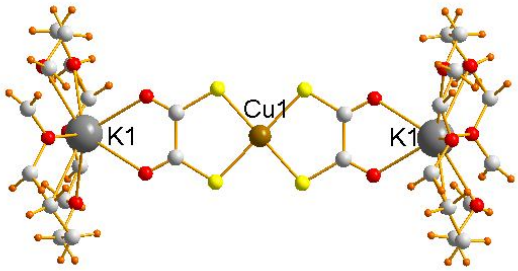


**Fig.1.3** [K(18-crown-6)Cu(dto)$_2$K(18-crown-6)].

The research on molecular magnetism has been devoted to metal dithiosquarates and dithiooxalates to obtain complexes with different topologies. In Fig.1.4 are shown three representative examples of high nuclearity dithiolene-based complexes.

Compound $[Cr(dto)_3(NiL)_3](ClO_4)_3$ [Wakita, 1993], Fig.1.4 a**,** is an example of discrete polymetallic complex where $[Cr(dto)_3]^{3-}$connects three $[NiL]^{2+}$, with L being a bulky tetraazamacrocycle ligand via C=O···Ni interaction.

Complex $[Cu(dto)_2Mn(H2O)_3]$, Fig.1.4 c, is one of the first ferromagnetic Mn(II)Cu(II) chain synthesized [Verdaguer, 1981, Verdaguer, 1984]. In this case $[Cu(dto)_2]^{2-}$is connected to Mn(II) anions by C=O···Mn coordination.

An example of metal complex bearing a 2D structure is $Pr_4N[Co(II)(dto)_3Fe(III)]$ [Kojima 2003] Fig.1.4 b. Three $[Co(dto)_3]^{2-}$ unities link a Fe(III) ion through -C=O group, forming two dimensional ferromagnetic layers of $[Co(II)(dto)_3Fe(III)]^{+}$.

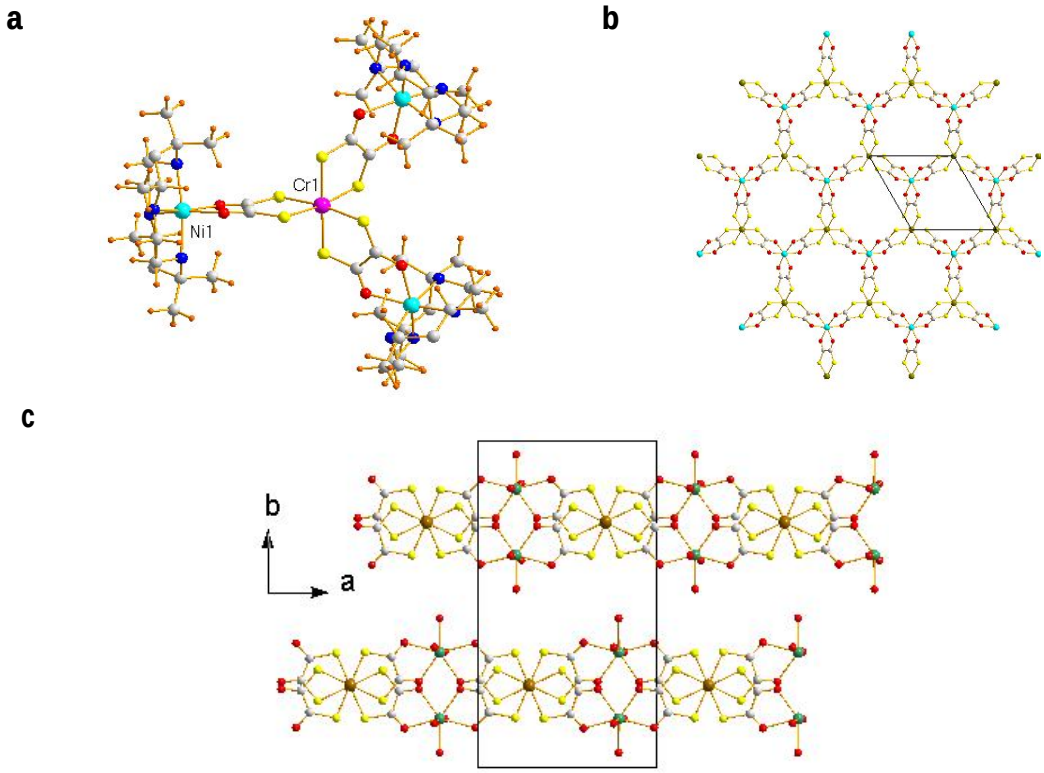


**Fig 1.4 a)**$[Cr(dto)_3(NiL)_3](ClO_4)_3$, **b)** $Pr_4N[Co(II)(dto)_3Fe(III)]$ and **c)** $[Cu(dto)_2Mn(H2O)_3]$.

Other metal dithiolene complexes possessing nitrogen donor–CN groups are those with the ligands maleonitrile 1,2 dithiolato (mnt) and 1-trifluoromethyl-2-cyano-1,2-dithiolato (tfadt), compounds **3** and **4** in Fig.1.2 respecetively.

In literature a lot of examples concerning $[M(mnt)_2]^n$ and alkali metals are present [Daqi, 2005, Wang, 2005, Daqi, 2005].

The more recent dithiolene complexes $[Cu(tfadt)_2]^{2-}$ and $[Ni(tfadt)_2]^{\cdot-}$ by reaction with other metal complexes with free coordination sites afforded polymetallic 1-D compounds, as for example $[Cu(tfadt)_2Ni(cyclam)]$ Fig 1.5 [Fourmigué, 2005], a chain of alternating spin S=1/2 and S=1 where $[Cu(tfadt)_2]^{2-}$ and $[Ni(cyclam)_2]^{2-}$ shows ferromagnetic interaction.

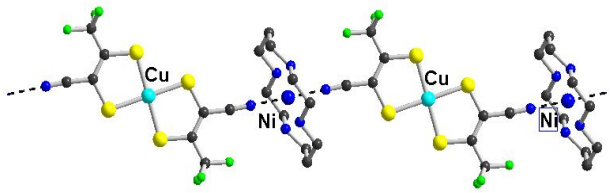


**Fig 1.5**[$Cu(tfadt)_2Ni(cyclam)$]

Another interesting example is compound $\{CuL_2(CH_3OH)\}\{CuL_2\}Gd(NO_3)\{Ni(mnt)_2\}][Ni(mnt)_2]$ [Madalan, 2008], a 3d-4f polymetallic complex where Cu(II) of $[CuL_2(CH_3OH)Gd(NO_3)CuL_2]^{3+}$ (Fig 1.6 b) are connected via -CN···Cu to the radical anion $[Ni(mnt)_2]^{\bullet-}$ affording discrete polynuclear complexes of formula $[\{CuL_2(CH_3OH)\}\{CuL_2\}Gd(NO_3)\{Ni(mnt)_2\}]^{+}$ (Fig 1.6 a).

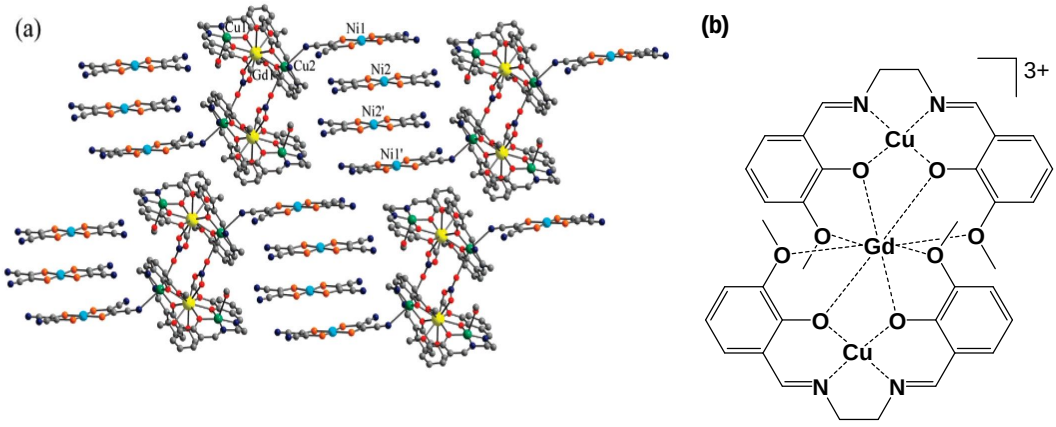


**Fig. 1.6 a)** $[\{CuL_2(CH_3OH)\}\{CuL_2\}Gd(NO_3)\{Ni(mnt)_2\}][Ni(mnt)_2]$ and **b)** $[CuL_2(CH_3OH)Gd(NO_3)CuL_2]^{3+}$ trinuclear unity.

Other examples involving metal dithiolene as metallo-ligands are present in literature. However, their number is relatively limited making the research in these field more intriguing because still unexplored.

In the next chapters, other examples of metallo-dithiolene based polynuclear compounds will be given in order to compare them with the complexes obtained in this work.

The next chapter is devoted to the general properties of metal dithiolene complexes, in order to give an overview of this particular and interesting class of coordination compounds and to understand why they are so appealing for the synthesis of molecular based materials.

**Bibliography**


Andruh, M. *Chem. Comm.* **2007**, 2565

Benedix, R.; Hennig, H. *Inorg. Chim. Acta* **1988**, 141, 21

Coucouvanis, D. *J. Am. Chem. Soc.* **1970,** 3875

Coucouvanis, D. et al. *Inorg. Chem.* **1985,** 1680

Dagi, ; Wang, D.-Q. *J. Coord. Chem.*, **2005**, 1597

Eisenberg, R.; Ibers, J. A.; Clark, R. J. H.; Gray, H. B. *J. Am. Chem. Soc.*, **1964**, 86, 113

Furlani, C.; Flamini, A.; Sgamellotti, A.; Bellitto, C. *J. Chem. Soc., Dalton Trans.* **1973**, 22, 2404

Hadad, C. M.; Rablen, P. R.; Wilberg, K. B. *J. Org. Chem.* **1998**, 63, 8668

Humphrey, M. S. *Inorg chem.* **2005**, 44, 5981

Jeannin, O.; Barrière, F.; Delaunay, J. ; Fourmigué, M. *Inorg. Chem.* **2005**, *44*, 9763

Joergensen, C. K. *Inorg. Chim. Acta* **1968**, 2, 65

Kojima, N. *Solid State Commun.,* **2003**, 291

Madalan; Avarvari, N.; Fourmigué, M.; Clérac, R.; Chibotaru, L.F.; Clima, S.; Andruh, M. *Inorg. Chem*. **2008**, *47*, 940

Pandolfo, L.; Maratini, F.; Bendova, M.; Schubert, U.; Bauer, M.; Rocchia, M.;

Venzo, A.; Tondello, E.; Gross, S. *Inorg. Chem*. **2011**, 50, 489

Stiefel, E.I.; Matsumoto, K. *Transition Metal Sulfur Chemistry: Biological and Industrial Significance (ACS Symp. Ser.* 653) **1996**

Stiefel, E.I. *Prog. Inorg. Chem.* **2004,** 52 John Wiley and Sons Ed.

Verdaguer, M. et al. *J. Am. Chem. Soc.*, **1981**, 7373

Verdaguer, M. et al. *J. Am. Chem. Soc.*, **1984**, 3727

Wakita, H. *Dalton Trans.*, **1993**, 2991

Wang, D.-Q. *Synth. React. Inorg., Met.-Org., Nano-Met. Chem.*, **2005**, 583

Wang, D.-Q. *J. Mol. Struct.*, **2005**, 79

# Chapter 2

## Metal dithiolene complexes: a general introduction

### 2.I Chemistry of metal-dithiolene complexes

Since 1960, resarch on metal dithiolene complexes has been an exciting topics especially for the particular redox behavior of such complexes.

As we have introduced in the previous chapter, the base ligand unity is ethylene 1,2 dithiolate (edt), considered as *non innocent* ligand because of its intrinsic redox properties [Gray, 1964; Stiefel, 2004]

Ethylene 1,2 dithiolate can be oxidized in a reversible way to the radical anion form, bearing an unpaired electron, while further oxidation yields the 1,2 thione form which is in a tautomeric equilibrium between the 1,2 dithiete form (Scheme 2.1)

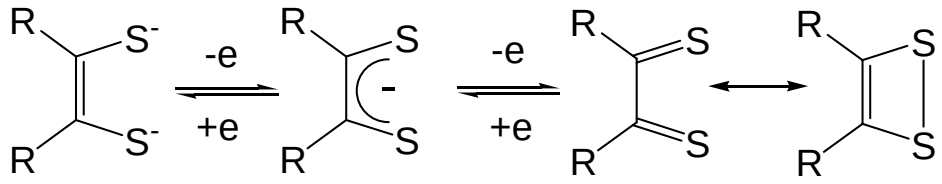


**Scheme 2.1** Ligand base unit $edt^{2-}$ in its different redox states.

From one to three dithiolene ligands could be engaged in the formation of their corresponding metal complexes. In Fig. 2.1 some examples of heterolpetic and tris-dithiolene complexes are shown.

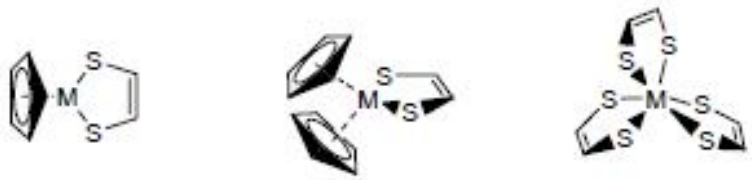

**Fig. 2.1 :** Examples of heteroleptic metal dithiolenes and metal tris-dithiolene complexes.

Metal bis-dithiolenes are known for groups 7 to 12 in the periodic table.

Depending on the type of dithiolene ligand involved and of the metal, different oxidation states are accessible within a bis-dithiolene complex.

For example, the most simple dithiolene ligand, edt, together with Ni(II) ion forms a square planar complex that is possible to isolate in four different oxidation states.

Dianionic complex $[Ni(edt)_2]^{2-}$ with spin S=0 undergoes reversible oxidation to the radical anion $[Ni(edt)_2]^{\cdot-}$ with S=1/2, neutral S=0 $[Ni(edt)_2]$ and finally cationic $[Ni(edt)_2]^{+}$ with spin S=1/2 (Scheme 2.2).

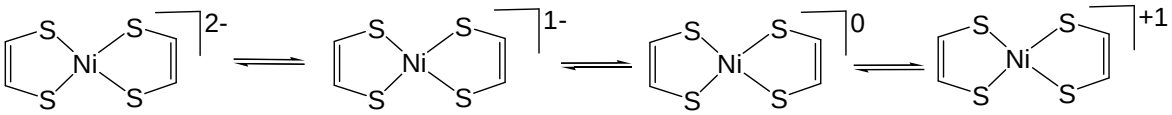

**Scheme 2.2**: Reversible oxidation of complex $Ni(edt)_2$ .

Functionalization of the dithiolene moiety with electro-withdrawing groups such as –CN, -$CF_3$, $CO_2R$ stabilizes the reduced oxidation states of dithiolene complexes. On the contrary, electron donating groups will favour the oxidized states of metal bis-dithiolenes. The interplay between the nature of the metal center and the type (electro-donating or electron-withdrawing) of the substituent groups on the dithiolene moiety makes metal-bis-dithiolene complexes very versatile compounds because they offer a great flexibility toward the choice of the spin and/or of the charge (Table 2.1).

| $d^9$ | $d^8$ | $d^7$ | $d^6$ | $d^5$ | |
|---|---|---|---|---|---|
| Cu | **$Cu(S_2C_2R_2)_2^{2-}$** | $Cu(S_2C_2R_2)_2^{1-}$ | — | — | — |
| Au | **$Au(S_2C_2R_2)_2^{2-}$** | $Au(S_2C_2R_2)_2^{1-}$ | **$Au(S_2C_2R_2)_2$** | — | |
| Ni | — | $Ni(S_2C_2R_2)_2^{2-}$ | **$Ni(S_2C_2R_2)_2^{-\bullet}$** | $Ni(S_2C_2R_2)_2^{0}$ | **$Ni(S_2C_2R_2)_2^{+}$** |
| Co | — — | **$Co(S_2C_2R_2)_2^{2-}$** | $Co(S_2C_2R_2)_2^{1-}$ | | |

**Table 2.1** : Charge variation of M-bis(dithiolenes) as a function of the metal. Bold: paramagnetic complexes.

The most common synthetic way towards metal bis-dithiolene complexes is displayed in Scheme 2.3.

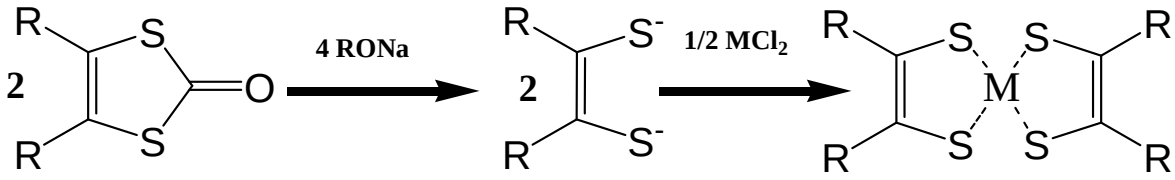


**Scheme 2.3** Reaction pathway to metal bis-dithiolene complexes.

Dithiolenes are generated by the nucleophilic opening of the proligand dithiolone, leading to the corresponding dithiolate dianion. Thereafter, half an equivalent of a metal salt are added to form *in situ* the metal bis-dithiolene complex in its dianionic form. The dianionic species could be isolated when electron-withdrawing substituent R are present in the dithiolene moiety. The dianionic complex can be oxidized by $O_2$ or other chemical oxidants such as $I_2$ or the cation ferricinium $Fc^+$ to monoanionic, neutral and cationic oxidation states, depending on the nature of the substituents.

A synthethic way that lead directly to neutral Ni bis(dithiolene) complexes involves the limit 1,2 dithiete form of the ligand and $Ni(CO)_4$ as nickel precursor, as depicted in Scheme 2.4.

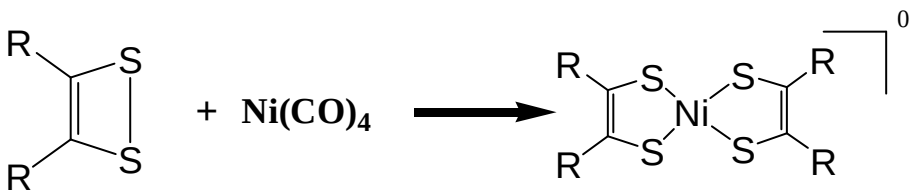


**Scheme 2.4**: Synthethic way to neutral Ni bis(dithiolene).

Unfortunately, the high toxicity of $Ni(CO)_4$ makes this synthesis difficult to carry out.

It has to be pointed out that bis-dithiolene complexes are generally stable from a chemical point of view but they are characterized by a certain reactivity in solution.

Five general types of reaction could be recognized [Stiefel, 2004]: ligand exchange, ligand addition, alkylation, cycloaddition and oxidation, summarized in Scheme 2.5.

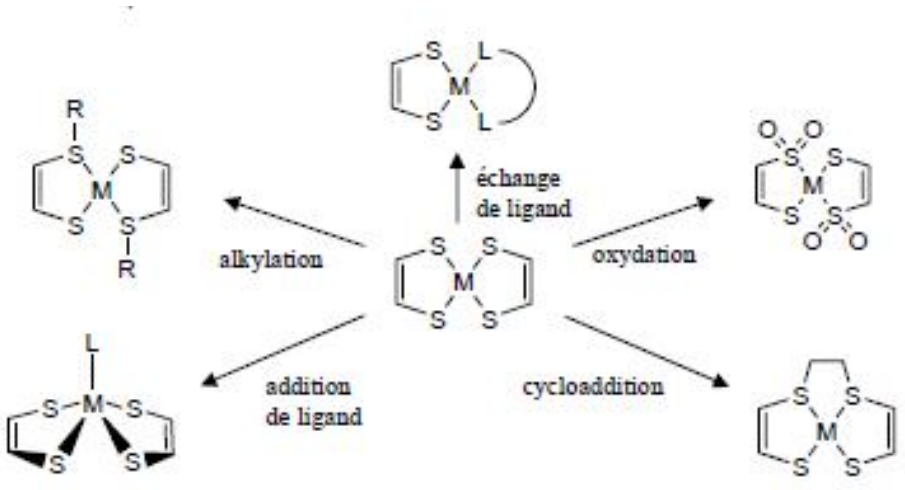


**Scheme 2.5** Solution reactivity of metal bis-dithiolene.

In the solid state, bis-dithiolene complexes show different coordination geometries and structures. They depend on the nature of the complexed metal, on the complex charge, on the type of ligand involved and finally on the crystal packing.

Complexes of $d^8$ metals Ni, Pd, Pt and Au are generally square planar while $d^9$ and $d^{10}$ metals as Cu, Zn, Hg have mostly tetrahedral geometries.

Electron poor dithiolene complexes of Fe and Co tend to form dimers via S⋯M interaction. With Pt, Pd and Au , they can dimerize via M⋯M interactions.

The extended delocalized electronic core of metal bis dithiolenes comprising the metal center, the four sulphur atoms, the C=C unity and, in some cases also the substituents, lead to a number of important properties such as the reversible rich electrochemical behaviour or the strong absorption in the UV-Vis-NIR regions.

The appropriate choice of 1,2 dithiolato ligands leads to a stabilization of radical redox states in the metal complex with the possibility of inter-molecular interactions in the solid state. It is possible to obtain crystalline materials that could be conductive, superconductive or magnetic [Stiefel, 2004].

For example complexes $[Ni(dddt)_2]$ and $[Ni(dmit)_2]$ (dddt= 5,6 dihydro-1,4-dithiin-2,3-dithiolato, dmit= 2-oxo 1,3 dithiole-4,5 dithiolato) bearing sulphur rich substituent groups, allowed to obtain mixed valence materials with conductive properties [Cassoux, 1991; Cassoux, 1999; Faulkmann 1993].

Dithiolene complexes can be employed as electrolytes during the electrocrystalization process of classic organic donors such as tetrathiafulvalene and derivatives, perylene and derivatives or other donor molecules.

## 2.2 Metal dithiolene complexes: functional properties

As far as electrical properties are concerned, the interest in using dithiolene complexes was inspired by the development of “organic metals” [Stiefel, 2004] conducting and superconducting systems.

This class of “organic” materials must obey some molecular ,structural and electronic criteria favoured by one dimensional infinite structures. Bis-dithiolene complexes are able

to organize through stacking interactions within their molecular planes along one direction. They provide good overlaps between stacked molecules and partial filled conduction bands can be generated by oxidation of the dithiolene complex.

For these reason they are suitable precursor for the synthesis of TTFs based materials.

For what concerns the magnetic properties, antiferromagnetism is the most commonly observed magnetic behaviour for dithiolene complexes [Stiefel, 2004; Cronin 2002] .

Very few dithiolene complexes exhibit unusual magnetic behaviours, such as undergoing a spin Peierls transition, behaving like spin ladder, or exhibiting ferromagnetic interactions or behaving as bulk ferromagnet [Stiefel, 2004].

It has to be remarked that almost all of the interesting dithiolene-based magnetic compounds known are relative to bis-dithiolene complexes, except for the tris-molibdenum complexes and for the compounds of the type $Cp_2M$(dithiolene).

To date no dithiolene based thin films have been studied for their magnetic properties and no patents has claimed the use of such complexes in this area [Stiefel, 2004].

Bis-dithiolene complexes are particulary prone to form spin ladder systems. In spin ladder systems unidimensional chains of S=1/2 spins are disposed one next to the other and this system can be regarded intermediate between 1D chains showing quasi-antiferromagnetic long range ordering or as 2D lattices with real long range antiferromagnetic ordering [Stiefel, 2004]. Depending on the number of coupling chains and upon the strength of the coupling the final magnetic properties of these systems are very different, from single chain magnet behaviour to short range spin interactions.

Depending on the nature of the counteraction, some metal bis-dithiolenes systems have a tendency to form stacks with side by side S····S contacts.

Salts of the complex $[Ni(mnt)_2]^{-\cdot}$ are unusual in providing ferromagnetic interactions.

However, the salt $[NH_4][Ni(mnt)_2]$, [Clemenson, 1988] orders as a ferromagnet at temperature below 4.5 K. In the solid state side by side stacks of planar $[Ni(mnt)_2]^{-1}$ form a two dimensional sheet. Each sheet is separated by $NH_4^+$ and $H_2O$ molecules. The stack provide that the anions are equidistant preventing any type of dimerization leading to a diamagnetic state.

Another example where the counter cation influences the magnetic properties is compound $Bu_4N[Ni(mnt)_2]$[Willett, 2005]. A transition between paramagnetic and

diamagnetic state is present and its origin arises from a structural change on $Bu_4N^+$: one carbon of this counteraction is disordered at room temperature keeping the dithiolene unities separated. On cooling, ordering of the $Bu_4N^+$ group allows the interaction between $[Ni(mnt)_2]^{-}$ leading to a diamagnetic state.

Compound [CpFe][Ni(tfadt)$_2$] [Fourmigué, 2006] is the ferricinium salt of the anionic $S = {}^1/_2$ dithiolene complex $[Ni(tfadt)_2]^{\bullet-}$. At room temperature its crystal structure reveals chains of $[Ni(tfadt)_2]^{\bullet-}$ unities separated by disordered $[CpFe]^+$ and the ordering of $[CpFe]^+$ causes the transition to a diamagnetic state.

In all these examples, the approach toward the synthesis of molecular based magnetic materials consists of combining paramagnetic $[M(dithiolene)_2]^{n}$ with classic "organic" counter cations such as $Bu_4N^+$, $NH_4^+$ , or $[CpFe]^+$ . The magnetism properties derive from the relative position in the lattice of counter cations and $[M(dithiolene)_2]^{n}$ and from their inter-and intramolecular interactions.

By discussing the examples mentioned here, a strong correlation is present between the solid state arrangement of dithiolene complexes and their magnetic properties.

A metallo-ligand approach is another way to organize metal dithiolene complexes with appropriate coordination compounds in order to obtain molecular based materials with magnetic properties.

**Bibliography**


Cassoux, P.; Valade, L.; Kobayashi, H.; Kobayashi, A.; Clark, R. A; Underhill, A. E. *Coord. Chem. Rev*. **1991**, 110, 115

Cassoux, P. *Coord. Chem. Rev*. **1999**, 186, 213

Clemenson, P. I.; Underhill, A.E.; Hursthouse M.B.; Short R.L. *J. Chem. Soc., Dalton Trans.* **1988**, 1689

Faulkmann, C.; Errami, A.; Legros, J. P.; Cassoux, P.; Yagubskii, E. B.; Kotov, A.I.; *Synth. Met*. **1993**, 56, 2057

Fourmigué M., *J. Am. Chem. Soc.* **2006**, 128, 14649

Robertson, N.; Cronin, L. *Coordination Chemistry Reviews 227* **2002**, 93

Stiefel, E.D. *Progr. Inorg. Chem.* **2003**, 52

Willett, R. D.; Gomez-Garcia C. J.; Ramakrishna, B. L.; Twamley, B. *Polyhedron* **2005**, 24, 2232

# Chapter 3

## Metal bis-dithiolene complexes as metallo-ligands

In this chapter "classical" metal bis-dithiolene complexes $[Ni(dmid)_2]^{\cdot-}$, $[Cu(mnt)_2]^{2-}$, $[Cu(tfadt)_2]^{2-}$ have been investigated as metallo-ligands towards three different cationic Mn-based building blocks: $[Mn(TTP)]^+$ (section 3.1), Mn(III)-salen complexes (section 3.2) and the mixed valence Mn(II)/Mn(III) complexes formed from Mn(II) and ligand hmp- (hydroxymethylpyridine) (section 3.3). For each section an introduction about the general structural an magnetic properties of each Mn-based complex is given together with the example concerning their assembli with metal bis-dithiolene complexes.

### 3.1 The radical bis-dithiolene complex (S = ½) $[Ni(dmid)_2]^{\cdot-}$ as metallo-ligand toward (meso-Tetraphenylporphinato)manganese(III)

The coordination chemistry of metal porphinato derivatives with dithiolene complexes (Scheme 3.1) has been previously barely explored, and with essentially two different goals in mind, as models of heme-based enzymes in the one hand, as novel magnetic heterobimetallic polymeric systems on the other hand. For example, iron porphyrine derivatives were used as models of the active site of the resting form of cytochrome *c* oxidase (CcO) where strong ligand-mediated antiferromagnetic coupling between copper(II) atom and an iron(III) heme had been proposed to explain the magnetic properties of the CcO active site [Palmer,1976]. For that purpose, $[Fe(TPP)]^+$ itself [Schauer, 1984; Serr, 1990] or the substituted [Elliott, 1982; Hatfield, 1987] $[Fe(Cl_4TPP)]^+$ have been associated with S = ½ $[Cu(mnt)_2]^{2-}$ complex into trimeric units where the porphyrine is sandwiched between two $[Cu(mnt)_2]^{2-}$ dithiolene complexes, through two short Fe···S contacts, with Fe···S distances ranging between 2.44 and 2.55 Å. Bimetallic complexes associating one $[Fe(TPP)]^+$ and one $[Cu(mnt)_2]^{2-}$ units through one single Fe···S interaction are also reported in three different complexes with Fe···S distances between

2.41 and 2.44 Å. The sixth coordination site about the iron atom of the anion is occupied by a THF molecule [Serr, 1992].

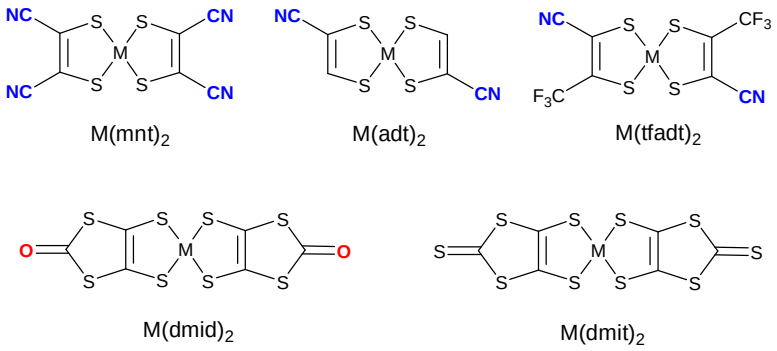


**Scheme 3.1**. Formula and acronyms of various dithiolene complexes.

A similar coordination mode was also reported in the reaction product of $Co^{II}$ [Co(TPP)] and $[Ni(tfd)_2]$ neutral complexes, which afford the dimeric unsymmetrical charge-transfer salt $[Co(TPP)]^+[Ni(tfd)_2]^-$ where the coordination sphere of $[Co(TPP)]^+$ is completed here by only one sulfur atom of the dithiolene radical anion complex $[Ni(tfd)_2]^-$ with Co···S distance at 2.293 Å [Shkolnik, 1975]. In the examples described above, it should be stressed that the coordination to the porphyrinic Fe atom occurs *via* one sulfur atom of the dithiolene complex metallacycle (Scheme 3.2a) rather than with the nitrogen atom of the nitrile substitutents (Scheme 3.2b).

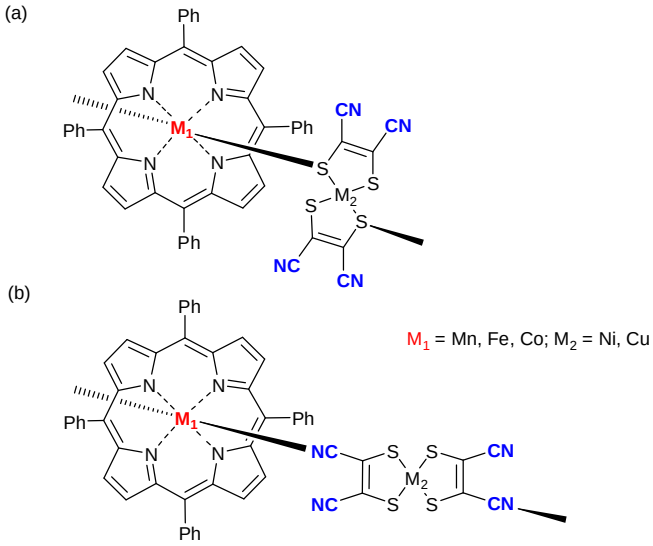


**Scheme 3.2**. Two coordination modes of $[Mn(TPP)]^+$ with $[M(mnt)_2]$ complexes.

Turning to the Mn porphyrine derivative $[Mn(TPP)]^+$, Miller was able to isolate and fully characterize the 1:1 $[Mn(TPP)][Ni(mnt)_2]$ and $[Mn(TPP)][Ni(adt)_2]$ salts [Dawe, 2005] where now infinite alternated chains of S = 2 $[Mn(TPP)]^+$ and S = ½ $[Ni(mnt)_2]^-$, or $[Ni(adt)_2]^-$ [Fourmiguè, 2000; Fourmiguè, 2003], ions are formed through the coordination to the nitrile nitrogen atom (Scheme 3.2 b), with Mn···N distances at 2.394(3) and 2.339(16) Å, respectively. This coordination mode is comparable to that observed in the $[Mn(TPP)][TCNE]\cdot 2PhMe$ salt [Day, 2002;Miller, 2002] where 1D coordination polymers are characterized by $[TCNE]^{-\cdot}$ radical anions trans–μ–N–σ–bound to $Mn^{III}$. The $[Mn(TPP)][Ni(mnt)_2]$ and $[Mn(TPP)][Ni(adt)_2]$ salts exhibit weak antiferromagnetic interactions and a ferrimagnetic order at 2.3 and 5.5 K respectively. Additionally, a modified Mn porphyrine with *tert*-butyl groups in the 3,5-positions, noted [Mn(TP'P)] afforded another salt with $[Ni(mnt)_2]^-$, where only one water molecule complete the coordination sphere of the $[Mn(TP'P)]^+$ cation.

What emerges from the few examples described above of metal porphyrine salts with dithiolene complexes as anionic metalloligands is already the variety of coordination modes of the metal porphyrine complex. The manganese $[Mn(TPP)]^+$ cation is known to coordinate easily through nitrogen atom with nitriles, amines or pyridines, as well as

through water, alcohols, ethers or ketones, amide, sulfoxydes oxygen atoms, but only a few examples have been reported with thiolates [Mu, 1997] or thioethers [Basolo, 1978; Jones, 1978]. On the other hand, the iron or cobalt derivatives are indeed coordinated by sulfur atom of the metallacycle of dithiolene complexes, despite sometimes strong distortions from planarity on both the porphyrin and the dithiolene complexes. Coordination chains similar to those already observed in the presence of $[Mn(TPP)]^+$ with $[Ni(mnt)_2]^{\cdot -}$ or $[Ni(adt)_2]^{\cdot -}$ could be prepared also with $[Ni(tfad)_2]^{\cdot -}$.

The dmid complex, that is $[Ni(dmid)_2]^{\cdot -}$, provides an other attractive alternative as the presence of the terminal oxygen atoms offers the possibility for Mn···O=C coordination motif.

### 3.1.1 Synthesis of $[Mn(TPP)(S)][Mn(TPP)(H_2O)][Ni_2(tto)(dmid)_2]$ complexes

In order to evaluate whether dithiolene complexes bearing other coordinating functions than the nitrile one could be used as metalloligands toward the formation of hetero bimetallic chains with a dithiolene complex based on the 1,3-dithiole-2-one-3,4-dithiolato ligand (dmid) was investigated. Accordingly, solutions of $[Mn(TPP)]BF_4$ and $Et_4N[Ni(dmid)_2]$ in THF or acetone were prepared, and diffusion of diethyl ether afforded in three different phases noted **1**, **2** and **3** compound of general formula $[Mn(TPP)(THF)]_2[Ni_2(tto)(dmid)_2]$.

#### *Crystal structure*

As shown in Fig. 3.1 , the structure of **1** involves two crystallographically independent $[Mn(TPP)]^+$ cations, coordinated on the Mn atom with either a THF or a water molecule. However, the starting $[Ni(dmid)_2]^-$ radical anion has evolved during the crystallisation process to give a bimetallic, dianionic species formulated as $[Ni_2(tto)(dmid)_2]^{2-}$ (tto= tetrathiooxalate) with two crystallographically independent complexes in the asymmetric unit, each located in an inversion centre. Such bimetallic dithiolene complexes are not unknown and have been already encountered in several instances from the aerial decomposition [Yang, 1994] of square planar bis- dithiolene complexes such as

$[Ni(dmit)_2]^-$,[Piotraschke, 1995; Pullen, 1996; Pullen, 1997; Pullen, 1997, Bai, 2000] $[Cu(dmid)_2]^-$,[Vicente, 1987] and more recently $[Ni(dmid)_2]^-$.[Batsanov, 2001] Compound **1** can therefore be formulated as: $[Mn(TPP)(THF)][Mn(TPP)(H_2O)][Ni_2(tto)(dmid)_2]^{\cdot}(THF)_2$. In the solid state, each $[Ni_2(tto)(dmid)_2]^{2-}$ complex is surrounded by two $[Mn(TPP)]^+$ cations through short S···Mn contacts, at 2.951(5) Å with $[Mn(TPP)(THF)]^+$ and at 2.865(3) Å with $[Mn(TPP)(H_2O)]^+$, demonstrating that the anticipated coordination of the Mn atom by the carbonyl function of the dmid ligand is clearly not favoured here, but rather an additional Mn···S interaction with one sulfur atom of the dithiolene complex metallacycle. In each case, the bridging interactions involving sulfur result in longer Ni–S bond distances to the bridging sulfur atoms and distortions from planarity for the $[Ni_2(dmid)_2(tto)]^{2-}$ anions. For example, when linked to $[Mn(TPP)(THF)]^+$ (Fig.3.1 ), the Ni–S distances amount to Ni1B–S2B (bridging) = 2.177(2) Å and Ni1B–S5B (nonbridging) = 2.169(2) Å; when linked to $[Mn(TPP)(H_2O)]^+$ (Fig. 3.1), one finds Ni–S distances at Ni1A–S2A (bridging) = 2.180(2) Å and Ni1A–S5A (nonbridging) = 2.164(2) Å. Not surprisingly, given the asymmetry of these axial interactions, the porphyrin are not planar any more but adopt a horse saddle shape.

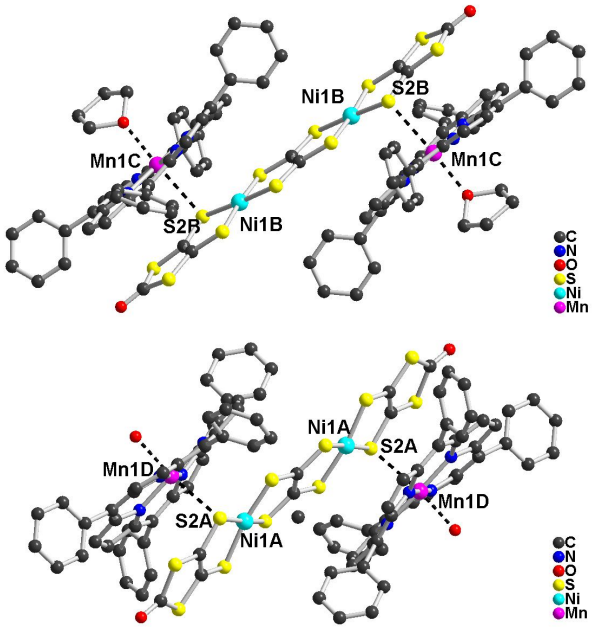


**Fig. 3.1**. A view of the two trimolecular motifs in **1** highlighting the S···Mn coordination.

These neutral trimeric motifs, $[Mn(TPP)(THF)]_2[Ni_2(tto)(dmid)_2]$ or $[Mn(TPP)(H_2O]_2[Ni_2(tto)(dmid)_2]$, form a chess board network in the (bc) plane (Fig. 3.2). Considering that the bimetallic nickel dithiolene complex $[Ni_2(tto)(dmid)_2]^{2-}$ is now diamagnetic –at variance with the starting $[Ni(dmid)_2]^{\cdot-}$ complex– we can anticipate that the magnetic response of **1** will be essentially due to the magnetically independent S = 2 $[Mn(TPP)]^+$ cations. Compound **2** differs only slightly from **1** as the THF molecule coordinating one $[Mn(TPP)]^+$ cation in **1** is now replaced in **2** by an acetone molecule, giving the following formulation $[Mn(TPP)(acetone)][Mn(TPP)(H_2O)][Ni_2(tto)(dmid)_2]\cdot(acetone)$ (one acetone molecule has been squeezed), where a solid state arrangement very similar to that observed in **3** is present. Hence, its crystal structure will not be further detailed here.

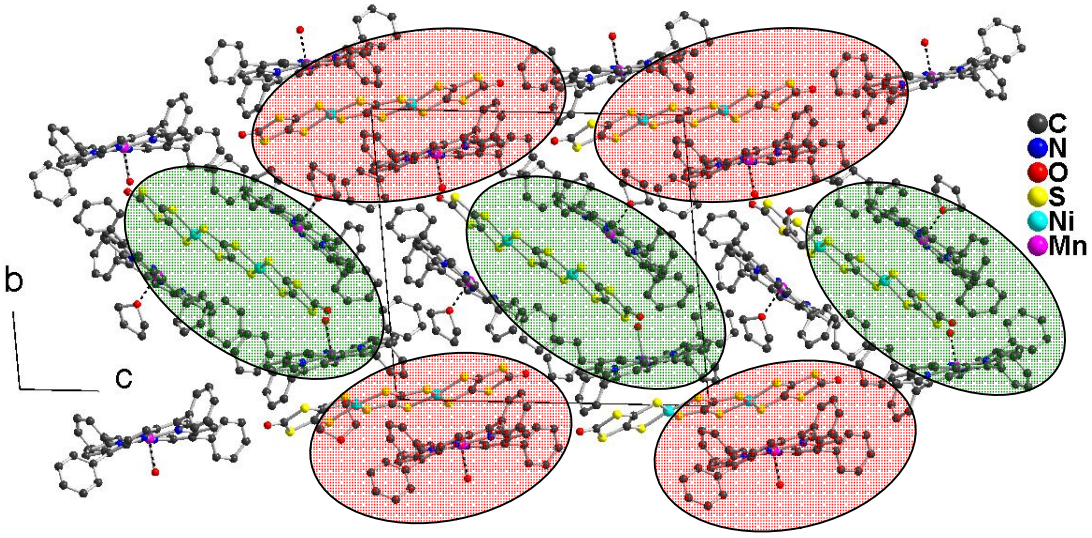


**Fig 3.2**. Projection view along *a* of the unit cell of **1**, showing the organization of the trimeric $[Mn(TPP)]_2[Ni_2(tto)(dmid)_2]$ motifs.

Compound **3** is also related to **1**, but with only one crystallographically independent $[Mn(TPP)(THF)]^+$ cation in general position and one $[Ni_2(tto)(dmid)_2]^{2-}$ on an inversion centre, together with two non-coordinated THF molecules. As shown in Fig. 3.3, a similar

trimeric motif formulated as $[Mn(TPP)(THF)]_2[Ni_2(tto)(dmid)_2]$ is found in **3**, with a Mn···S distance at 2.804(4) Å, that is notably shorter than in **1** or **2**. As in **1**, it is accompanied by longer Ni–S bond distances to the bridging sulfur atoms, with Ni1–S2A (bridging) at 2.182(6) Å and Ni1–S5A (nonbridging) at 2.173(4) Å. Note also the stronger deviations of planarity of the $[Ni_2(tto)(dmid)_2]^{2-}$ dianionic complex, when compared with the structures in **1** or **2** (Fig. 3.3) with a tetrahedral distortion around the Ni atom which amounts to 10.18(6)° and a folding of the central $NiS_2C_2$ metallacycle along the S---S hinge of 11.6(1)°.

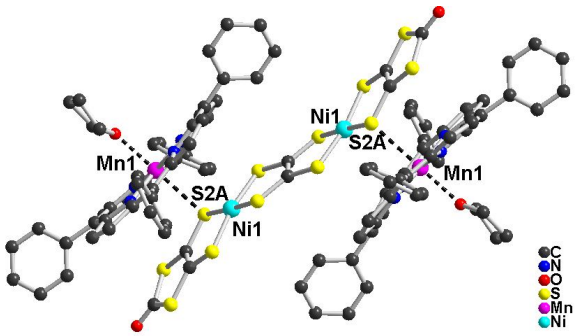


**Fig 3.3**. View of the neutral trimeric entity $[Mn(TPP)THF]_2[Ni_2(tto)(dmid)_2]$ in **3**.

***Magnetic properties of 1–3.***

As the bimetallic $[Ni_2(tto)(dmid)_2]^{2-}$ species in **1-3** are closed-shell, the magnetic susceptibility of the three compounds is expected to originate only from the S = 2 $[Mn(TPP)]^+$ species. Temperature dependence of the χT product (per Mn atom) for the three compounds (Fig. 3.4) shows values at 300 K close to the expected χT = 3 value for a S = 2 complex with *g* close to 2. The deviations from 3 for compounds 1 and 2 are due to uncontrollable desolvatation processes and to the fact that crystals in 1 and 2 were obtained together with a black powder that probably contaminated the samples. It is reasonable that during the crystallization process other by-products deriving from the process $[Ni(dmid)_2]^{\cdot-} \rightarrow [Ni_2(tto)(dmid)_2]^{2-}$ which involves the opening of the C=O moiety. Another impurity could be the by product of the methatesis, $Et_4NBF_4$ .

At lower temperatures, anisotropy or inter-chain antiferromagnetic interaction effects become relevant, which can be modelised through a Curie-Weiss fit with θ(1) = –5.9 K, θ(2) = –6.9 K and θ (3) = –5.8 K.

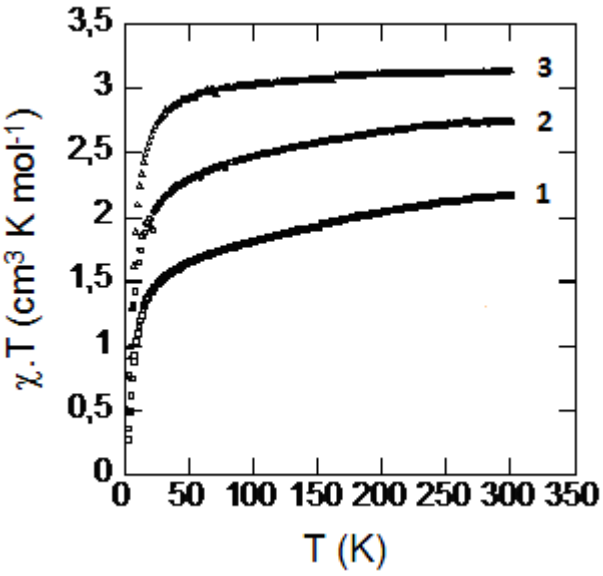


**Fig. 3.4**. Temperature dependence of the χT product for **1**–**3**.

Contextually with $[Ni(dmid)_2]^{\cdot-}$**,** this work had dealt also with another bis-dithiolene complexes together with $[Mn(TPP)]^+$, $[Ni(tfadt)_2]^{\cdot-}$ . For comparison purposes, a brief illustration of the results obtained in the same framework of $[Ni(dmid)_2]^{\cdot-}$ is given.

Compound $[Mn(TPP)][Ni(tfadt)_2]$ was obtained by Jeannin (Jeannin O., PhD work Université d'Angers) by the methathesis reaction between $[Mn(TPP)]BF_4$ and $Bu_4N[Ni(tfadt)_2]$ in $THF/CH_2Cl_2$ by slow evaporation of the solvent (Fig.3.5 a).

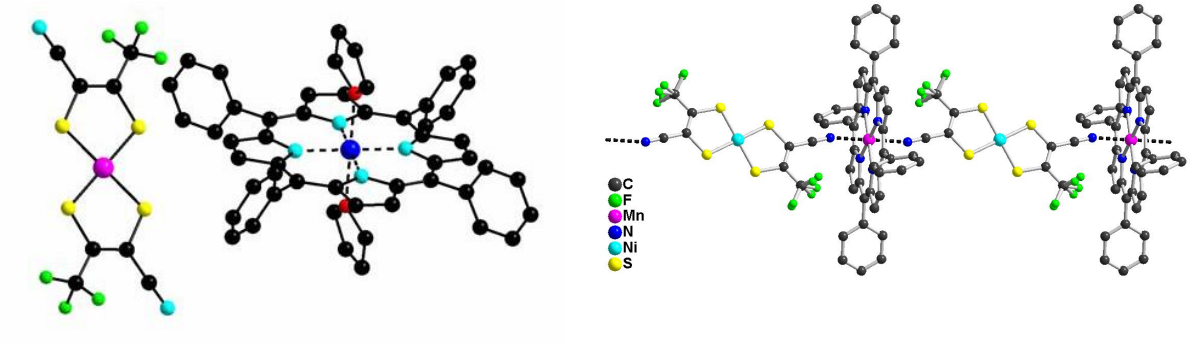


**a** **b**

**Fig 3.5 a)**[Mn(TPP)][Ni(tfadt)$_2$]·2THF and **b)** {[Mn(TPP)][Ni(tfadt)$_2$]}$_n$

In this case the coordination of –CN to Mn(III) is not observed in the crystal structure and Mn(III) is coordinated by two molecules of THF.

This example has shown the low coordination tendency of CN group, especially in solvents such as THF that could act as an oxygen donor ligand. By changing the solvent, the methathesis reaction between [Mn(TPP)]$BF_4$ and $Bu_4N$[Ni(tfadt)$_2$] in $CH_2Cl_2$ has led to heterobimetallic chains of formula {[Mn(TPP)][Ni(tfadt)$_2$]}$_n$ (Fig.3.5 b) (Jeannin, 2005) after layering with cyclohexane or pentane.

## 3.2 The dianionic bis-dithiolene complex (S=1/2) $[Cu(mnt)_2]^{2-}$ as metallo-ligand towards Mn(III)-salen type complexes

The formation of the heterobimetallic Mn-Ni-Mn chains has not be observed by reacting $[Mn(TPP)]^+$ with $[Ni(dmid)_2]^{\cdot-}$because of the dimerization of $[Ni(dmid)_2]^{\cdot-}$ leading to trimers of the type [Mn(TPP)][$Ni_2$(tto)(dmid)$_2$][Mn(TPP)]. For these reasons, we have switched to the paramagnetic $[Cu(mnt)_2]^{2-}$ bis-dithiolene complex which is relatively stable in solution with respect to $[Ni(dmid)_2]^{\cdot-}$. The basic idea is to connect complexes Mn(III)-salen and derivaties with $[Cu(mnt)_2]^{2-}$ as a bridging metallo-ligand through –CN···Mn(III) interaction.

### 3.2.1 The Mn(III)-salen derivatives as paramagnetic molecular building blocks

This bis-dithiolene has already been investigated in the formation of polymetallic coordination compounds together with $[Mn(TPP)]^+$ complexes (see paragraph 3.1).

However, the current outstanding development in the coordination chemistry of manganese, especially for what concerns molecular magnetism, has pushed us to study the quadridentate Schiff-base complexes of Mn(III), where the basic-ligand is represented by N,N- ethylene-bis(salicylideneiminate), most commonly called *salen* (Fig. 3.5).

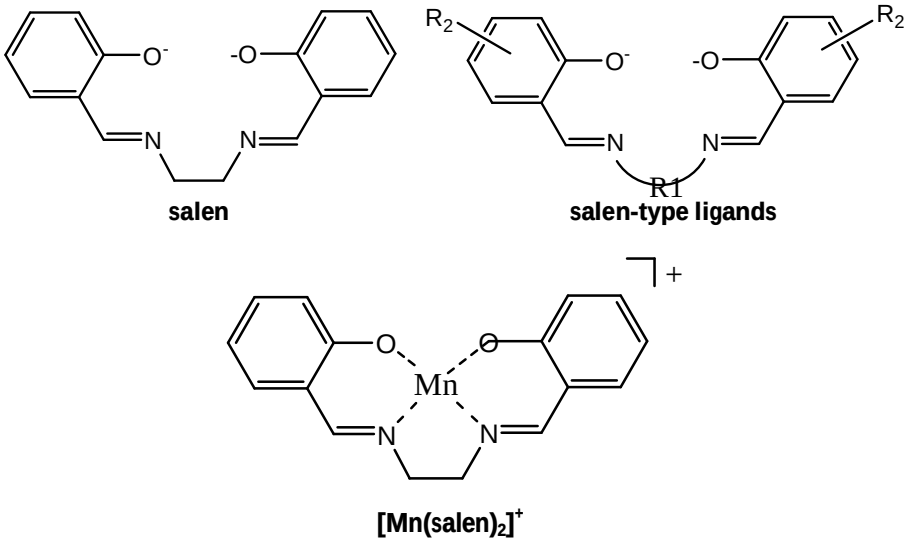


**Fig 3.5** The ligand salen and its derivatives (top).
The quasi-planar Mn(III) salen complex $[Mn(salen)_2]^+$ (bottom).

The stable quadridentate salen chelate $MnO_2N_2$ is reminiscent of the porphyrine framework [Myasaka, 2007]. Most of the times, the Mn-$N_2O_2$ is quasi-planar and coordination is completed by two molecules of solvent or by one molecule of solvent and one oxygen atom from a second Mn(III) salen unity, affording dimers of the type $[Mn_2(salen)_2(L)_2]_2^+$ through a bi-phenolate bridge (Fig. 3.6).

Because of the labile apical solvent molecules, Mn(III)-salen complexes can be regarded as "acceptor" coordination compounds toward other ligands or metallo-ligands. When Mn(III) is coordinated by bifunctional ligands such as $NCS^-$ anions, they can act as

metallo-ligand able to coordinate other metal centers by N-or S-donor atoms of $NCS^-$ anion [Myasaka, 2007].

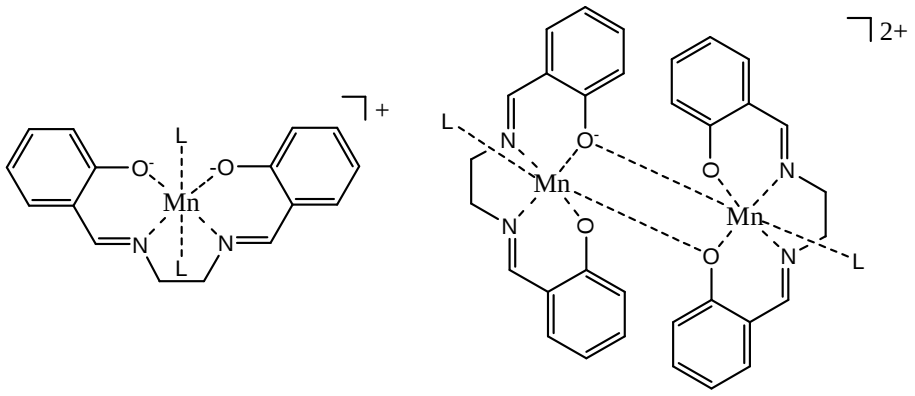

**Fig 3.6** Monomer $[Mn(salen)(L)_2]^+$ and dimer $[Mn_2(salen)_2(L)_2]^{2+}$.

This versatility makes Mn(III)-salen complexes suitable building block for the synthesis of polymetallic complexes with magnetic properties.

$[Mn(salen)]^+$ has spin S=2 and it is Jahn Teller distorted. The axis of the tetragonal distorsion is perpendicular to the Mn-$N_2O_2$ plane and it is located on the same direction corresponding to the free coordination sites for additional ligand, as depicted in Fig.3.7.

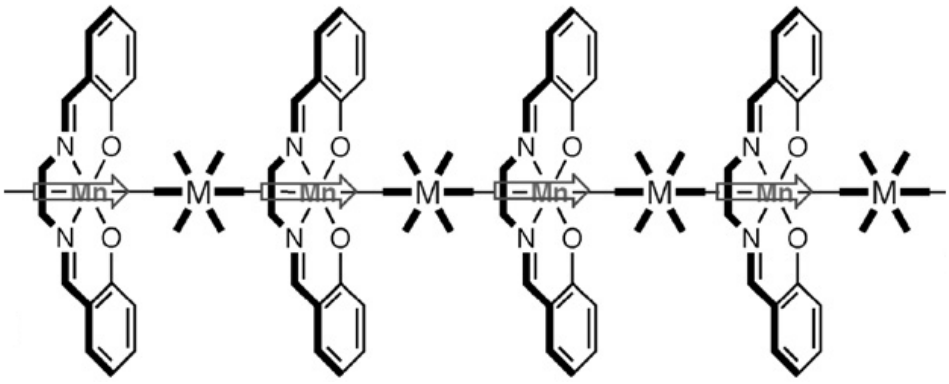

**Fig. 3.7** An example of Mn(salen) assemblies with general $M(L)_6$ complexes. The arrow is the Jahn Teller axis.

One unpaired electron is located on the $dz^2$ orbital laying in the direction of the Jahn Teller axis. As it can be observed in Fig 3.7, in the assembly of several $[Mn(salen)]^+$ unities with $M(L)_6$ metallo ligands, the ligands L of $M(L)_6$ bridge two unities and are magnetic "mediators" between Mn(III) and the metal M. However, the magnetic properties depend also on the type of the salen ligand in Mn(III) because of the ligand field in the equatorial plane affecting the energy of the $dz^2$ by the tetragonal distortion.

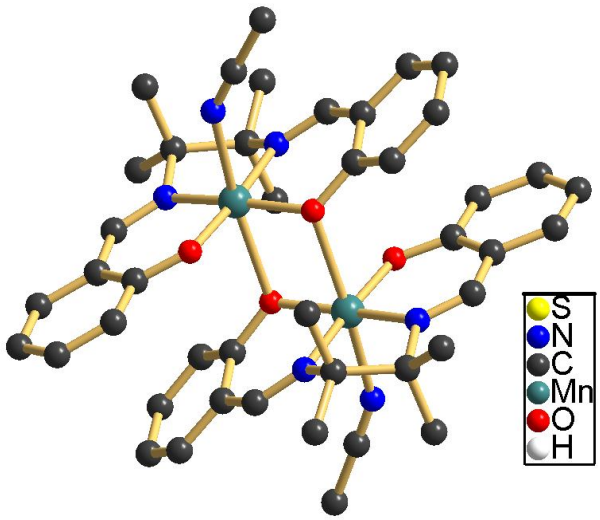


**Fig. 3.8** $[Mn_2(saltmen)_2(CH_3CN)_2]^{2+}$ dimmer.

The out of plane dimers such as $[Mn_2(saltmen)_2(ReO_4)_2$ [Clerac, 2005] $[Mn(saltmen)(O_2CCH_3)]_2.2CH_3COOH$, $[Mn(saltmen)(N_3)]_2$, $[Mn(salen)(NCO)]_2$, [Lu, 2004; Myasaka, 2004] are considered to be SMMs with an intra-dimer ferromagnetic interaction through the bi-phenolate bridge occurring between the two $[Mn(salen)]^+$ , generating a spin ground state S=4.

### 3.2.2 Examples of metal bis-dithiolenes as metallo-ligands toward Mn(III)salen-derivatives in the literature

In literature a lot of examples of high nuclearity complexes or polynuclear 1-D chains based on monomeric or dimeric Mn(III)-salen derivatives are described [Myasaka 2007;

Myasaka, 2005; Lecren, 2007]. These complexes are linked together by polyfunctional organic ligands or metal complexes bearing coordinative groups [Myasaka, 2007].

A limited number of compounds involving metal bis-dithiolene complexes as metallo-ligands towards the Mn(III) center in Mn(III) salen is present.

The compounds $[Mn(5\text{-}MeOsaltmen)\{Ni(dmit)_2\}]_2$ e $[Mn(5\text{-}Mesaltmen)\{Ni(dmit)_2\}]_2$ (Fig. 3.9) were synthesized by Fourmigué [Fourmigué, 2009] from paramagnetic S=1/2 $[Ni(dmit)_2]^{\bullet-}$ with $[Mn_2(5\text{-}MeOsaltmen)_2]^{2+}$ or $[Mn_2(5\text{-}Mesaltmen)_2]^{2+}$ .

In both compounds, Mn(III) is coordinated by the sulphur atom of the –C=S group of $[Ni(dmit)_2]^{\bullet-}$, forming a trimeric structure of the type Ni-$Mn_2$-Ni (Fig. 3.9).

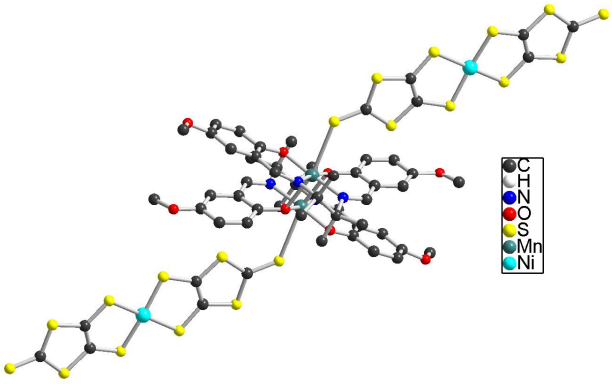


**Fig. 3.9** Complex $[Mn(5\text{-}MeOsaltmen)\{Ni(dmit)_2\}]_2$

Another example is compound is $[\{Mn(salph)(H_2O)\}_2\{Cu(mnt)_2\}]4DMF$ (Fig X) , where two $[Mn(salph)H_2O]^+$ are coordinated via Mn(III)···S interaction with the dianionic $[Cu(mnt)_2]^{2-}$ complex giving a neutral trimeric structure. The magnetic behaviour of such complex has not been studied.

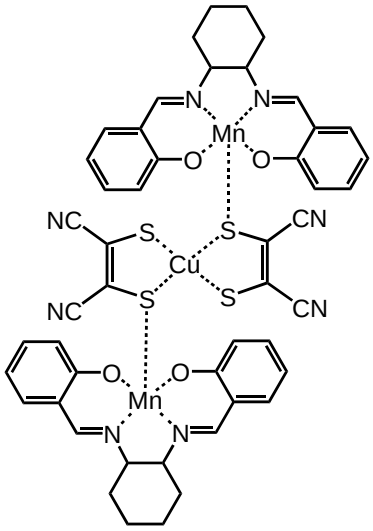

**Fig 3.10** [{Mn(salph)($H_2O$)}$_2${Cu(mnt)$_2$}].

The limited number of compounds where a metal bis-dithiolene acts as metallo-ligand toward Mn(III)-salen type complexes has prompted us to investigate whether a metal-bis-dithiolene is able to coordinate Mn(III)-salen derivatives.

### 3.2.3 Synthesis of $[Et_4N]_2[\{Mn(salen)(NCS)\}_2\{Cu(mnt)_2\}]$

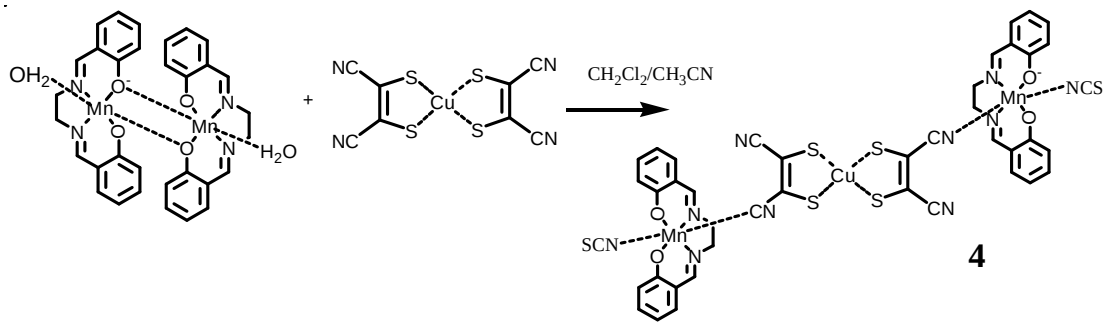


**Scheme 3.4**

The complex $[Et_4N]_2[\{Mn(salen)(NCS)\}_2\{Cu(mnt)_2\}]$ (**4** in Scheme 3.4) was obtained by the metathesis reaction of $[Et_4N]_2[Cu(mnt)_2]$ with $[Mn_2(salen)_2(H_2O)_2][PF_6]_2$ in a 1/1 mixture of $CH_2Cl_2/CH_3CN$ (Scheme 3.4) upon slow diffusion of diethyl ether after 14 days. It has to be mentioned that together with the crystals a brown-black powder was also present.

***Crystal structure***

$[Et_4N]_2[\{Mn(salen)(NCS)\}_2\{Cu(mnt)_2\}]$ crystallizes in the monoclinic system, space group P21/c with Cu atoms located on an inversion centre. The $[\{Mn(salen)(NCS)\}_2\{Cu(mnt)_2\}]^{2-}$ unity contains two cationic $[Mn(salen)]^+$ linked by a trans-bridging $[Cu(mnt)_2]^{2-}$ through –CN···Mn interaction leading to a trimeric complex Mn···Cu···Mn with three spins S=2, S=1/2, S=2. Surpisingly, a thiocyanate group $NCS^-$ is found to coordinate each Mn(III) with the nitrogen atom, giving a global charge of -2 for $[\{Mn(salen)(NCS)\}_2\{Cu(mnt)_2\}]^{2-}$. The charge is balanced by two $Et_4N^+$ disordered cations.

Cu-$S_4$ dithiolene core is in this case planar and bond distances Cu-S (Table 3.1) are in the range 2.250 Å -2.308 Å for Cu-S typical for a dianionic oxidation state of $[Cu(mnt)_2]$ [Stiefel, 2004]. The distance for C=C bond is consistent with the 1,2 dithiolate form of ligand mnt [Rabaça, 2009].

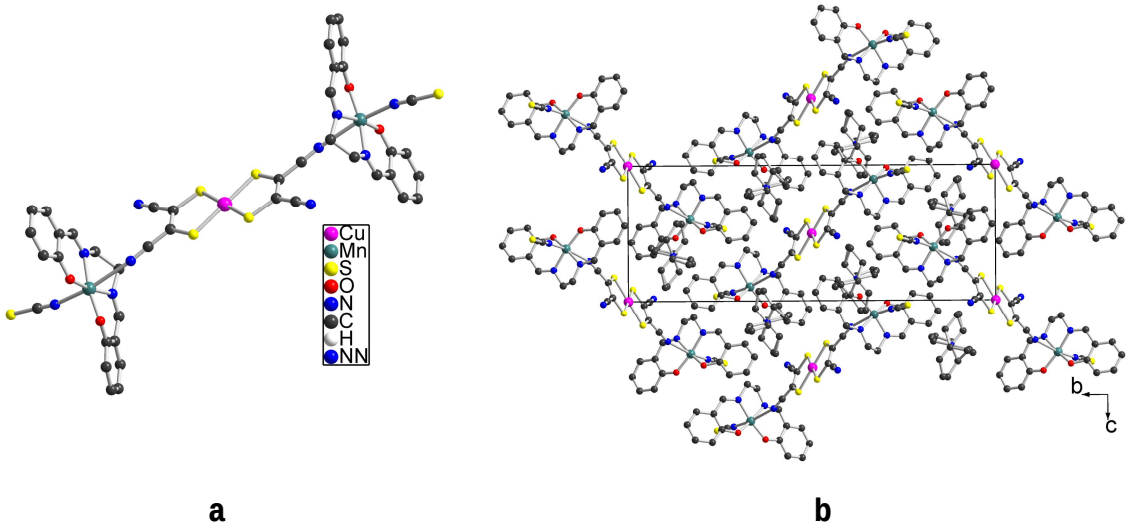


**a** **b**

**Fig. 3.11 a)** The $[\{Mn(salen)(NCS)\}_2\{Cu(mnt)_2\}]^{2-}$ unity and **b)**$[Et_4N]_2[\{Mn(salen)(NCS)\}_2\{Cu(mnt)_2\}]$ along crystallographic axis a.

In Table 3.1 Cu-S, C=C and C-S distances are reported together with those found for dianionic $[Bu_4N]_2[Cu(mnt)_2]$ [Plumlee, 1975] and monoanionic [BrPyH][$Cu(mnt)_2$] [Xiao, 2006], confirming the dianianionic state of $[Cu(mnt)_2]^{2-}$ in $[\{Mn(salen)(NCS)\}_2\{Cu(mnt)_2\}]^{2-}$.

| | **$[Et_4N]_2[\{Mn(salen)(NCS)\}_2\{Cu(mnt)_2\}]$** | **$[Bu_4N]_2[Cu(mnt)_2]$** | **[BrPyH][$Cu(mnt)_2$]** |
|---|---|---|---|
| Cu-S (Å) | 2.268(1) ; 2.294(1) | 2.264(4); 2.286(4) | 2.186 (13) ; 2.178 (21) 2.175 (14); 2.179 (14) |
| C-S (Å) | 1.734(4); 1.736(4) | 1.729(2); 1.726(2) | 1.741(3); 1.730(3) 1.732(3); 1.726(3) |
| C=C (Å) | 1.373(4) | 1.358 (32) | 1.344(20); 1.354(20) |

**Table 3.1** Selected bond distances for $[Et_4N]_2[\{Mn(salen)(NCS)\}_2\{Cu(mnt)_2\}]$, $[Bu_4N]_2[Cu(mnt)_2]$ and [BrPyH][$Cu(mnt)_2$].

Mn(III) is in an octahedral coordination geometry, with $O_2N_2$ salen in the equatorial positions and the $NCS^-$ with –CN(dihiolene) in apical positions. These last two Mn-N distances are longer than the equatorial ones because of the Jahn-Teller elongation for a $d^4$ Mn(III) ion. Mn(III)-salen is monomeric, and indication of the equilibrium $[Mn_2(salen)_2]^{2+} \rightarrow 2[Mn(salen)]^+$ .

Selected bond length are displayed in Table 3.2.

| | **Mn ($O_2N_2$)** | **Mn-N(dithiolene)** | **Mn-N(NCS)** |
|---|---|---|---|
| **Mn-N (Å)** | 1.981(1);1.986(1) | 2.749(2) | 2.235(1) |
| **Mn-O (Å)** | 1.877(1);1.886(1) | | |

**Table 3.2** Selected bond distances for$[Et_4N]_2[\{Mn(salen)(NCS)\}_2\{Cu(mnt)_2\}]$.

In the solid state the trimers are separated by $Et_4N^+$ cations in the crystal lattice and no short contacts are present.

For what concerns the two $NCS^-$ coordinated anions, it has to be pointed out that thiocyanate anion was not exhogenous and it probably derives from decomposition in solution of ligand mnt, deriving from $[Cu(mnt)]^{2-}$. This could be an evidence of a certain reactivity in solution for metal bis-dithiolene [Stiefel, 2004]. Uncoordinated mnt ligand probably derives from the ligand exchange reaction that could occurs between a planar $[Cu(mnt)]^{2-}$ and $[Mn_2(salen)_2]^{2+}$ as we will se in the next paragraph.

Anyway, all the attempts to obtain polymetallic complexes where $[Cu(mnt)]^{2-}$ acts as bridging ligand with the same synthetic conditions as for $[Et_4N]_2[\{Mn(salen)(NCS)\}_2\{Cu(mnt)_2\}]$ have failed. The presence of $NCS^-$ anions has been considered pivotal for the isolation of the trimetallic Mn---Cu---Mn coordination compound, view that the same trimer Mn---Cu---Mn without $NCS^-$ has not been isolated yet. In order to better control the reaction conditions, attempts to synthetize $[Et_4N]_2[\{Mn(salen)(NCS)\}_2\{Cu(mnt)_2\}]$ starting from $[Et_4N]_2[Cu(mnt)_2]$ and $[Mn_2(salen)_2][PF_6]_2$ and adding exhogenous $[Et_4N][NCS]$ as a source of thiocyanate ions were done. By refluxing $CH_3CN$ solutions of $[Et_4N]_2[Cu(mnt)_2]$, $[Mn_2(salen)_2][PF_6]_2$, $[Et_4N][NCS]$ led only to recrystalization of $[Et_4N]_2[Cu(mnt)_2]$ from the filtrate.

Slow diffusion of a $CH_3CN$ solution containing $[Et_4N][NCS]$ to $[Et_4N]_2[Cu(mnt)_2]$ and $[Mn_2(salen)_2][PF_6]_2$ in $CH_2Cl_2/CH_3CN$ afforded crystals identified as $[Mn_2(salen)_2(NCS)_2]$ by means of single crystal X-ray analysis. In fact, $[Mn_2(salen)_2(NCS)_2]$ is very poorly soluble in $CH_3CN$ and slightly soluble in $CH_2Cl_2$. Consequently recrystallization of $[Mn_2(salen)_2(NCS)_2]$ is favoured over the isolation of $[Et_4N]_2[\{Mn(salen)(NCS)\}_2\{Cu(mnt)_2\}]$.

The decomposition of $mnt^{2-}$ ligand from $[Cu(mnt)_2]^{2-}$ is slow enough to allow first the formation of a trimetallic unity of the type $[\{Mn(salen)\}_2\{Cu(mnt)_2\}]$ in solution and then the coordination of $NCS^-$ anions to the Mn—Cu---Mn trimer, leading to the less soluble species $[Et_4N]_2[\{Mn(salen)(NCS)\}_2\{Cu(mnt)_2\}]$.

All the attempts where very diluited $[Et_4N][NCS]$ $CH_3CN$ solutions were diffused onto $[Et_4N]_2[Cu(mnt)_2]$ and $[Mn_2(salen)_2][PF_6]_2$ in $CH_2Cl_2/CH_3CN$ were unsuccessfull.

A synthetic way considered is to form first $[Mn_2(salen)_2(NCS)_2]$ and then makes him reacting with $[Et_4N]_2\{Cu(mnt)_2]$. To date, attempts done in DMF ($[Mn_2(salen)_2(NCS)_2]$ is

soluble only in DMF) were unsuccesfull. Anyway the work is still on progress using different reaction conditions in order to provide a magnetic characterization for the unusual trimer $[Et_4N]_2[\{Mn(salen)(NCS)\}_2\{Cu(mnt)_2\}]$.

### 3.2.4 Synthesis of $[Mn(salen)Cu(salen)]_2[Cu(mnt)_2]$: a competition with $[Et_4N]_2[\{Mn(salen)(NCS)\}_2\{Cu(mnt)_2\}]$?

During the several attempts to carry out the reaction leading to the desired $[Et_4N]_2[\{Mn(salen)(NCS)\}_2\{Cu(mnt)_2\}]$, crystals of the salt $[Mn(salen)Cu(salen)]_2[Cu(mnt)_2]$ (Fig. 3.12) were found upon slow diffusion of diethylether or slow evaporation of solution in $CH_3CN$ containing $[Mn_2(salen)_2(NCS)_2]$ and $[Et_4N]_2[Cu(mnt)_2]$.

The asymmetric unit (Fig. 3.12, a) consists of a half dithiolene molecule of $[Cu(mnt)_2]^{2-}$ with the Cu(II) occupying an inversion center and the mixed Mn(III) Cu(II) dimer $[Mn(salen)Cu(salen)]^+$ in general position. So, for each $[Cu(mnt)_2]^{2-}$ , the charge is balanced by two $[Mn(salen)Cu(salen)]^+$ molecules.

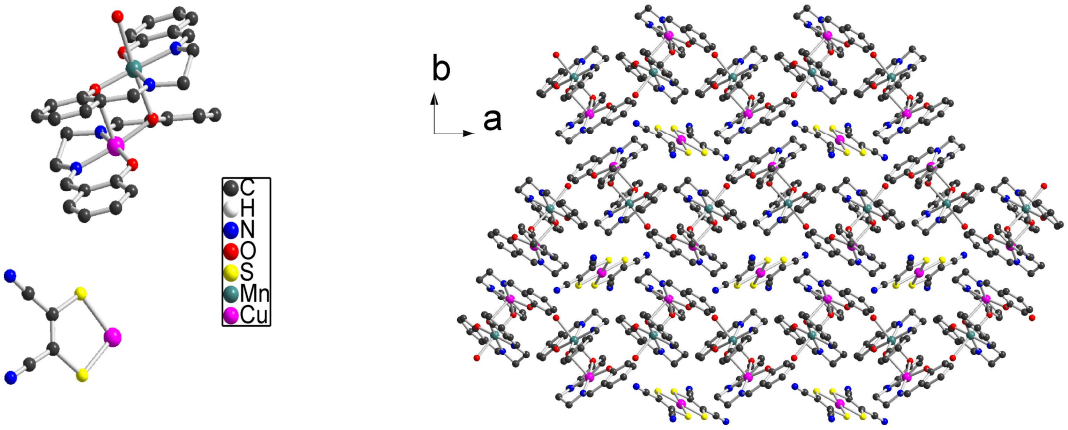


**a** **b**

**Fig 3.12 a)** asymmetric unity of $[Mn(salen)Cu(salen)]_2[Cu(mnt)_2]$ and **b)** crystal packing along c axis.

In Fig. 3.12 b, unit cell packing is shown along c axis. It can be observed that the $[Cu(mnt)_2]^{2-}$ are segregated by six molecules of $[Mn(salen)Cu(salen)]^+$.

The Cu-$S_4$ core of the dithiolene complex is planar and Cu-S distances are reported in Table 3.3 together with C=C and C-S distances. By comparison with the previously discussed $[Et_4N]_2[\{Mn(salen)(NCS)\}_2\{Cu(mnt)_2\}]$ and monoanionic $[BrPyH][Cu(mnt)_2]$ it can be confirmed that $[Cu(mnt)_2]$ in $[Mn(salen)Cu(salen)]^+$ is in its dianionic state.

| | **$[Et_4N]_2[\{Mn(salen)(NCS)\}_2\{Cu(mnt)_2\}]$** | **$[Mn(salen)Cu(salen)]_2[Cu(mnt)_2]$** | **$[BrPyH][Cu(mnt)_2]$** |
|---|---|---|---|
| Cu-S (Å) | 2.268(1) ; 2.294(1) | 2.260(1); 2.287() | 2.186 (13) ; 2.178 (21) 2.175 (14); 2.179 (14) |
| C-S (Å) | 1.734(4); 1.736(4) | 1.732(1); 1.733(1) | 1.741(3); 1.730(3) 1.732(3); 1.726(3) |
| C=C (Å) | 1.373(4) | 1.370 (0) | 1.344(20); 1.354(20) |

**Table 3.3** Selected bond distances for $[Et_4N]_2[\{Mn(salen)(NCS)\}_2\{Cu(mnt)_2\}]$, $[Bu_4N]_2[Cu(mnt)_2]$ and $[BrPyH][Cu(mnt)_2]$ **.**

In $[Mn(salen)Cu(salen)]^+$, neutral $[Cu(salen)]$ interacts via a bi-phenolate bridge with the $[Mn(salen)]^+$ molecule, as usually found for $[Mn_2(salen)_2]^{2+}$ in solid state.

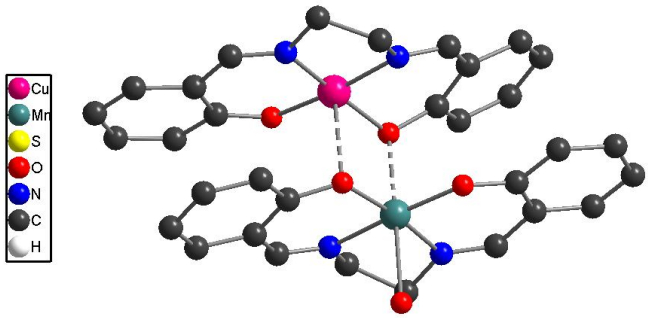


**Fig 3.12** The cationic unity of $[Mn(salen)Cu(salen)]_2[Cu(mnt)_2]$, $[Mn(salen)Cu(salen)]^+$ . Dashed line: the bi-phenolate bridge.

Cu(II) is in a square planar environment while Mn(III) is in a distorted octahedral geometry. Cu-N and Cu-O bond distances are reported in Table 3.4 together with Mn-N and Mn-O values.

| | **$M(O_2N_2)$** | **$M-H_2O$** | **M-O(μ-O)** |
|---|---|---|---|
| **Cu-N (Å)** | 1.947(1);1.932(0) | --- | --- |
| **Cu-O (Å)** | 1.931(1);1.909(0) | --- | 2.563(0) |
| **Mn-N (Å)** | 1.987(1); 1.983(0) | --- | --- |
| **Mn-O (Å)** | 1.886(1); 1.896(1) | 2.380(0) | 2.293(1) |

**Table 3.4** Selected bond distances for $[Mn(salen)(H_2O)Cu(salen)]_2[Cu(mnt)_2]$,

The bond distances found for Cu(II) are consistent for those of [Cu(salen)] complexes and related compounds already published [Kahn, 1997]. The Cu-O distance relative to the phenolate bridge in $[\{Mn(salen)(H_2O)Cu(salen)]_2[Cu(mnt)_2]$ is slightly lower than the one of 2.80 Å for the complex $\{[Cu(salen)\{Pr(hfac)_3\}_2(bpy)](CHCl_3)_2\}$ [Pontillart, 2010] where the Cu(II) from a [Cu(salen)] unity is connected to the $[Pr(hfac)_3]$ via Cu(II)-O(hfac) interaction.

To date, no examples of mixed Cu(II)/Mn(III) salen dimers have been synthesized.

Its formation is indicative of a possible exchange reaction that occurs between $[Mn(salen)]^+$ and $[Cu(mnt)_2]^{2-}$, view that Cu(II) has been introduced only as $[Cu(mnt)_2]^{2-}$.

This is consistent with the formation of $NCS^-$ from the free ligand mnt as discussed in paragraph 3.3.3.

In chapter 2 we introduced the possible chemical reactivity in solution of metal bis-dithiolene complexes. One type of reaction that can occurs for planar dithiolenes is the ligands exchange.

Similarly to other square planar complexes, metal bis-dithiolenes undergo ligand exchange reaction with other bis-chelating ligand in poorly coordinating solvents[Stiefel, 2004], as shown in Scheme 3.5.

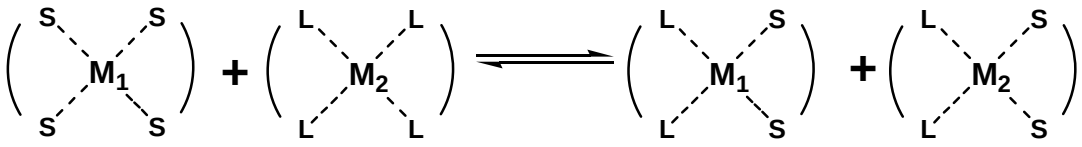


**Scheme 3.5** Ligand exchange equilibrium between a bis-dithiolene complex with a bis-chelated metal square planar metal complex.$M_1$, $M_2$ = Fe, Co, Ni, Pd, Pt, Cu, Au

The reaction in Scheme 3.5 is an equilibrium and generally it is slow at room temperature. A reaction mechanism has been proposed for this ligand exchange between metal bis-dithiolenes and other bis-chelated complexes [Stiefel, 2004].

A stacking dinuclear intermediate, compound **1** in scheme 3.6 is believed to form in solution and then the mixed ligand dinuclear species **2** is formed from isomeration of **1**. The dinuclear species **2** then dissociates to give the mixed ligand complexes.

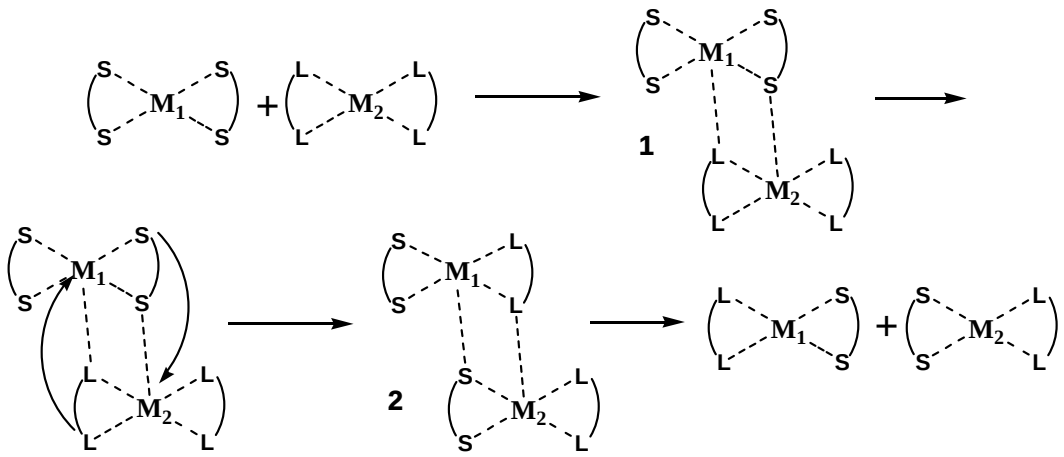


**Scheme 3.6** Reaction mechanism for the ligand exchange reaction between a planar bis-dithiolene complex and a general square planar $ML_4$ metal complex.

It has also to be pointed out that many heteroleptic bis-dithiolene complexes are synthetized through exchange reactions between two different homoleptic metal bis-dithiolenes in acetone, dichlorometane and acetonitrile, as reported by McLeverty [McLeverty, 1964].

Taking into account that both $[Cu(mnt)_2]^{2-}$ and $[Mn(salen)]^+$ are planar and considering the affinity of Mn(III) for sulphur donor atoms, a similar reaction path as in Scheme 3.6 with dimeric intermediates is reasonable to justify the formation of the mixed $[\{Mn(salen)(H_2O)Cu(salen)]^+$. Crystals of $[Mn(salen)Cu(salen)]^+$ were isolated in low yelds but the reaction is reproductible. In particular, in some batches crystals of $[Mn(salen)Cu(salen)]_2[Cu(mnt)]$ were isolated together with compound $[Mn_2(salen)_2(NCS)_2]$. This is a further indication of the decomposition in solution of $mnt^{2-}$ ligand to give thiocyanate ions, as discussed in paragraph 3.4.3 for $[Et_4N]_2[\{Mn(salen)(NCS)\}_2\{Cu(mnt)_2\}]$.

To clarify the solution behaviour of $[Mn(salen)]^+$ and $[Cu(mnt)]^{2-}$ complexes, electron paramagnetic resonance measurement are in progress on DMF and $CH_3CN$ solutions. DMF was choosen as solvent to prevent the formation of crystals or precipitates. To date, on DMF solutions, only signal of $[Mn(salen)]^+$ and $[Cu(mnt)]^{2-}$ were detected.

A more hindered Mn(III)-salen complex was reacted with $[Cu(mnt)]^{2-}$ because we wanted to check whether the effect of a bulkier group could influence the exchange reaction, considering that exchange reactions have dimeric intermediates, as shown in Scheme 3.6.

The metal exchange was observed also by reacting $[Et_4N]_2[Cu(mmt)]$ with the steric hindered, di-phenyl-disubstitued, $[Mn_2(R,R\text{-}1,2diphenyl\text{-}salen)_2(H2O)_2]^{2+}$. Crystals of compound [Cu (R,R-1,2-diphenyl-salen)](CH3CN) Fig.**3.13** were isolated from acetonitrile solutions after one week.

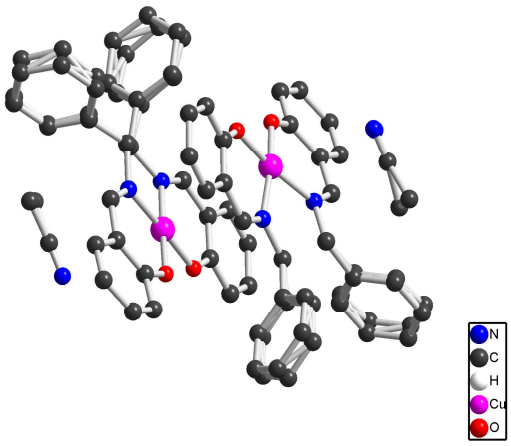


**Fig. 3.13** Asymmetric unit for [Cu (R,R-1,2-diphenyl-salen)](CH3CN).

The complex [Cu(R,R-1,2-diphenyl-salen)](CH3CN) crystallizes in the monoclinic system, space group C2. The asymmetric unity is composed of two [Cu(R,R-1,2-diphenyl-salen)] molecules and two $CH_3CN$ molecules. The two Cu(II) ions are located on two binary axis. Each Cu(II) is in square planar coordination geometry. Cu(II)-N and Cu(II)-O distances are reported in Table 3.5 together with the corresponding distances for $[Mn(salen)Cu(salen)]^+$

| | **[Cu (R,R-1,2-diphenyl-salen)]** | **$[Mn(salen)Cu(salen)]^+$** |
|---|---|---|
| **Cu(II)-N (**Å) | 1.938; 1.941 | 1.947; 1.932 |
| **Cu(II)-O (**Å) | 1.890; 1.906 | 1.931; 1.909 |

**Table 3.5** selected Cu(II)-N and Cu(II)-O for $N_2O_2$ binding core of [Cu (R,R-1,2-diphenyl-salen)] and $[Mn(salen)Cu(salen)]^+$

It is clear that $[Cu(mnt)_2]^{2-}$ undergoes ligand exchange reaction in acetonitrile with planar Mn(III)- salen complexes. We have demonstrated that also with a bulkier substituent on the salen moiety, the exchange occurs. EPR measurements are on course with other bulkier Mn(III) salen complexes to further confirm our statements.

### 3.2.5 Synthesis of $[Mn_2(saltmen)_2(CH_3CN)_2][Cu(mmt)].CH_3CN$

We have considered a third Mn(III)-salen derivative, $[Mn_2(saltmen)_2\ (H_2O)_2]^{2+}$. The salen moiety in $[Mn_2(saltmen)_2\ (H_2O)_2]^{2+}$ is 1, 2 substituted by four methyl groups.

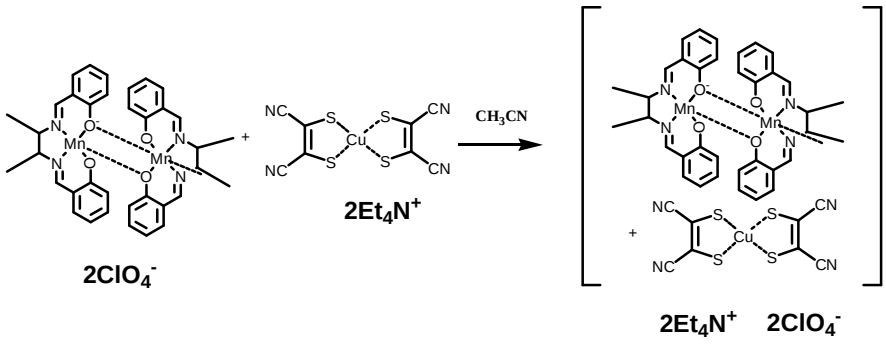


**Scheme 3.7:** Co-crystallization of $[Mn_2(saltmen)_2(CH_3CN)_2][Cu(mmt)]$ from $[Mn_2(saltmen)_2(H_2O)_2](ClO_4)_2$ together with $[Et_4N]_2[Cu(mmt)]$.

By reacting $[Mn_2(saltmen)_2(H_2O)_2](ClO_4)_2$ together with $[Et_4N]_2[Cu(mmt)]$, a simple methathesis reaction occurs in acetonitrile solutions, affording crystals of the compound $[Mn_2(saltmen)_2(CH_3CN)_2][Cu(mmt)]$, where a $[Cu(mnt)_2]^{2-}$ co-crystallizes together with dimeric $[Mn_2(saltmen)_2\ (CH_3CN)_2]^{2+}$.

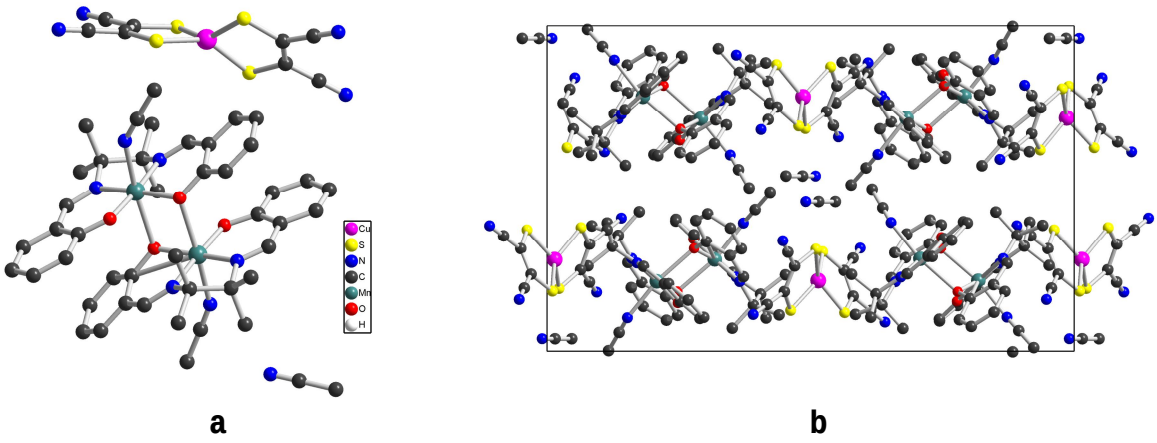


**Fig 3.14 a** Asymmetric unity of $[Mn_2(saltmen)_2(CH_3CN)_2][Cu(mmt)]\cdot(CH_3CN)$ and **b** view of the crystal packing along axis.

$[Mn_2(saltmen)_2(CH_3CN)_2][Cu(mmt)].CH_3CN$ crystallizes in the monoclinic system, space group P21/n. The dimeric Mn(III) complex and $[Cu(mnt)_2]^{2-}$ are both on general positions and a molecule of $CH_3CN$ is present as co-crystallization solvent.

The copper bis-dithiolene is not planar, presenting a quasi-tetrahedral distortion. The dihedral angle between the two $MS_2C_2$ ring constituting $[Cu(mnt)_2]^{2-}$ is 47.44°. In Table 3.6 are reported the Cu-S, C=C and C-S distances relative to $[Cu(mnt)_2]^{2-}$ and the corresponding values of $[Mn(salen)Cu(salen)]_2[Cu(mnt)_2]$ and $[BrPyH][Cu(mnt)_2]$ for comparison purposes.

| | **$[Mn(saltmen)(CH_3CN)_2][Cu(mnt)_2]$** | **$[Mn(salen)Cu(salen)]_2[Cu(mnt)_2]$** | **$[BrPyH][Cu(mnt)_2]$** |
|---|---|---|---|
| Cu-S (Å) | 2.253(1); 2.247(1); 2.257(2) | 2.260(1); 2.287() | 2.186 (13); 2.178 (21)<br>2.175 (14); 2.179 (14) |
| C-S (Å) | 1.730(1); 1.741(0) | 1.732(1); 1.733(1) | 1.741(3); 1.730(3)<br>1.732(3); 1.726(3) |
| C=C (Å) | 1.368(1); 1.372(0) | 1.370 (0) | 1.344(20); 1.354(20) |

**Table 3.6** Selected bond distances for $[Mn_2(saltmen)_2(CH_3CN)_2][Cu(mnt)_2]$, $[Mn(salen)Cu(salen)]_2[Cu(mnt)_2]$ and $[BrPyH][Cu(mnt)_2]$

From the bond distances analysis, $[Cu(mnt)_2]$ is in a dianionic oxidation state.

Mn(III) in $[Mn_2(saltmen)_2(CH_3CN)_2][Cu(mmt)]$ is in an octahedral coordination and the apical coordination is provided by a $CH_3CN$ molecule and the μ-oxygen of the phenolate.

| | **$[Mn(saltmen)(CH_3CN)_2][Cu(mnt)_2]$** | **$[Mn(salen)Cu(salen)]_2[Cu(mnt)_2]$** |
|---|---|---|
| Mn-O (Å) | 1.859(1); 1.815(1)<br>1.868(1); 1.915(1) | 1.886(1); 1.896(1) |
| Mn-N (Å) | 1.973(1); 1.992(1)<br>1.975(1); 1.995(1) | 1.987(1); 1.983(0) |
| Mn-O (μ-O)(Å) | 2.414(1); 2.440(1) | 2.293(1) |
| Mn-N ($CH_3CN$) (Å) | 2.321(1); 2.291(0) | --- |

**Table 3.7** Selected bond distances for $[Mn_2(saltmen)_2(CH_3CN)_2][Cu(mnt)_2\}]$ and $[Mn(salen)Cu(salen)]_2[Cu(mnt)_2]$.

The apical distances on Mn(III) appears more elongated with respect to $[Mn(salen)]^+$ in $[Mn(salen)Cu(salen)]_2[Cu(mnt)_2]$. In table 3.6 are reported the Mn-O and Mn-N distances for both $[Mn_2(saltmen)_2(CH_3CN)_2][Cu(mmt)]$ and $[Mn(salen)Cu(salen)]_2[Cu(mnt)_2]$.
As it can be observed in Fig**.** 3.6 , each $[Cu(mnt)_2]^{2-}$ is segregated by Mn(III) saltmen dimer and there are no short contacts between $[Cu(mnt)_2]^{2-}$ and between $[Cu(mnt)_2]^{2-}$ and $[Mn_2(saltmen)_2(CH_3CN)_2]^{2+}$.

The reaction that leads to $[Mn_2(saltmen)_2(CH_3CN)_2][Cu(mmt)].CH_3CN$ is reproductible and the compound has been obtained with reasonable yields.

## 3.3 The dianionic bis-dithiolene complexes $[Cu(mnt)_2]^{2-}$ and $[Cu(tfadt)_2]^{2-}$ as metallo-ligands towards mixed valence Mn(II)/Mn(III) complexes.

The reactivity in solution of Mn(III) salen type complexes in the presence of square planar metal bis-dithiolenes towards ligand exchange reaction has prompted us to choose another Mn-derivative as a possible cationic building block for the synthesis of polymetallic complexes together with $[Cu(mnt)_2]^{2-}$ and $[Cu(tfadt)_2]^{2-}$ complexes.

The complex $[Mn_4(hmp)_6][ ClO_4]_4$ has been thought to be a good candidate, because of its peculiar magnetic and structural features.

### 3.3.1 The $[Mn_4(hmp)_6]^{4+}$ cationic unity

The ligand 2-hydroxymethylpyridine (Hhmp) has been extensively used in coordination chemistry to build up transition metal complexes with high nuclearity. Manganese forms a series of polymetallic complexes with different nuclearities such as $Mn_7$- [Bolcar, 1997], $Mn_{10}$[Harden 2003], $Mn_{12}$ [Boskovic, 2002], $Mn_{18}$ [Brechin,2002; Sanud, 2003; Gupta, 2004], $Mn_{21}$ [Sanudo, 2004].

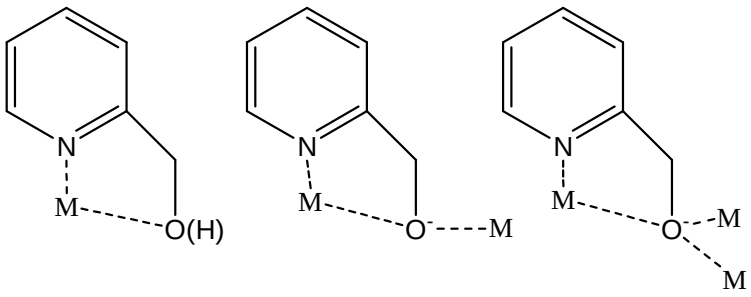


**Fig 3.16** Different coordination modes for ligand $hmp^-$.

The family of tetrameric $Mn_4$ compounds characterized by the cationic unity $[Mn_4(hmp)_6]^{4+}$- a mixed valence complex with 2Mn(II) and 2 Mn(III) [Hendrickson, 2001; Yoo, 2001; Yang, 2003]- is known for the properties of SMM. $[Mn_4(hmp)_6]^{4+}$ bears two spin S=2 and two spin S=5/2 showing a ferromagnetic interaction leading to a spin ground state S=9.

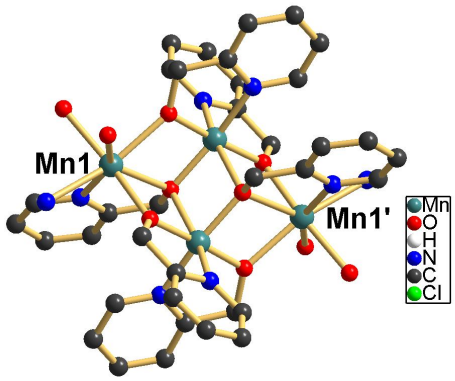


**Fig 3.16**: $[Mn_4(hmp)_6(H_2O)_4]^{4+}$: an example of $Mn_4$-hmp complex.
On Mn and Mn' labile $H_2O$ molecules are shown.

$[Mn_4(hmp)_6]^{4+}$ presents two possible coordination sites on the Mn(II) atoms when non-coordinant counter anions are employed during its synthesis. In this case, water or solvent labile coordinated molecules are exchangeable with many different anions. This coordination ability gives to these complexes a high flexibility that can be used to build new architectures.

$[Mn_4(hmp)_6]^{4+}$ has been used as cationic building block for the synthesis of higher nuclearity complexes [Lecren, 2005] by connecting discrete $Mn_4$ unities with polyfunctional ligands, with inorganic coordinating anions as for example in $\{[Mn_4(hmp)_6(Cl)_2](ClO4)_2\}$ [Yoo, 2005], or with other metal complexes bearing coordinative functional ligands (Fig 3.17).

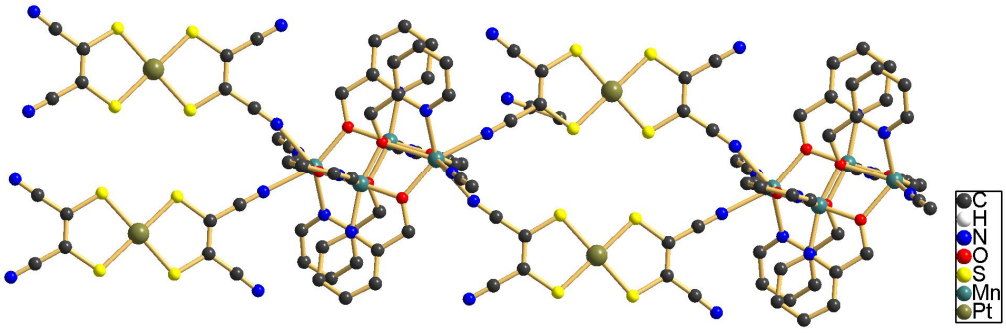


**Fig. 3.17** $[\{Mn_4(hmp)_6(CH_3CN)_2\}\{Pt(mnt)_2\}_4][Pt(mnt)_2]_2$ (the two $[Pt(mnt)_2]^n$) have been omitted for clarity.

Examples where metal bis-dithiolene complexes act as metallo-ligands towards these $Mn_4$ complexes are scarce. Recently, complexes[{$Mn_4(hmp)_6(CH_3CN)_2$}{$Pt(mnt)_2$}$_2$][$Pt(mnt)_2$]$_2$· 2 $CH_3CN$ (Fig.3.16) and [{$Mn_4(hmp)_6(CH_3CN)_2$}{$Pt(mnt)_2$}$_4$][$Pt(mnt)_2$]·2$CH_3CN$ were obtained by reacting $[Pt(mnt)_2]^{\bullet-}$ with a solution containing the cationic $[Mn_4(hmp)_6(S)_6]^{4+}$ (S= solvent) unity. The structure of [{$Mn_4(hmp)_6(CH_3CN)_2$}{$Pt(mnt)_2$}$_2$][$Pt(mnt)_2$]$_2$·2$CH_3CN$ is depicted in Fig. X. It can be observed that –CN groups of $[Pt(mnt)_2]^n$ coordinate the Mn(II) centers of $[Mn_4(hmp)_6(S)_6]^{4+}$ affording a polymetallic chain where two $[Pt(mnt)_2]^n$ coordinate two unities $[Mn_4(hmp)_6(S)_6]^{4+}$. To date, the two complexes here mentioned are the only examples where $[Mn_4(hmp)_6(S)_6]^{4+}$ cationic unities are connected by metal a bis-dithiolene complexes.

In this framework, we investigated the behaviour of $[Cu(mnt)]^{2-}$, $[Ni(mnt)]^{-}$ and $[Cu(tfadt)_2]^{2-}$ with the in situ solution formation of $[Mn_4(hmp)_6]^{4+}$, in order to evaluate the possibility of obtaining polymetallic complexes via –CN···Mn(II) interaction.

### 3.3.2 Synthesis of $[Mn_7(hmp)_{12}][Cu(mnt)_2]_2$ and $[Mn_7(hmp)_{12}][Cu(tfadt)_2]$

Usually, the mixed valence Mn(II)Mn(III) unity $[Mn_4(hmp)_6]^{4+}$ is generated in situ starting from $CH_3CN$ solutions of a Mn(II) precursor such as $Mn(ClO_4)$*$6H_2O$, the ligand Hhmp and a base, often tetraalkyl-ammonium hydroxide [Clerac, 2005] Thereafter, polyfunctional ligands or metallo-ligands that are able to connect the single $[Mn_4(hmp)_6]^{4+}$ are added to the solution containing the Mn(II)Mn(III).

This synthetic strategy has been considered in this work for the investigation of $[Cu(mnt)]^{2-}$, $[Ni(mnt)]^{-}$ and $[Cu(tfadt)_2]^{2-}$ toward the coordination of $[Mn_4(hmp)_6]^{4+}$.

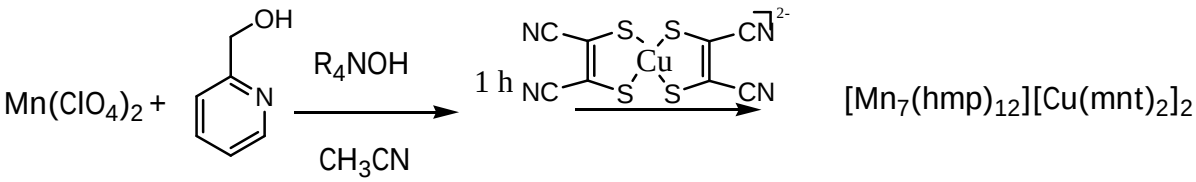


**Scheme 3.8** Reaction path leading to $[Mn_7(hmp)_{12}][Cu(mnt)_2]_2$·(8+x)$CH_3CN$.

However, upon addition $[Et_4N]_2[Cu(mnt)]$ to a solution containing $Mn(ClO_4)_2$, Hhmp and a $R_4NOH$ (any tetraalkylammonium-hydroxide base) (Scheme 3.8), compound $[Mn_7(hmp)_{12}][Cu(mnt)_2]_2$, $(8+x)CH_3CN$ was obtained with 60% yields upon slow diffusion of diethylether. Molecular formula of this compound as been established by X-ray single crystal diffraction.

***Crystal structure***

$[Mn_7(hmp)_{12}][Cu(mnt)_2]_2 \cdot (8+x)CH_3CN$ crystallizes in the triclinic system, space group P-1. $[Mn_7(hmp)_{12}]$, $[Cu(mnt)_2]$ and 8 $CH_3CN$ molecules have clearly been identified and refined, the residual electronic density in two 95$Å^3$ voids has been squeezed using PLATON program.

In Fig 3.18 it is shown the asymmetric unity of $[Mn_7(hmp)_{12}][Cu(mnt)_2]_2 \cdot (8+x)CH_3CN$ consisting of one molecule of $[Cu(mnt)_2]^{2-}$ with half a $[Mn_7(hmp)_{12}]$ heptamer, with the central Mn atom occupying an inversion center.

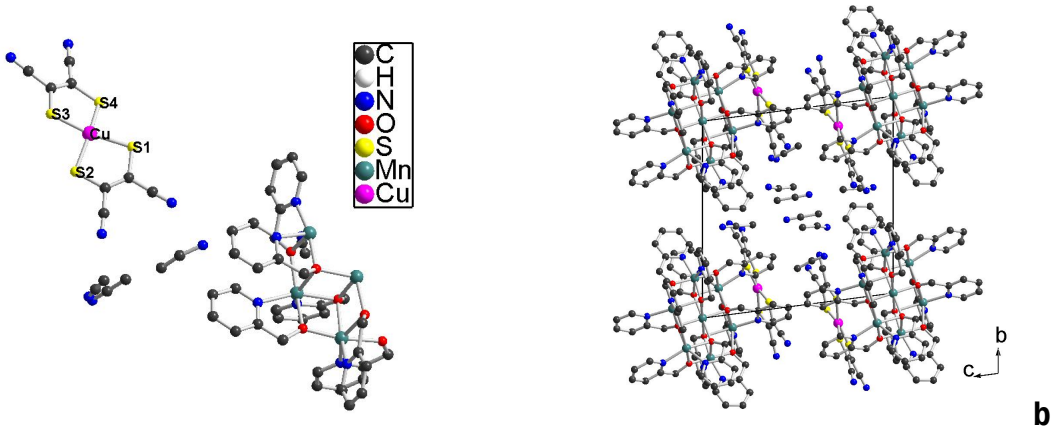


**a** **b**

**Fig 3.18 a)** Asymmetric unity for $[Mn_7(hmp)_{12}][Cu(mnt)_2]_2(8+x)CH_3CN$ and **b)** view of the crystal along a axis.

$[Cu(mnt)_2]^{2-}$ in $[Mn_7(hmp)_{12}][Cu(mnt)_2]_2 \cdot (8+x)CH_3CN$ shows a non planar Cu-$S_4$ core, with a dihedral angle between the two $CuC_2S_2$ rings of 25.9°. This distorded tetrahedral geometry is typical of $Cu(mnt)_2$ dianions. Cu-S, C=C and C-S distances are also in good

agreement with a dianionic complex [Plumlee, 1975] (see Table 3.8). In Table 3.8 are reported also the values for a monoanionic $Cu(mnt)_2$ in [BrPyH][$Cu(mnt)_2$] [Ren, 2006 ]. Considering that the two [$Cu(mnt)_2$] are dianions, it follows that [$Mn_7(hmp)_{12}$] has a charge of 4+ and it is supposed also to be a mixed valence Mn(II)/Mn(III) complex.

| | **[$Mn_7(hmp)_{12}$][$Cu(mnt)_2$]$_2$** | **[$Bu_4N$]$_2$[$Cu(mnt)_2$]** | **[BrPyH][$Cu(mnt)_2$]** |
|---|---|---|---|
| Cu-S | 2.277(3) ; 2.262(2) 2.278(3) ; 2.264(2) | 2.264(4); 2.286(4) | 2.186 (13) ; 2.178 (21); 2.175 (14); 2.179 (14) |
| C-S | 1.720(4); 1.741(3) 1.744(4); 1.731 (1) | 1.729(2); 1.726(2) | 1.741(3); 1.730(3) 1.732(3); 1.726(3) |
| C=C | 1.364(5); 1.365(6) | 1.358 (32) | 1.344(20); 1.354(20) |

**Table 3.8**: Relevant bond distances for [$Mn_7(hmp)_{12}$][$Cu(mnt)_2$]$_2$·(8+x)$CH_3CN$; [$Bu_4N$]$_2$[$Cu(mnt)_2$] and [BrPyH][$Cu(mnt)_2$].

$[Mn_7(hmp)_{12}]^{4+}$shows a pseudo C3 symmetry (Fig. 3.18) were six manganese atoms are disposed to give an hexagon with a seventh manganese atom located in the centre. Four crystallographically independent manganese atoms are present. The central Mn2 atom shows an octahedral coordination geometry which arises from six oxygen atoms of six different $hmp^-$ molecules. This oxygen atom connects the central Mn2 atom to the peripheral Mn atoms via a monoatomic $\mu_3$ bridging coordination.

Each peripheral manganese is then coordinated by a $\mu_3$-O bridge and two $\mu_2$-O which bridges two adjacent manganese ions. Coordination is completed by two nitrogen atoms of two different $hmp^-$ ligands, the first connects the external atom with its neighbour and the second one binds the peripheral metal to central Mn2.

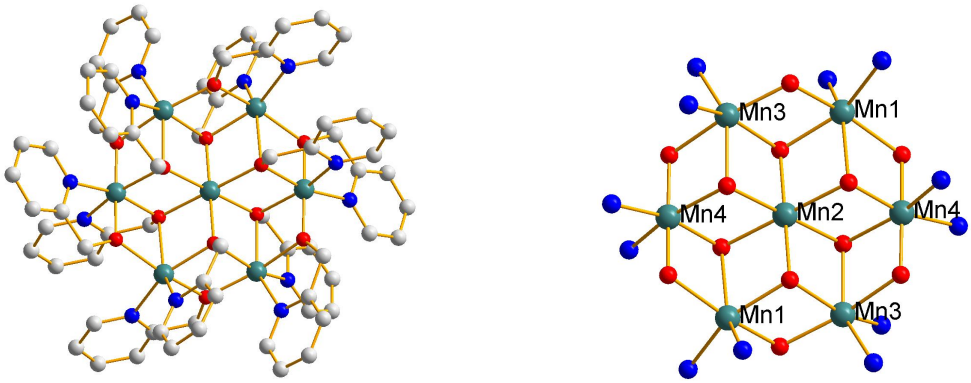


Fig. 3.19 View of the cationic complex $[Mn_7(hmp)_{12}]^{4+}$

All the Mn atoms are six-coordinate and posses quasi–octahedral coordination geometry. Hmp$^-$ acts as an N, O chelating and O bridging ligand. The solvent is present as co-crystallization molecule and does not participate to the coordination of manganese atoms.

On the basis of bond valence sum calculations and by the identification of the elongated Jahn Teller axis, this $Mn_7$ has been determined to be mixed valent Mn(II)/Mn(III).

Mn4 (Fig. 3.19) and its corresponding crystallographical equivalent atom generated by the inversion symmetry operation have been identified as Mn(III). The elongation axis is along atoms N5-Mn4-O1, involving a $\mu_3$-O and a nitrogen atom of a different hmp$^-$ ligand (selected atom distances in Table 3.9). The five remaining manganese atoms are Mn(II), to give finally a $Mn(III)_2/Mn(II)_5$ mixed valence complex.

| | **Mn1** | **Mn2** | **Mn3** | **Mn4** |
|---|---|---|---|---|
| **Mn-N** | 2.220(3); 2.223(3) | - | 2.193(3); 2.251(3) | 2.049(3); **2.217(3)** |
| **Mn-O** | 2.160(3); 2.390(3) | 2.119(3); 2.227(3) | 2.184(3); 2.203(3) | 1.889(3); 1.886(3) |
| | 2.081(3); 2.163(3) | 2.202(3) | 2.061(3); 2.257(3) | **2.204(3)**; 2.005(3) |

**Table 3.9**: Selected bond distances in $[Mn_7(hmp)_{12}][Cu(mnt)_2]_2 \cdot (8+x)CH_3CN$.

In bold: the Jahn Teller distances.

The cubane-like structure found here for $[Mn_7(hmp)_{12}]^{4+}$ has already be encountered in the literature with compound $[Mn_7(OH)_3(hmp)_{12}[Cl)_3](Cl][ClO_4]$ [Harden, 2003].
However, $[Mn_7(hmp)_{12}][Cu(mnt)_2]_2$ and $[Mn_7(OH)_3(hmp)_9(Cl)_3](Cl)(ClO_4)$ have different coordination features. In this last complex, together with nine $hmp^-$ ligands, three $OH^-$ anions and three $Cl^-$ groups coordinate the metal centers. In $[Mn_7(OH)_3(hmp)_9(Cl)_3](Cl)(ClO_4)$, $OH^-$ connects in $\mu_3$-O bridging way two peripheral Mn atoms with the central Mn while in our $Mn_7$ complex the $\mu_3$-O is provided by three $hmp^-$ instead of $OH^-$ ions. $Hmp^-$ connects adjacent peripheral Mn atoms by a $\mu_2$-O. For three Mn atoms the coordination is completed by two nitrogen from two bridging hmp molecules. For the other three Mn coordination is completed by $Cl^-$ anions occupying apical position.
$[Mn_7(OH)_3(hmp)_{12}(Cl)_3](Cl)(ClO_4)$ has been identified as mixed valence $Mn(II)_4\,Mn(III)_3$ complex.

It is interesting to compare the synthethic conditions employed to obtain the heptameric $[Mn_7(hmp)_{12}][Cu(mnt)_2]_2$, **$Mn_7$1,** obtained in this work with the one synthesized by Harden, [Harden, 2003], $[Mn_7(OH)_3(hmp)_{12}(Cl)_3](Cl)(ClO_4)$, **$Mn_7$2.**
In Table 3.10 the synthethic conditions for **$Mn_7$1** and **$Mn_7$2** are summarized together with the synthesis of $[Mn_4(hmp)_6(CH_3CN)_4(H_2O)][ClO_4]_4$, **$Mn_4$,** reported by Clérac [Clérac, 2005].

| | **$Mn_7$1** | **$Mn_7$2** | **$Mn_4$** |
|---|---|---|---|
| **Mn source** | $MnCl_2$ and $[Bu_4N][MnO_4]$ | $Mn(ClO_4)2$ | $Mn(ClO_4)2$ |
| **Mn(II)/hmp (mol/mol)** | 3.3 | 2.5 | 2.5 |
| **Solvent** | $CH_3CN$ | $CH_3CN$ | $CH_3CN$ |
| **Co-solvent** | n-hexane | $Et_2O$ | Toluene |

**Table 3.10** Synthethic conditions for **$Mn_7$1**, **$Mn_7$2** and **$Mn_4$**

**$Mn_7$1** was obtained by a comproportionation reaction between $MnCl_2$ and $[Bu_4N][MnO_4]$ in the presence of Hhmp and a source of $ClO_4^-$ [Harden, 2003].

In **$Mn_7$2,** Mn(II) undergoes aereal oxidation yielding the mixed valence Mn(II)/Mn(III).

**$Mn_7$2** in this work was obtained under the same synthetic condition as for $Mn_4$ (Table 3.10), with the difference that $[Cu(mnt)]^{2-}$ was added and the resulting solution was recrystalized from $Et_2O$ (Table 3.10) [[Clerac, 2005].

In order to avoid the formation of the $Mn_4$ brick alone, diethyl ether was used instead of toluene and this has led to the described $[Mn_7(hmp)_{12}][Cu(mnt)_2]_2.(8+x)CH_3CN$.

However, other $Mn_7$ mixed valence complexes are known: $[Mn_7(OH)_3(hmp)_9(Cl)_3](Cl)_2$, $[Mn_7(OH)_3(hmp)_9\ (Br)_3](Br)_2$ and $[Mn_7\ (hmp)_9(OH)_3(NCS)_3]$ with the same $Mn_7$ core as for $[Mn_7(OH)_3(hmp)_{12}(Cl)_3](Cl)(ClO_4)$ have been isolated by Lecren [Lecren, 2006] as the minor product in solution containing the tetrameric $[Mn_4(hmp)_6]^{4+}$ unity. However, crystals of these $Mn_7$ species appeared after 2-3 days [lecren PhD thesis Université de Bordeaux april 2006) while salts comprising the $[Mn_4(hmp)_6]^{4+}$ unity have been isolated after one week from the liquor.

In our case, the mother solutions of $[Mn_7(hmp)_{12}][Cu(mnt)_2]_2{\cdot}(8+x)CH_3CN$ afforded only a white powder.

By carrying out the reaction in Scheme 3.6 without adding $[Cu(mnt)_2]^{2-}$, the salt $[Mn_7(hmp)_{12}](ClO_4)_4$ was obtained upon diffusion of diethyl ether, identified by means of single crystal X-ray diffraction. The structure is not reported because the twinned nature of crystals $[Mn_7(hmp)_{12}](ClO_4)_4$ (space group R-3) and the high degree of disorder of the $ClO_4$ did not allow a reasonable refinement.

Anyway, we can state that $Mn_7$ species form also without the presence of $[Cu(mnt)_2]^{-2}$ as counter-anion.

To overcome the formation of $Mn_7$ species, we decided to isolate the $[Mn_4(hmp)_6]^{4+}$ synthesizing the related compound $[Mn_4(hmp)_6(H2O)_4][ClO_4]_4{\cdot}2H_2O$ following the reported procedure [Clérac, *J. Am. Chem. Soc.* 2005, 127, 17355].

This $Mn_4$ complex has been obtained by using the same synthesis conditions of the $Mn_7$ species, except that toluene was added as co solvent to obtain fragile prismatic pink

crystals of $[Mn_4(hmp)_6(H2O)_4]$ $[ClO_4]_4 \cdot 2H_2O$. The rapid solvent loss does not allow us to collect the unit cell parameters and this compounds was characterized by means of FT-IR and elemental analysis, with reference to the reported work by Clérac [Clérac, *J. Am. Chem. Soc.* 2005, 127, 17355].

Reaction between $[Mn_4(hmp)_6$ $(H2O)_4][ClO_4]_4 \cdot 2H_2O$ with two equivalents of $[Cu(mnt)_2]^{2-}$ in $CH_3CN$ or mixed $CH_3CN/CH_2Cl_2$ solution afforded crystals of $[Mn_7(hmp)_{12}][Cu(mnt)_2]_2$ (Fig 3.19) upon diffusion of diethylether.

***Crystal structure***

$[Mn_7(hmp)_{12}][Cu(mnt)_2]_2$ is another phase of the same compound obtained by *in situ* addition of the copper dithiolene complex. $CH_3CN$ molecules are present in the crystal lattice and they have been all squeezed for a corresponding volume of 754 $Å^3$.

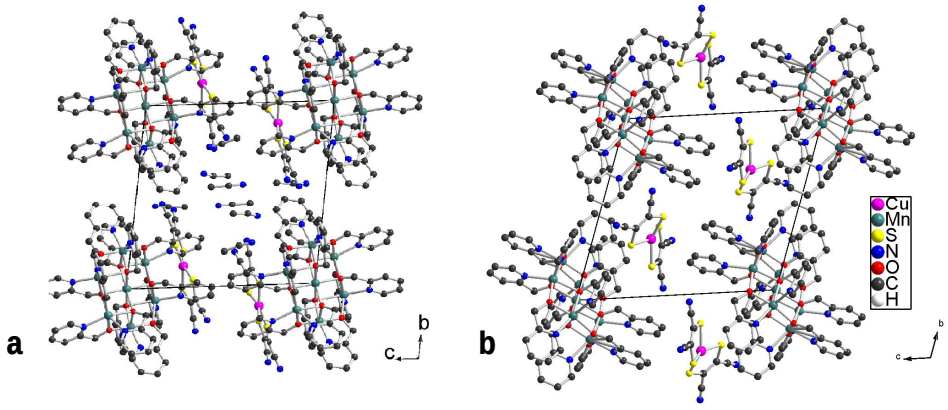


**Fig 3.19**: View along a axis of **a)** $[Mn_7(hmp)_{12}][Cu(mnt)_2]_2 \cdot (8+x)CH_3CN$ and its polymorph **b**) $[Mn_7(hmp)_{12}][Cu(mnt)_2]_2 \cdot xCH_3CN$.

Once angain, $[Cu(mnt)_2]^{2-}$ deviates from planarity with a an angle between the two $CuS_2C_2$ rings of 25.77°, a value smaller than the one found for the first polymorph.

In tab X the main interatomic distances are reported and compared with those of dianioni $Cu(mnt)_2$ and monoaninioc $Cu(mnt)_2$ in $[BrPyH][Cu(mnt)_2]$ .

| | **$[Mn_7(hmp)_{12}][Cu(mnt)_2]_2$, $xCH_3CN$** | **$[Mn_7(hmp)_{12}][Cu(mnt)_2]_2$ $(8+x)CH_3CN$** | **$[Bu_4N]_2[Cu(mnt)_2]$** | **$[BrPyH][Cu(mnt)_2]$** |
|---|---|---|---|---|
| **Cu-** | 2.267(1) ; 2.269(1) | 2.277(3); 2.262(2) | 2.264(4); 2.286(4) | 2.186(1) ; 2.178(2) |
| **S** | 2.262(1); 2.260(1) | 2.278(3); 2.264(2) | | 2.175(1); 2.179(1) |
| **C-S** | 1.732(3); 1.738(4) | 1.720(4); 1.741(3) | 1.729(2); 1.726(2) | 1.741(3); 1.730(3) |
| | 1.745(4); 1.738(4) | 1.744(4); 1.731(1) | | 1.732(3); 1.726(3) |
| **C=C** | 1.368(6); 1.345(6) | 1.364(5); 1.365(6) | 1.358(3) | 1.344(2); 1.354(2) |

**Tab 3.11** Selected bond distances for $[Mn_7(hmp)_{12}][Cu(mnt)_2]_2 \cdot xCH_3CN$.

Concerning $[Mn_7(hmp)_{12}]^{4+}$ analogous consideration as for the solvate $[Mn_7(hmp)_{12}][Cu(mnt)_2]_2$, $(8+x)CH_3CN$ can be done, identifying it as a $Mn(II)_5$ $Mn(III)_2$ mixed valence. A Jahn Teller elongation axis is present in the octahedrally coordinated Mn3 atom and it passes through N3-Mn3-O5 atoms (see Table 3.12).

| | **Mn1** | **Mn2** | **Mn3** | **Mn4** |
|---|---|---|---|---|
| *Mn-N* | 2.227(1); 2.232(1) | | 2.043(1); **2.245(1)** | 2.215(1); 2.237(2) |
| *Mn-O* | 2.151(2); 2.085 (1) | 2.195(3) , | 1.885(2); 1.879(1) | 2.086(1); 2.190(3) |
| | 2.166(1); 2.333(1) | 2.174(1) | **2.190(1)**; 2.003(2) | 2.214(1); 2.245(1) |
| | | 2.166(1) | | |

**Table 3.12**: Selected bond distances for $[Mn_7(hmp)_{12}][Cu(mnt)_2]_2$, $xCH_3CN$. Bold: Jahn Teller distances.

From these results, it is clear that the formation of $Mn_7$ mixed valence complex is strongly favoured under the conditions here employed and it derives also from the evolution in acetonitrile solutions of $[Mn_4(hmp)(H_2O)_4](ClO_4)_4$. in the presence of $[Cu(mnt)_2]^{2-}$.
When toluene is added to $[Cu(mnt)_2]^{2-}$ solutions containing the $Mn_4$ precursor synthesized prior to use or generated *in situ*, $[Mn_4(hmp)(H_2O)_4](ClO_4)_4$ has been obtained, identified by means of micro analysis and FT-IR spectroscopy.

Furthermore, other two compounds containing the $[Mn_7(hmp)_{12}]^{4+}$ units have been isolated, $[Mn_7(hmp)_{12}][Cu(tfadt)_2]_2 \cdot 3CH_3CN$ and $[Mn_7(hmp)_{12}][Ni(mnt)_2]_2$. The structures are not reported here.

***Magnetic characterization of $[Mn_7(hmp)_{12}][Cu(mnt)_2]_2$.***

As we have previously said, the $[Mn_7(hmp)_{12}]^{4+}$ is a new compound in the family of high nuclearity mixed valence Mn(II)Mn(III) complexes. We have discussed its crystals structure and through crystal field considerations about Jahn Teller elongation axis, we have found that there are two Mn(III) and five Mn(II).

$[Mn_7(hmp)_{12}][Cu(mnt)_2]_2$ bears two spins S=1/2 from the two $[Cu(mnt)_2]^{2-}$ molecules while from $Mn_7$ five spin S=5/2 and two spin S=2 are present.

The magnetic molar susceptibility χTof $[Mn_7(hmp)_{12}][Cu(mnt)_2]_2 8CH_3CN$ and for the polymorph $[Mn_7(hmp)_{12}][Cu(mnt)_2]_2$ were measured as a function of the temperature T in the range 1.8 K – 298 K with a field of 5000 Oe. In Fig.3.20, χT is reported as a function of the temperature T. The $CH_3CN$ molecules were not taken into account because of desolvation processes occurring on the crystals.

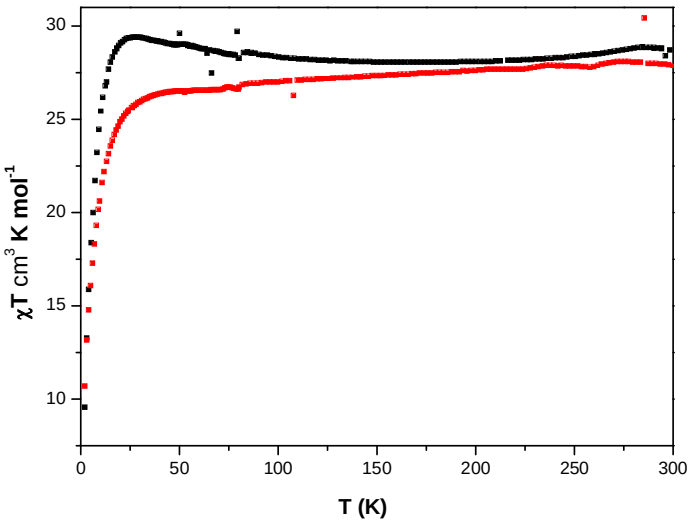


**Fig 3.20** χT vs. T for $[Mn_7(hmp)_{12}][Cu(mnt)_2]_2 8CH_3CN$ (black) and for the polymorph $[Mn_7(hmp)_{12}][Cu(mnt)_2]_2$ (red)

At 294 K the experimental χT value is 28.8 K $cm^3$ $mol^{-1}$ and 27.8 K $cm^3$ $mol^{-1}$ for $[Mn_7(hmp)_{12}][Cu(mnt)_2]_2 8CH_3CN$ and $[Mn_7(hmp)_{12}][Cu(mnt)_2]_2$ respectevely, consistent with the presence of five S=5/2, two S=2 and two S=1/2 non interacting spins. The calculated χT value considering a g factor of 2 is 28.7 K $cm^3$ $mol^{-1}$. The value found $[Mn_7(hmp)_{12}][Cu(mnt)_2]_2 \cdot xCH_3CN$ is slightly lower probably because of uncontrollable desolvation processes.

However, the values found for χT are a further confirmation of the presence of five Mn(II) and two Mn(III) in the $Mn_7$ unity.

In $[Mn_7(hmp)_{12}][Cu(mnt)_2]_2.(8+x)CH_3CN$, χT slightly decrease to a 28.0 K $cm^3$ $mol^{-1}$ within the range 298 K -65 K and on cooling χT increases and reach the the maximum value of 29.4 K $cm^3$ $mol^{-1}$ at 27 K, indicative of a a larger spin ground state. χT decreases after 27 K because of the zero field splitting or intermolecular antiferromagneti interactions or both.

In $[Mn_7(hmp)_{12}][Cu(mnt)_2]_2 \cdot xCH_3CN$, the trend is different and χT decreases smoothly until 25K then below this temperature χT abruptly decreases because of the zero field splitting.

For comparison purposes, it is reasonable to consider the reported $[Mn_7(OH)_3(hmp)_{12}(Cl)_3](Cl)(ClO_4)$ [Harden, 2003]. This complex has been magnetically characterized and shows a maximum for χT at nearly 10 K of 37.9 K $cm^3$ $mol^{-1}$, a value higher than the one measured for In $[Mn_7(hmp)_{12}][Cu(mnt)_2]_2.(8+x)CH_3CN$.

$[Mn_7(OH)_3(hmp)_{12}(Cl)_3](Cl)(ClO_4)$ has found to have a large spin ground state S= 10-11 but it does not display a SMM magnet behaviour.

$[Mn_7(OH)_3(hmp)_{12}(Cl)_3](Cl)(MnCl4)$ [Bolcar, 1997] have a similar χT vs. T as for $[Mn_7(OH)_3(hmp)_{12}(Cl)_3](Cl)(ClO_4)$ but the maximum value of 27.7 K $cm^3$ $mol^{-1}$ is found at 30 K. These values are corrected for the paramagnetic contribution of S=5/2 $MnCl4^-$.

In $[Mn_7(hmp)_{12}][Cu(mnt)_2]_2 \cdot xCH_3CN$ no evidence of high spin ground state is present, as expected considering $[Mn_7(hmp)_{12}][Cu(mnt)_2]_2.(8+x)CH_3CN$.

Investigations of the magnetic behaviour of these compounds are in progress to determine the spin of the ground state and also to understand the difference in the magnetic behaviour within the two phases.

## 3.4 Conclusions

Three compounds of general formula $[Mn(TPP)(S)]_2[Ni_2(tto)(dmid)_2]$ were obtained because of the tendendcy of $[Ni(dmid)_2]^{\cdot-}$ toward dimerization in solution. Complex $[Ni_2(tto)(dmid)_2]^{2-}$is diamagnetic and the magnetic behaviour of $[Mn(TPP)(S)]_2[Ni_2(tto)(dmid)_2]$ is consistent with two independent spins S=2 for the two Mn(III) atom.

In $[Mn(TPP)(S)]_2[Ni_2(tto)(dmid)_2]$ Mn(III) interact via S···Mn(III) contacts with $[Ni_2(tto)(dmid)_2]^{2-}$ demonstrating the affinity of Mn(III) for sulphur with respect to the C=O oxygen.. However, Mn····M(dithiolene)····Mn metallic chains with $[Ni(dmid)_2]^{\cdot-}$are not known to date and in general examples where $[Ni(dmid)_2]^{\cdot-}$ participates with C=O coordination in the formation of the polymetallic complexes has never been reported, probably for problem related to its dimerization in solution.

We have observed that $[Cu(mnt)_2]^{2-}$ together with some Mn(III) salen complexes has a strong tendency to undergo exchange ligand reaction. For this reason, to date we are not able to isolate the desired polymetallic complexes through –CN···Mn coordination.

In the case of Mn(III) saltmen only the co-crystallization of $[Cu(mnt)_2]^{2-}$ with the dimeric $[Mn_2(saltmen)_2(CH_3CN)_2]^{2+}$ occurs and no coordination of –CN to Mn(III) is observed.

As we have seen in paragraph 3.2, a dithiolene –CN group can coordinate a Mn(III) of a $[Mn(TPP)]^+$ and the corresponding bimetallic chains are known and characterized. However, the limited number of such complexe is justified by the low coordinating ability of –CN groups. Most of the time, the solvent is in competition with –CN for the coordination of the metal centres. The interplay between the coordination ability of -CN metallo-ligands and the solubility of the different species in solution are determinant for the formation in the solid state of the desired polymetallic complexes.

Even if most of the time the reactions that lead to high nuclearity complexes are simple methathesis between two complexes salt, the synthesis of such complexes is not trivial and requires a systematic investigation.

The approach to the synthesis of polymetallic complexes starting from bis-dithiolenes and mixed valence Mn(II)Mn(III) $Mn_4$ has found to be very difficult to control because of the equilibrium of different nuclearities for the Mn(II)Mn(III) species. This has led to the heptameric compound $[Mn_7(hmp)_{12}]^{4+}$, which does not offer possible coordination sites on the seven Mn atoms because they are all coordinated by hmp ligand instead of labile molecules such as the solvent.

The presence of Cu(II) bis dithiolene complexes allows to isolate $[Mn_7(hmp)_{12}]^{4+}$ in reasonable yields from acetonitrile upon diethylether layering.

However, it has to be remarked that in this work the $Mn_7$ is different from the already published heptameric mixed valence Mn(II) Mn(III) species and to date no reference were found for all the $[Mn_7(hmp)_{12}]^{4+}$ base compounds here obtained.

$[Mn_7(hmp)_{12}][Cu(mnt)_2]_2.(8+x)CH_3CN$ shows a large ground spin state and investigation it are in progress by the group of Dr. Clérac, Université de Bordeaux.

**Bibliography**


Bai, J.-F.; Zuo, J.-L.; Shen, Z.; You, X.-Z.; Fun, H.-K.; Chinnakali, K. *Inorg. Chem.* **2000**, 39, 1322

Basolo, F.; Jones, R. D.; Summerville, D. A. *Acta Chem. Scand.* **1978**, A32, 771

Batsanov, A. S.; Bryce, M. R.; Dhindsa, A. S.; Howard, J. A. K.; Underhill, A. E. *Polyhedron* **2001**, 20, 537

Bolcar, M.A.; Aubin, S.M.J.; Folting, K.; Hendrickson, D.N., Christou, G. *Chem. Comm.* **1997,** 1485

Brechin, E. K.; Boskovic, C.; Wernsdorfer, W.; Yoo, J.; Yamaguchi, A.; Sañudo, E. C.; Concolino, T.; Rheingold, A.; L. Ishimoto, H.; Hendrickson, D.N.; Christou, G. *J. Am. Chem. Soc.* **2002**, 124, 9710

Brechin, E. K.; Soler, M. Davidson, J. Hendrickson, D. N. Parsons, S. Christou, G. *Chem. Commun.* **2002**, 2252.

Clérac, R. *J. Am. Chem. Soc.* **2005**, 127, 17355

Dawe, L. N.; Miglioi, J.; Turnbow, L.; Taliaferro, M. L.; Shum, W. W.; Bagnato, J. D.; Zakharov, L. N.; Rheingold, A. L.; Arif, A. M.; Fourmigué, M.; Miller, J. S. *Inorg. Chem.* **2005**, 44, 7530

Day, P. *Notes Rec. R. Soc. London* **2002**, 56, 95

Elliott, C. M.; Akabori, K. *J. Am. Chem. Soc.* **1982**, 104, 2671

Fourmigué, M.; Bertran, *J. N. Chem. Commun.* **2000**, 2111

Fourmigué, M.; Mézière, C.; Dolou, S. *Cryst Growth Design* **2003**, 3, 805

Harden, N.C., Bolcar, M.A.; Wernsdorfer, W.; Abboud, K.A., Streib, W.E.; Christou, G. *Inorg. Chem.* **2003**, 42, 7067

Hatfield, W. E.; Elliott, C. M.; Ensling, J.; Akaborit, K. *Inorg. Chem.* **1987**, 26, 1930

Jeannin, O. *PhD work Université d'Angers* **2005**

Jones, R. D.; Summerville, D. A.; Basolo, F. *J. Am. Chem. Soc.* **1978**, 100, 4416

Miller, J. S. *Adv. Mater.* **2002**, 14, 1105

Mu, L.; Huang, J.; Zhou, Y.; Shen, P. *Polyhedron* **1997**, 16, 2885

Palmer, G.; Babcock, G. T.; Vickery, L. E. *Proc. Natl. Acad. Sci. U.S.A.* **1976**, 73, 2206

Piotraschke, J. J.; Pullen, A. E.; Abboud, K. A.; Reynlds, J. R. *Inorg. Chem.* **1995**, 34, 4011

Plumlee, K.W.; Hoffman B.M.; Ibers, J.A.; Soos, Z.G. *J. Chem. Phys* **1975,** 63, 1923

Pullen, A. E.; Olk, R.-M.; Zeltner, S.; Hoyer, E.; Abboud, K. A.; Reynolds, J. K. *Inorg. Chem.* **1997**, 36, 958

Pullen, A. E.; Zelter, S.; Olk, R.-M.; Hoyer, E.; Abboud, K. A.; Reynolds, J. R. *Inorg. Chem.* **1996**, 35, 4420

Pullen, A. E.; Zeltner, S.; Olk, R.-M.; Hoyer, E.; Abboud, K. A.; Reynolds, J. R. *Inorg. Chem.* **1997**, 36, 4163

Schauer, C. K.; Akabori, K.; Elliott, C. M.; Anderson, O. P. *J. Am. Chem. Soc.* **1984**, 106, 1127

Serr, B. R.; Headford, C. E. L.; Aaderson, O. P.; Elliott, C. M.; Spartalian, K.; Fainzilberg, V. E.; Hafield, W. E.; Rohrs, B. R.; Eaton, S. S.; Eaton, C. R. *Inorg. Chem.* **1992**, 31, 5450

Serr, B. R.; Headford, C. E. L.; Anderson, O. P.; Elliot, C. M.; Schauer, C. K.; Akabori, K.; Spartalian, K.; Hatfield, W. E.; Rohrs, B. R. *Inorg. Chem.* **1990**, 29, 2663

Shkolnik, G. M.; Geiger, W. E. Jr. *Inorg. Chem.* **1975**, 14, 313

Vicente, R.; Ribas, J.; Alvarez, S.; Segui, A.; Solans, X.; Verdaguer, M. *Inorg. Chem.* **1987**, 26, 4004

Xiao-Ming Ren; Guang-Xiang Liu; Heng Xu; Akutagawa, T.; Nakamura T. *Acta. Cryst. E. m.* **2006**, 3134, 62

Yang, X.; Doxsee, D. D.; Rauchfuss, T. B.; Wilson, S. R. *J. Chem. Soc. Chem. Commun.* **1994**, 821

# Chapter 4

## Novel coordinating metal-dithiolene complexes

It has been observed that the formation of polynuclear complexes by use of metal bis-dithiolenes such as $[Cu(mnt)_2]^{2-}$, $[Cu(tfadt)_2]^{2-}$, and $[Ni(dmid)_2]^{\cdot-}$ as metallo-ligands towards manganese metal complexes has been hamped by the reactivity in solution of $[Cu(mnt)_2]^{2-}$, $[Ni(dmid)_2]^{\cdot-}$ together with the particular solution chemistry associated to polynuclear Mn complexes and the relatively low tendency of –CN group to coordinate a metal centre.

These limitations have prompted to focus a part of this work on the synthesis of new 1,2 dithiolate ligands conveniently functionalized with coordinating groups.

### 4.1 New bifunctional 1,2 dithiolato ligands

The aim was to synthesize a series of ligands able to coordinate transition metals as well as lanthanide ions. Ln(III) ions have the advantage that they bear higher spin values with respect to 3d metals allowing the formation of high spin complexes even with relatively few paramagnetic centre within the complex. For these reasons they are appealing metals for the synthesis of molecular magnets.

Lanthanides ions are oxophylic and compounds where Ln(III) is coordinated by sulphur donor atoms are scarce, even if tris-dithiolene complexes of Ne(III) and Ce(III) has been synthesized by Fourmigué et al. [Fourmigué et al., 2005].

Examples of metal bis-dithiolenes bearing an oxygen donor which exhibits a certain tendency toward the coordination of Ln(III) are known and characterized. In the pentanuclear $\{[Ni(dto)_2]_3[Ln(H2O)_6]_3\}$ [J.Galy, 1984] the diamagnetic $[Ni(dto)_2]^{2-}$ dithiolene is connected to Ln(III) ions via C=O···Ln(III) interactions. Other examples of such a coordination concern $[Ni(dts)_2]^{2-}$.

To the best of our knowledge, compounds where Ln(III) ions are connected to paramagnetic metal-dithiolene complexes have not been synthesized yet.

The main idea was to synthesize a stable radical monoanionic dithiolene complex able to coordinate Ln(III) ions or certain paramagnetic 3d metals.

Crown ethers macrocycles were chosen as appealing candidates as substituent groups for 1,2 dithiolato ligands. Their selectivity toward Ln(III) is given by the presence of oxygen atoms on the macrocycle. It has been found that 18-crown-6 ether and its derivatives are able to complexate Ln(III) ions in particular Gd(III) [Sadafumi, 2003 ]. It is also well known the high affinity of 18-crown 6-ether toward $Na^+$ ions. The ionic radius of Gd(III) is 0.108 nm, comparable with the one of 0.095 nm for $Na^+$. Furthermore, by changing the size of the macrocycle it possible to modulate this selectivity and extend it towards 3d metals.

In literature it has been found only one dithiolene complex bearing a dithia 18-crown- 6 – ether macrocycle as functional group, the heteroleptic [Pt(dbbpy)(4O-C2S4)] (fig 1) [Yong, *2008*] where dbbpy is a bypyridil derivative while $4O\text{-}C_2S_4$ is 1,4,7,10-tetraoxo-13,16-dithiacyclooctadec-14-ene-14,15-dithia-2-one.

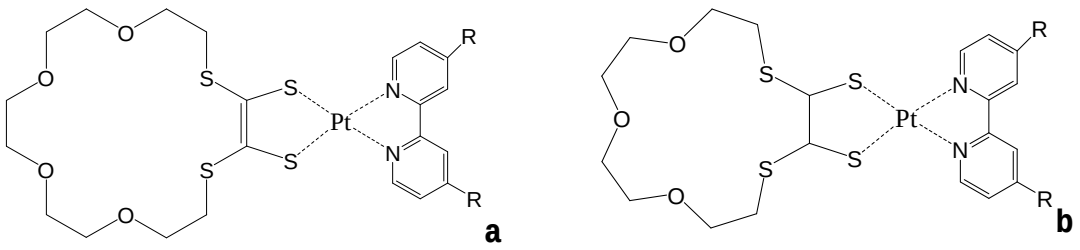


**Fig4. 1 a)** [Pt(dbbpy)($4O\text{-}C_2S_4$)] and **b)** [Pt(dbbpy)($3O\text{-}C_2S_4$)]

The three oxygen-analog, [Pt(dbbpy)($3O\text{-}C_2S_4$)] (fig. 1a)), was synthesized contextually to [Pt(dbbpy)($4O\text{-}C_2S_4$)] (Fig. 4.1b) and bears a dithia-15-crown-5 ether as substituent. The crystal structures have not been determined but the complexes have been characterized by NMR spectroscopy and elemental analysis.

These two compounds are diamagnetic and they were synthesized in order to obtain receptors toward $Na^+$ cations.

The complex [Cu(3O-$C_2S_4$)$_2$Na] and the complex [$Cp_2$Mo(3O-$C_2S_4$)] were synthesized by Green [J Chem SocDalton Trans 1990 3789]. No X-ray structural data are available for these complexes and they are diamagnetic.

In order to modulate the metal selectivity, we have decided to synthesize a series of crown ether functionalized-1,2-dithiolato ligands with different crown ether sizes (fig X , page X) to obtain the corresponding Ni bis-dithiolene complexes in the radical anion oxidation state with spin S=1/2.

The next step involved the use of these Ni bis-dithiolenes here obtained as radical metallo-ligands toward the coordination of 3d metals or Ln(III) ions.

## 4.2 Synthesis of crown-1 and crown-4-Ni(dithiolene)$_2$ complexes

The synthetic way that is generally followed to obtain different metal bis dithiolenes involves the derivatives of 1,3-dithiol-2-one as proligands. The corresponding dithiolate ligands are obtained by cycle nucleophilic opening reaction. Bases such as NaOMe, $Me_4NOH$, $Et_4NOH$, $Bu_4NOH$ etc. are usually employed to generate the 1,2-dithiolate ligand.

The crown-1, crown-2, crown-3 and crown-4 dithioketones reported as **2a, 2b, 2c, 2d** in Fig.4.2 have been obtained in this work as proligands for the corresponding 1,2 dithiolates.

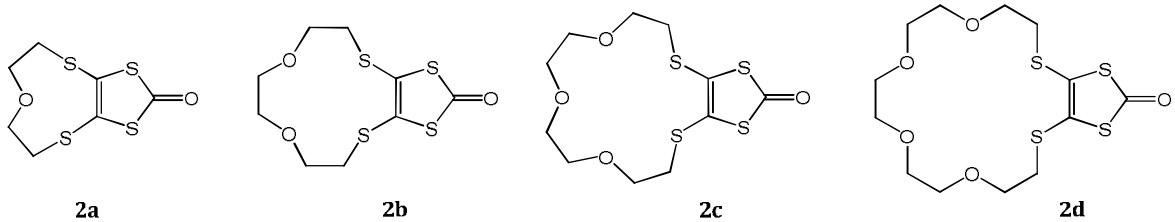


Fig. 4.2: Dithiolone derivatives for crown ether functionalized dithiolate ligands.

The compounds **2a, 2b, 2c** and **2d** are obtained from the corresponding thione derivatives (compound **1** Scheme 4.1). These are synthetized starting from $[Et_4N]_2[Zn(dmit)_2]$ (dmid**=**1,3-dithiole-2-thione-3,4-dithiolato) and the corresponding precursors for the macrocycle, i. e. ditosylate- or dihalogen derivatives of general formula $X\text{-}CH_2(CH_2OCH_2)_nCH_2\text{-}X$. The reaction conditions chosen are different depending on the size of the macrocycle considered. Anyway, a general scheme of the reaction path is given in Scheme 4.1.

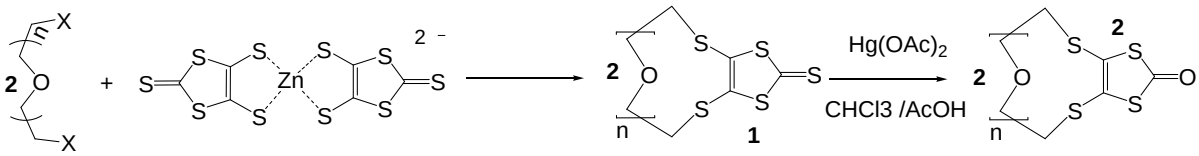


**Scheme 4.1**: General pathway to dithiolone derivatives

The idea of using macrocycles such as crown ethers for the functionalization of dithiolene moieties arises from the work firstly performed by Becher, who has reported synthethic methods to obtain annelated bis-crown ethers based on a tetrathioethene unit [Becher J J Org chem. 33 21 3035 1992]. Thereafter, Becher and his group, prompted by the concept of building up molecular systems as sensors (or as antennae), combined the redox active TTF moiety with crown ethers macrocycles. In the work done by Becher et al., the key starting precursor for obtaining this kind of materials is the thione derivative (compound **1**, Scheme 1), the same precursor molecule that has been used in this work to obtain macrocycle functionalized 1,2 dithiolene ligands.

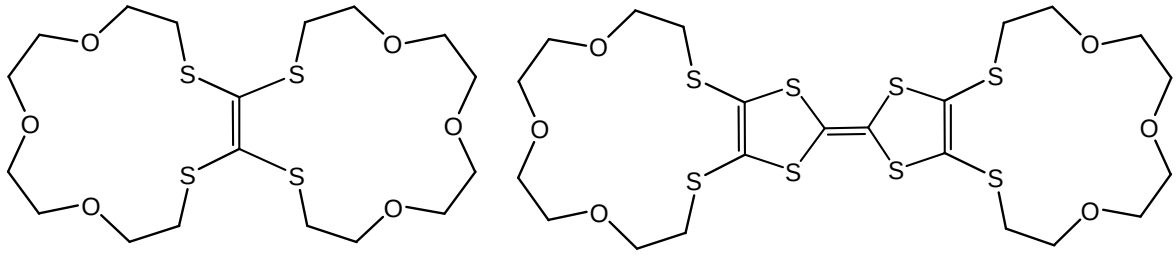

**Fig 4.3 a)** Annelated bis-crown-ethers **b)** TTF-annelated-bis crown ether

In Scheme 4.2 is reported the original synthetic way to obtain the thione [Becher J J Org Chem 57 1992 6405], different from the one used in this work (Scheme 4.1). 4,5-bis(benzoylthio)-1,3dithiol-2-thione (**3**), is deprotected by reaction with 2 eq. of a base such as NaOEt giving 1,3-dithiole-2thione-4,5-dithiolate **4**, which gives the thione-crown ether derivative **1** after adding one equivalent of the corresponding bis alkylating agent ($BrCH_2(CH_2O\ CH_2)_nCH_2Br$). It must be noticed also that oligomers such compound **6** forms as by-products of the reaction and this makes strictly necessary a long workup to purify the product.

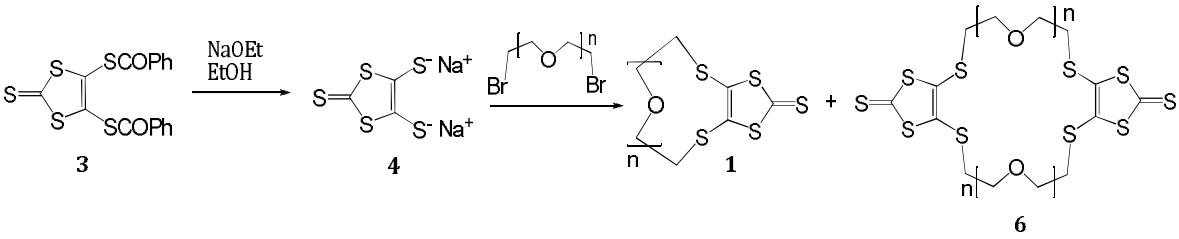


**Scheme 4.2**

The reaction conditions and the choice of the solvents for the reactions in Scheme 2 depend on the size of the macrocycle. Furthermore, the procedure requires a pump with syringes apparatus to carry out the reaction under high dilution conditions to maintains relative high yields (about 65%).

### 4.2.1 Synthesis of crown-1 Ni(dithiolene)$_2$ complexes.

#### 4.2.1.1. Synthesis of 1-oxo-4,7-dithiacyclopenta 5-ene 5,6-dithio-2-one (crown-1-dithioketone)

In this work we decided to carry out alkylation reaction of $[Zn(dmit)_2]^{2-}$ to synthetize **1a.** This was inspired by a work published by Echegoyen et al. [2000], where it is reported the synthesis of **1** with n=3,4,5 by refluxing acetone solutions of $[Zn(dmit)_2]^{2-}$ together with corresponding dibromo ethylene glycol derivatives, giving yields of about 65% . This synthetic procedure is easier than the one reported by Becher and no pump and syringes are required to carry out the reaction. Furthermore, the large availability of salt $[Et_4N]_2[Zn(dmit)_2]$ in the laboratory pushed us to choose this synthetic method to try the synthesis **2a**. We have tried $ClCH_2(CH_2O\ CH_2)CH_2Cl$ and $ICH_2(CH_2OCH_2)CH_2I$ instead of $Br\text{-}CH_2(CH_2O\ CH_2)\text{-}CH_2Br$ as alkylating agents. The di-iodo derivative has been thought to be more reactive than the reported di-bromo and it can be obtained by reaction of $ClCH_2(CH_2OCH_2)CH_2Cl$ with NaI in cyclohexanone at 110-120 °C for 3 h, followed by vacuum distillation of the crude. Unfortunately $ICH2(CH_2O\ CH_2)CH_2I$ is not a very stable compound and it has to be freshly synthesized before use. The stable dichloro derivative has the advantage of being less expensive than the dibromo one.

By using the di-iodo derivative, **1** (n=1) was obtained with yield of 26%. 2 eq. of $ICH_2(CH_2OCH_2)CH_2I$ were put together with $[Et_4N]_2[Zn(dmit)_2]$ in refluxing acetone for 15 hours, under high dilution conditions. Switching to the dichloro derivative, carrying out the reaction of 2 eq. of $ClCH_2(CH_2OCH_2)CH_2Cl$ with $[Et_4N]_2[Zn(dmit)_2]$ in refluxing acetone in high dilution conditions did not give **1** (n=1), even maintaining the heating for 11 days. The use of cyclohexanone (b.p. 160 °C) as solvent was considered, inspired by its use for the synthesis of the di-iodo derivative. A first attempt was made by heating a mixture of $ClCH_2(CH_2OCH_2)CH_2Cl$ and $[Et_4N]_2[Zn(dmit)_2]$ at 100-110°C for 7 days, but the desired product seemed not to form. In refluxing cyclohexanone, after 15 hours, the desired product was obtained with yield = 21%. In this case , the yield is slightly lower than the one found for $ICH_2(CH_2O\ CH_2)CH_2I$. However, $ClCH_2(CH_2OCH_2)CH_2Cl$ is stable, commercially available and cheap.

The low yield is due to the formation of by-products such as **6** and multimers involving more than two thione moieties as observed by Becher [Becher, 1993](Fig 4.4). This makes purification of **1a** not easy, but still feasible.

**Fig 4.4**: Trimer and pentamer, by-products in the synthesis of **1a**

The dithiolone **2a** is easily obtained by reacting **1a** with 2 eq. of $Hg(OAc)_2$ in a mixture 3/1 of $CH_3COOH/CHCl_3$ at room temperature for three hours with yield 87% (Scheme 4.3). It has been seen that the same reaction carried out using one equivalent of $Hg(OAc)_2$ in refluxing $CH_3COOH/CHCl_3$ 3/1 (v/v) gives **2a** in slightly lower yields, 81 %.

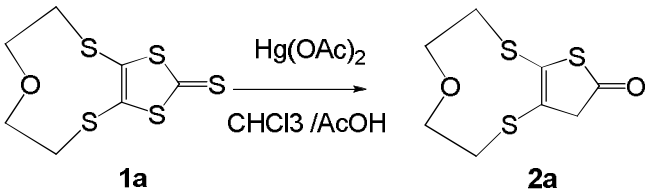


**Scheme 4.3**

### 4.2.1.2. Synthesis of $Bu_4N[Ni(C_6H_8S_4O)_2]$, (crown-1-Ni(dithiolene)$_2$)

The reaction of the crown-1-dithioketone **2a** with 2 equivalents of $Bu_4NOH$ in MeOH gives 1-oxo-4,7-dithiacyclopenta-5-ene-5,6-dithio-1,2-dithiolate within 1 hour. Thereafter 0.5

eq. of nickel chloride hexahydrate are added to the solution yielding directly $Bu_4N[Ni(C_6H_8S_4O)_2]$ (**7**).

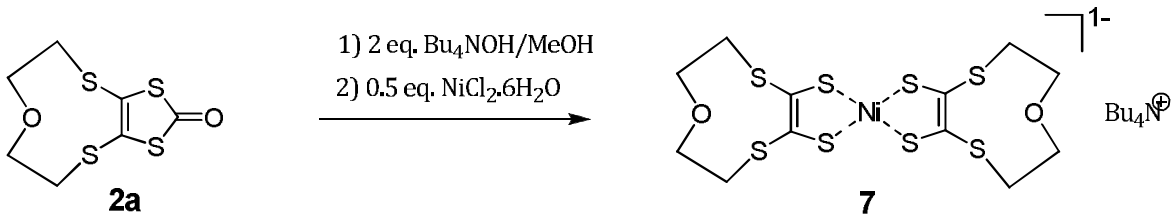


**Scheme4.4**: Synthesis of $Bu_4N[Ni(C_6H_8S_4O)_2]$

$Bu_4N[Ni(C_6H_8S_4O)_2]$ is highly soluble in $CH_3CN$, $CH_2Cl_2$, DMF. Crystals have been grown by slow diffusion of $Et_2O$ vapours in DMF solution of **(7)**

***Crystal structure***

$[Bu_4N][Ni(C_6H_8S_4O)_2]$DMF crystallizes in the monoclinic system with space group C 2/c. The cation $Bu_4N^+$ and one molecule of DMF (disordered on two positions) are localized on two-fold axis and the nickel atom the dithiolene complex on an inversion center.

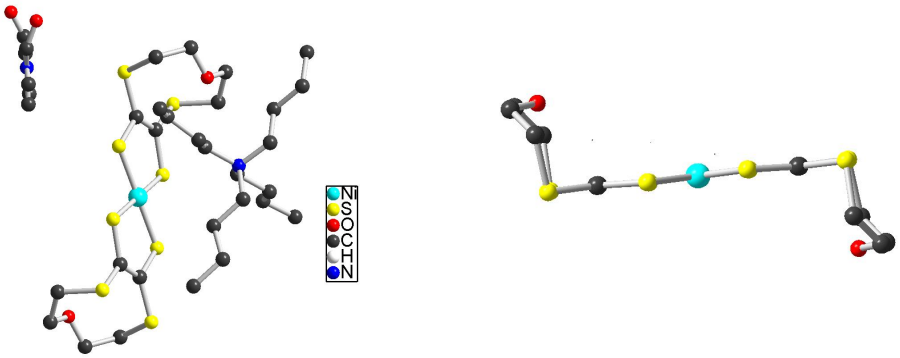


**Fig 4.5:** _$Bu_4N[Ni(C_6H_8S_4O)_2]$ DMF.

The coordination geometry around nickel atom is square planar. Ni-S distances in $[Ni(C_6H_8S_4O)_2]^{\cdot-}$ are 2.150 Å and 2.149 Å which, compared with the corresponding distances of complex $[Ni(pddt)]^{\cdot-}$ of 2.143 Å and 2.152 Å [Zuo, 1995], are indicative of the monoanionic state.

The C=C distance in the $MS_2C_4$ cycle, that is roughly correlated to the oxidation state of the complex, has a value of 1.357 Å in $[Ni(C_6H_8S_4O)_2]^{\cdot-}$ while the monoanionic $[Ni(pddt)]^{\cdot-}$ it has been found to be 1.358 Å. Another feature which correlates with the oxidation state is the C=C stretching frequency that is 1385 $cm^{-1}$ for $[Ni(C_6H_8S_4O)_2]^{\cdot-}$ while for $[Ni(ttdt)]^{\cdot-}$ it is 1380 $cm^{-1}$ [Takahashi, 1998].

Along c axis $[Ni(C_6H_8S_4O)_2]^{\cdot-}$ unities are disposed to develop a column of planar dithiolenes, each separated by a $Bu_4N^+$ cation and a molecule of disordered DMF (omitted in Fig 4.6). $[Ni(C_6H_8S_4O)_2]^{\cdot-}$ are staggered forming an angle of 90° between the two planes.

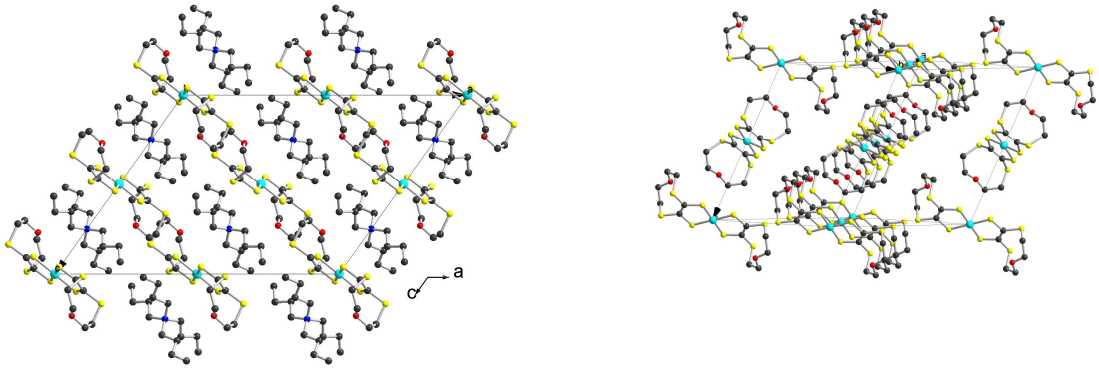


**a** **b**

Fig.4.6: **a)** $Bu_4N^+$ cations between $[Ni(C_6H_8S_4O)_2]^{\cdot-}$**,** view along b **b)** staggered $[Ni(C_6H_8S_4O)_2]^{\cdot-}$ planes.

The distance between two nickel atoms of two $[Ni(C_6H_8S_4O)_2]^{\cdot-}$ along the c axis is 8.668 Å . In the crystal structure, intermolecular S-S short contacts are not present.

Paramagnetic $[Ni(C_6H_8S_4O)_2]^{\cdot-}$ are well isolated in the solid state and do not interact. It is reasonable to predict a Curie type behaviour for the magnetic susceptibility of this compound as a function of temperature.

***Electrochemical behaviour***

Cyclic voltammetry measurements were performed on $Bu_4N[Ni(C_6H_8S_4O)_2]$ in $CH_2Cl_2$ .

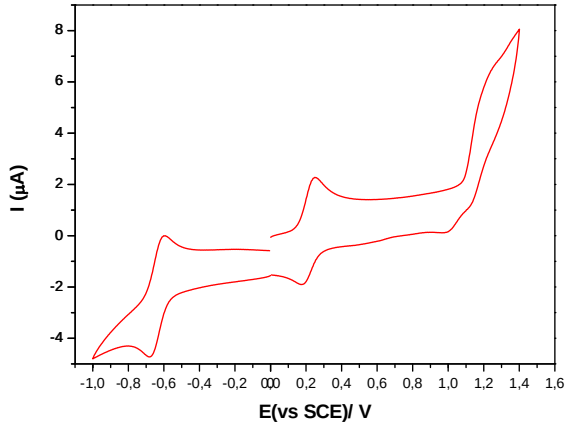


**Fig. 4.7**- Voltammogram of $Bu_4N[Ni(C_6H_8S_4O)_2]$ ($Bu_4NPF_6$/ $CH_2Cl_2$/Pt/0.5 $Vs^{-1}$).

As it can be seen from Fig. X, three waves are visible: two reversible waves at -0.643 V and 0.213 V and a quasi reversible wave at 1.250 V . The wave at -0.643 V corresponds to the process $[Ni(C_6H_8S_4O)_2]^{2-} \rightarrow [Ni(C_6H_8S_4O)_2]^{\cdot-}$ while the reversible peak at 0.213 V is relative to the oxidation to neutral species $[Ni(C_6H_8S_4O)_2]^{\cdot-} \rightarrow [Ni(C_6H_8S_4O)_2]^{0}$. The irreversible peak at 1.250 V is attributed to $[Ni(C_6H_8S_4O)_2]^{0} \rightarrow [Ni(C_6H_8S_4O)_2]^{+}$ . In table 4.1, peak potentials for different Ni-bis(dithiolene) complexes are reported for comparative purposes.

| Compound | $E^0$ -2/-1 (V) | $E^0$ -1/0 (V) | $E^0$ 0/+1 (V) | Ref |
|---|---|---|---|---|
| 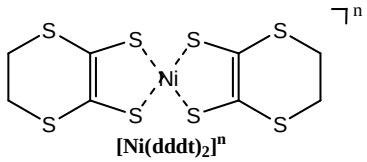 $[Ni(dddt)_2]^n$ | -0.790 | 0.013 | 0.834 | $CH_2Cl_2$ vs. SCE [a] |
| 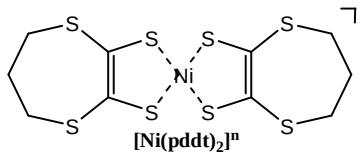 $[Ni(pddt)_2]^n$ | -0.645 V | 0.260 | 0.830 | $CH_2Cl_2$ vs. SCE [a] |
| 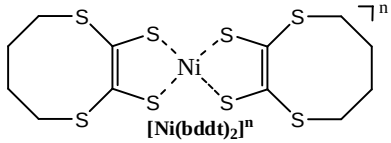 $[Ni(bddt)_2]^n$ | -0.625 | 0.300 | 0.907 | $CH_2Cl_2$ vs. SCE [a] |
| 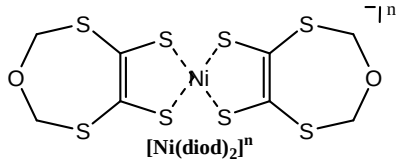 $[Ni(diod)_2]^n$ | -0.64 | 0.28 | 1.15 | $CH_3CN$ vs. SCE [b] |
| 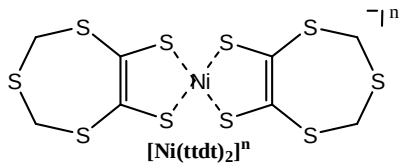 $[Ni(ttdt)_2]^n$ | -0.59 | 0.21 | | $CH_3CN$ vs. SCE [c] |
| 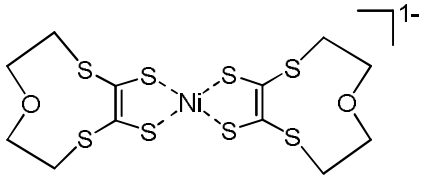 | -0.643 | 0.213 | 1.250 | $CH_2Cl_2$ vs. SCE |

**Table 4.1** : Redox potentials for some Ni-bis(dithiolene) complexes.

The values of the first two anodic peaks are consistent with those found for $[Ni(ttdt)]^{-}$ in $CH_3CN$ *vs.* SCE [a,Soras,2010] and with those of the oxygen analogue $[Ni(diod)]^{-}$ in $CH_3CN$ vs. SCE [b, Underhill,1995). The first two oxidation waves are found to be reversible for both $[Ni(ttdt)]^{-}$ and $[Ni(diod)]^{-}$.

The wave at 1.250 V is irreversible and this could be due to the decomposition of $[Ni(C_6H_8S_4O)_2]^{+}$ to give organic radicals [Cassouw, 1996] as for complex $[Ni(dddt)_2]^{+}$. Other data available for comparative purposes concern complexes $[Ni(pddt)_2]^{-}$, $[Ni(bddt)_2]^{-}$ and

$[Ni(dddt)_2]^{\cdot-}$ (Table 4.1) in $CH_2Cl_2$ vs. SCE. By comparing these three complexes, it could be observed that generally the oxidation potentials for the couple -1/0 is shifted toward more positive values within the series $[Ni(bddt)_2]^{\cdot-}$ **>** $[Ni(pddt)_2]^{\cdot-}$ **>** $[Ni(dddt)_2]^{\cdot-}$. The size of the macrocycle substituents follows the trend $[Ni(bddt)_2]^{\cdot-}$ **>** $[Ni(pddt)_2]^{\cdot-}$ **>**$[Ni(dddt)_2]^{\cdot-}$. On these basis, one should expect values for $[Ni(C_6H_8S_4O)_2]^{\cdot-}$ more anodic than for $[Ni(bddt)_2]^{\cdot-}$ because of its bigger macrocycle substituent chain and because of the presence of electronegative oxygen atom within the chain.

In $[Ni(C_6H_8S_4O)_2]^{\cdot-}$, only the third oxidation potential relative to $[Ni(C_6H_8S_4O)_2]^{0} \rightarrow [Ni(C_6H_8S_4O)_2]^{+1}$ presents a sensible shift with respect to $[Ni(bddt)_2]^{\cdot-}$ The first oxidation wave and the second one are quite similar to the value found for $[Ni(bddt)_2]^{\cdot-}$ and $[Ni(pddt)_2]^{\cdot-}$. Probably, over a certain substituent chain size, the associated electron donating ability does not show sensible changes in increasing the size of the chains and consequently also the presence of the oxygen heteroatom does not cause meaningful shifts of the oxidation potential.

These observation are supported by Vis-NIR absorption measurements where the shifts on the absorption energies for the transition $2b_{1u}$-$3b_{2g}$ are not so marked between $[Ni(bddt)_2]^{\cdot-}$ $[Ni(pddt)_2]^{\cdot-}$, [Ni(ttdt)]$^{\cdot-}$ and [Ni(diod)]$^{\cdot-}$, while they are quite different from $[Ni(dddt)_2]^{\cdot-}$ .

### 4.2.1.3 Synthesis of a bimetallic complex: {$[Ni(C_6H_8S_4O)_2][Ni(Cl)(DMF)_4]$} (8)

$[Ni(C_6H_8S_4O)_2][Ni(Cl)(DMF)_4]$ is obtained by adding an excess of $NiCl_2$ to a $CH_3CN$ solution of $Bu_4N[Ni(C_6H_8S_4O)_2]$. After two days, the dark precipitate that appears is filter and redissolved in DMF. Slow diffusion of diethyl yields crystals of **8** within 20 days (Scheme 4.5).

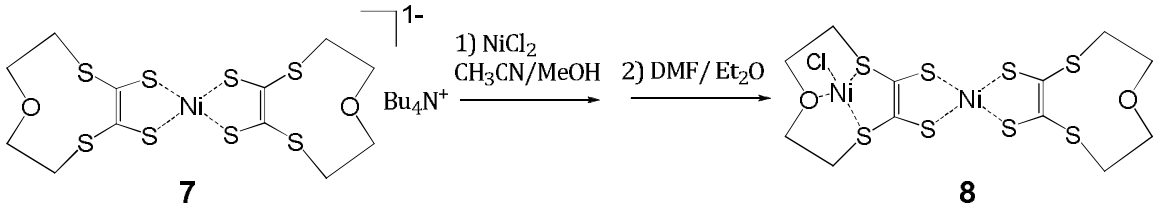


**Scheme 4.5** : Reaction between $Bu_4N[Ni(C_6H_8S_4O)_2]$ and $NiCl_2$

***Crystal structure***

{[Ni($C_6H_8S_4O)_2$][Ni(Cl)$(DMF)_2$]} crystallizes in the monoclinic system with space group C 2/m. The two Ni atoms of the complex lie on a mirror plane. The Ni-$S_4$ dithiolene core is planar and Ni-S distances are 2.164 Å and 2.149 Å. Ni-S bonds connected to the same side of the coordinating thio-ether moiety are slightly elongated respect to Ni-S in $Bu_4N$[Ni($C_6H_8S_4O)_2$]. The C=C distance is 1.363 Å, comparable with the one found for $Bu_4N$[Ni$(ttdt)_2$] of 1.37 Å.

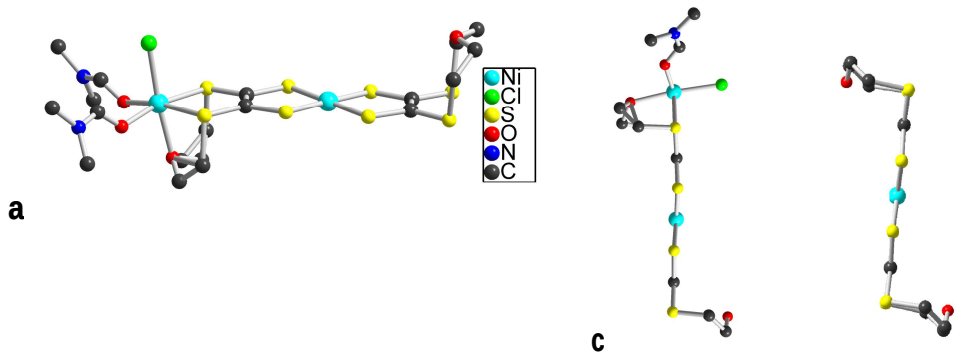


**Fig 4.8** a) {[Ni($C_6H_8S_4O)_2$][Ni(Cl)$(DMF)_2$]}
b) Comparison between{[Ni($C_6H_8S_4O)_2$][Ni(Cl)$(DMF)_2$]} and $Bu_4N$[Ni($C_6H_8S_4O)_2$]

The second Ni atom is in an octahedral environment, with equatorial coordination of the two sulphur atoms and two oxygen atoms from two DMF molecules. The oxygen atom from the thio-ether moiety and a $Cl^-$ anion complete the apical coordination. Two DMF and one $Et_2O$ molecules present as included solvent has been squeezed for the refinement by using PLATON in Wingx software. In Fig 4.8 {[Ni($C_6H_8S_4O)_2$][Ni(Cl)$(DMF)_2$]} is shown together with its parent compound $Bu_4N$[Ni($C_6H_8S_4O)_2$]. In this last complex, the oxygen of the thio-ether moiety points toward the Ni-$S_4$ dithiolene core. Upon coordination of the Ni(II) the oxygen atom points in the opposite direction respect to Ni-$S_4$.

Concerning the solid state arrangement of {[Ni($C_6H_8S_4O)_2$][Ni(Cl)($DMF)_2$]}, each bimetallic unity is well isolated to each other (fig X) and no short S···S intermolecular contacts are present, the thio-ether moiety and coordinated DMF molecules keep the unities well isolated (Fig. 4.9).

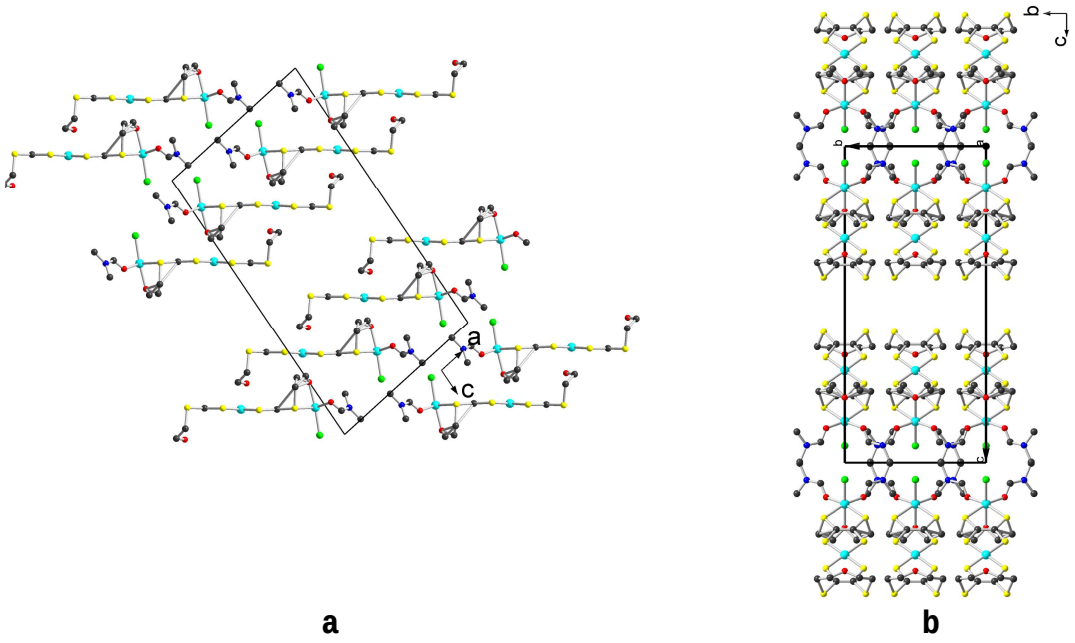


**Fig. 4.9**: {[Ni($C_6H_8S_4O)_2$][Ni(Cl)($DMF)_2$]} viewed along **a**) b axis and **b)** a axis.

Generally, crystallisation of {[Ni($C_6H_8S_4O)_2$][Ni(Cl)($DMF)_2$]} yields small crystals together with a brown powder. Attempts to grow pure {[Ni($C_6H_8S_4O)_2$][Ni(Cl)($DMF)_2$]} crystals, suitable for magnetic susceptibility measurement, are on course.

With this compound we demonstrate the coordination ability of our new metaloligand, giving a nice example of binuclear compound bearing two spins: S=1/2 from the Ni(III) dithiolene and spin S=1 from an Ni(II) in a $O_h$ environment.

Now we can expect the synthesis of polynuclear complexes of higher nuclearity: a non chlorinated $Ni^{2+}$ salt as reactant has been supposed to avoid the coordination of $Cl^-$ on the $Ni^{2+}$ and consequently to favour the formation of a trimetallic complex by coordination of two dithiolenes complexes through the crown ether moieties on the central $Ni^{2+}$.

The mixture of $CH_3CN$ solutions of $[Bu_4N][Ni(C_6H_8S_4O)_2]$ and $Ni(ClO_4)_2{\cdot}6H_2O$ yields a black polycrystalline precipitate. Crystallisation by slow diffusion of $Et_2O$ vapours into DMF solution gave big needle-like black crystals within 1-2days. X-ray single crystal diffraction experiment reveals that, instead of the expected trinuclear complex,we obtain a compound formulated $[Ni(C_6H_8S_4O)_2]_2[Ni(DMF)_6]$ **(9)** (Scheme 4.9)

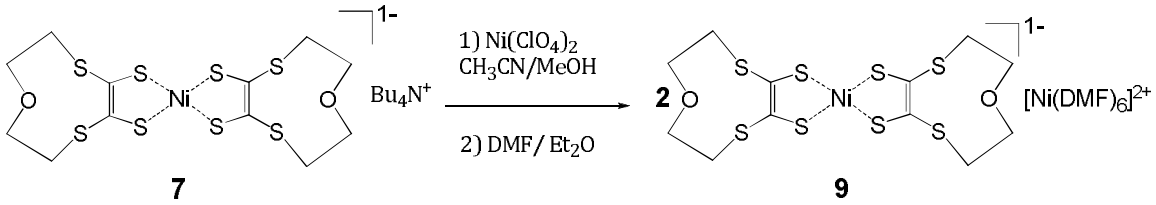


**7** **9**

**Scheme 4.9**

***Crystal structure of $[Ni(C_6H_8S_4O)_2]_2[Ni(DMF)_6]$(9)***

$[Ni(C_6H_8S_4O)_2]_2[Ni(DMF)_6]$ crystallizes in the triclinic system, space group P-1.

$[Ni(C_6H_8S_4O)_2]^{\cdot-}$ complex is located in general position and $[Ni(DMF)_6]^{2+}$ lie on an inversion center. Each DMF molecules coordinated to $Ni^{2+}$ is disordered on two positions with 50/50 occupation factors.

The Ni-$S_4$ core of the dithiolene complex is planar, Ni-S distances are found to be 2.151 Å, 2.147 Å, 2.145 Å, as for a monoanionic dithiolene complex. C=C distances are 1.355 Å and 1.345 Å, consistent with the values observed for the parent compound, $Bu_4N[Ni(C_6H_8S_4O)_2]$.

| **Compound** | Selected bond distances (Å) | | Ref |
|---|---|---|---|
| 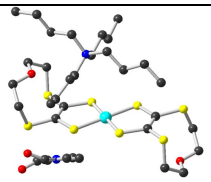 | Ni-S<br>C=C | 2.150, 2.149<br>1.357 | This work |

| | | | |
|---|---|---|---|
| 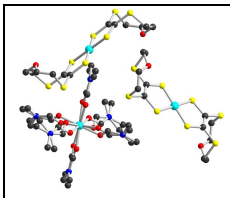 | Ni-S<br>C=C<br>Ni-O | 2.151, 2.147, 2.145<br>1.355, 1.345<br>2.047, 2.059, 2.055,<br>2.036 | This work |
| 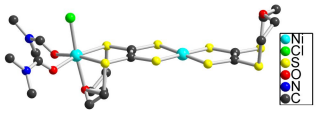 | Ni-S<br>C=C<br>Ni-Cl<br>Ni-O(DMF)<br>Ni-O<br>Ni-S(crown) | 2.164, 2.149<br>1.363<br>2.337<br>2.039<br>2.169<br>2.399 | This work |

**Table 4.2**: selected bond distances for $[Bu_4N][Ni(C_6H_8S_4O)_2]$,$[Ni(C_6H_8S_4O)_2]_2[Ni(DMF)_6]$, and $[Ni(C_6H_8S_4O)_2Ni(DMF)_2Cl]$

As it can be observed in Fig. 4.10, each $[Ni(DMF)_6]^{2+}$ cation is on a vertex of the cell and short contacts between them and $[Ni(C_6H_8S_4O)_2]^{-}$ are not present. Also the dithiolene unities are far to each others, preventing any type of short contact.

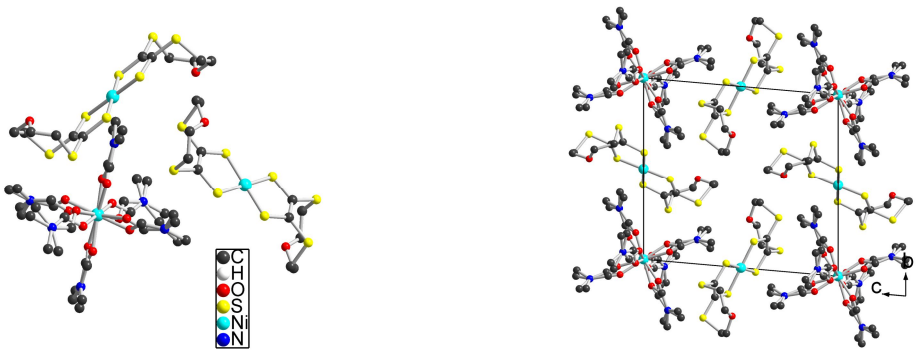


**a** **b**

**Fig. 4.10:** a) complex $[Ni(C_6H_8S_4O)_2]_2[Ni(DMF)_6]$ and b) view of along a axis.

***Magnetic properties:***

The magnetic susceptibility of a sample of $[Ni(C_6H_8S_4O)_2]_2[Ni(DMF)_6]$ has been mesured in the 2-300K range. As anticipated from the crystal structure, the magnetic behaviour of

this compound is well modelised with a Curie law of two S=1/2 spins and one S=1 spin with g values of 2 and 2.2 respectively (g values around 2.2 are usualy admitted for $Ni^{2+}$ in octahedral environement).

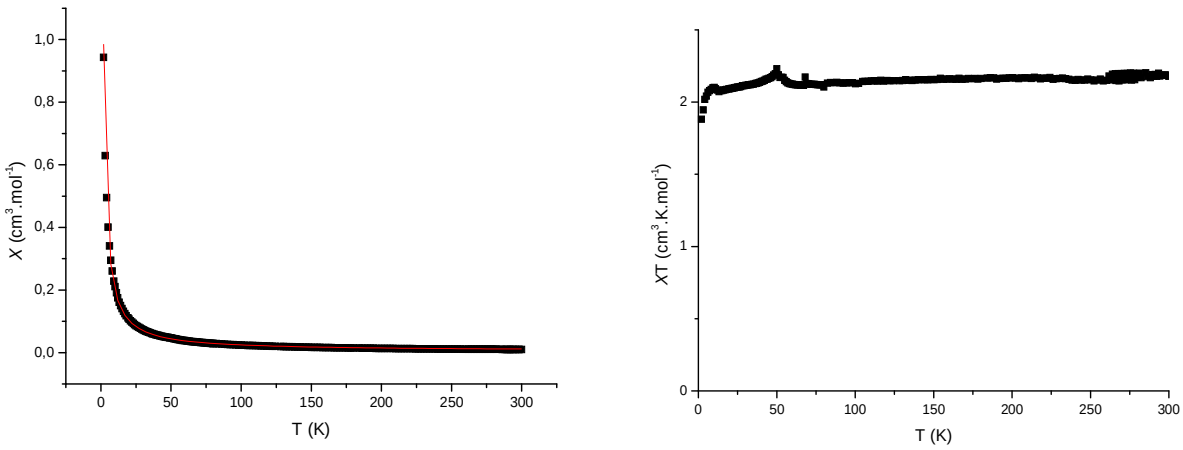


**Fig. 4.11** X vs T plot (fitting cuve in red) and XT vs T plot for $[Ni(C_6H_8S_4O)_2]_2[Ni(DMF)_6]$

We demonstrate here the coordination ability of a Ni dithiolene complex functionalized with small crown ether. Substitution of the dithiolene core with larger crown ether can enhance their coordination ability. We describe in the following part the synthesis and some coordination compound base on crown-4 functionalized Ni-dithiolene complex.

### 4.2.2 Synthesis of crown-4 Ni(dithiolene)$_2$ complexes

#### 4.2.2.1 Synthesis of 1,4,7,10-tetraoxo-13,16-dithiacyclooctadec-14-ene- 14,15- dithia-2-one, crown-4-dithioketone

As for the synthesis of **1a**, $[Zn(dmid)_2]^{2-}$ has been chosen as precursor material for the synthesis of crown-1-dithioketone **1d** and its oxygen analogue crown-4-dithioketone **2d**. The synthetic conditions were changed with respect to the already published procedures [Becher,2005; Echegoyen, 2000 ] 3292]] for the same reason mentioned above. Inspired

by the work done by Green [Green, 1990] TsO-$(CH_2OCH_2)_4$OTs was used as alkylating reagent (Scheme 4.11).

The reaction between $[Zn(dmid)_2]^{2-}$ and TsO-$(CH_2OCH_2)_5$OTs in refluxing acetone under high dilution conditions afforded after one week compound **1b** with a yield of 20%. The same reaction carried out in refluxing cyclohexanone for 24h yield 20% of **1b**.

As for compound **1a**, purification of the crude is not easy due to the formation of other by-products, such as dimeric compounds and oligomers.

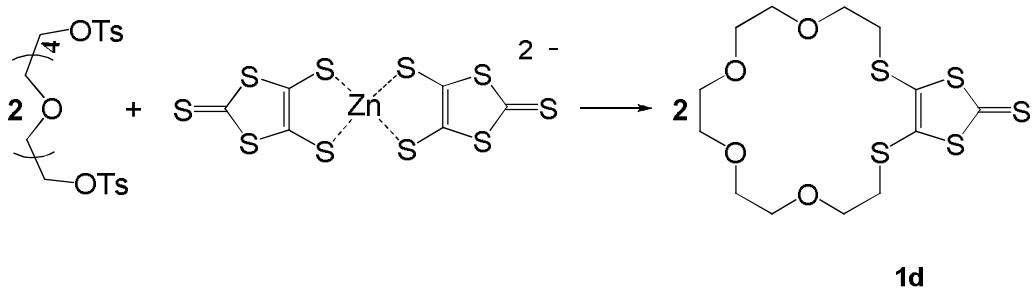


**Scheme 4.11**

Thione **1d** was reacted with 2.2 eq. of $Hg(OAc)_2$ in a mixture 3/1 of $CH_3COOH/CHCl_3$ (Scheme X) at room temperature for two hours affording **2d** in 88% yield. It has been found that purification of the crude **2d** can be done by $SiO_2$ column chromatography eluiting with light petrole/acetone 6/2 (v/v), obtaining a nearly transparent oil which affords needle-shape crystals upon cooling. Yields are similar if the reaction is carried out by refluxing the mixture for 2 Hours.

### 4.2.2.2. Synthesis of {[Ni($C_{12}H_{20}S_4O_4$)$_2$Na]} (11)

In order to test the coordination ability of the dithia 18-crown-6 ring in a dithiolene complex, we decided first to synthesize the $Na^+$ salt of $[Ni(C_{12}H_{20}S_4O_4)_2]^{-}$

Using the classical ring opening reaction, with NaOMe as nucleophile, yields directly the desired compound in good yields (70%) (Scheme 4.12).

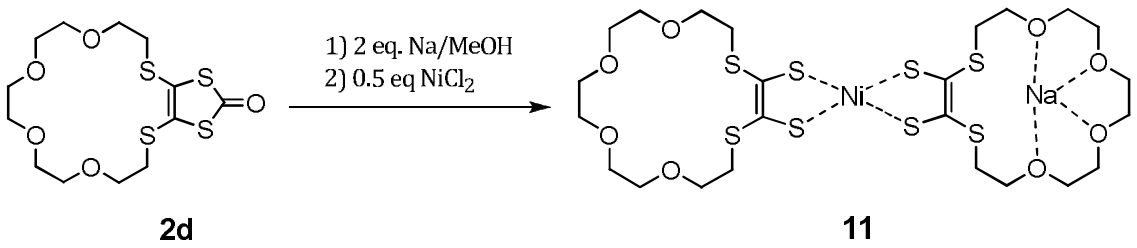


**2d** **11**

**Scheme 4.12**

$[Ni(C_{12}H_{20}S_4O_4)_2Na]$ has been crystallized from DMF solution upon diffusion of vapours of diethyl ether.

***Crystal structure:***

$\{[Ni(C_{12}H_{20}S_4O_4)_2Na]\}$ crystallizes in monoclinic system, space group C 2/c.

The asymmetric unity consists of half dithiolene molecule with Ni occupying an inversion center and a $Na^+$ cation on a binary axis. The dithiolene unity $[Ni(C_{12}H_{20}S_4O_4)_2Na]$ presents a square planar Ni-$S_4$ core, with Ni-S distances of 2.142 Å and 2.155 Å, and C=C distances of 1.37 Å are consistent with a monoanionic dithiolene complex. The energy of C=C antsymmetric stretching which correlates roughly with the oxidation state of the dithiolene is at 1370 $cm^{-1}$, confirming the monoanionic character of the dithiolene complex. Three of the four oxygen atoms of the crown-4 dithiolene complex are coordinated to the $Na^+$ developing uniform chains by symmetry.

$Na^+$ presents a "sandwich like" coordination fashion with Na-O distances of 2.451 Å, 2.463 Å and 2.523 Å. Each chain is well separated from the adjacent one and no inter-chain short contacts are present (Fig.4.12).

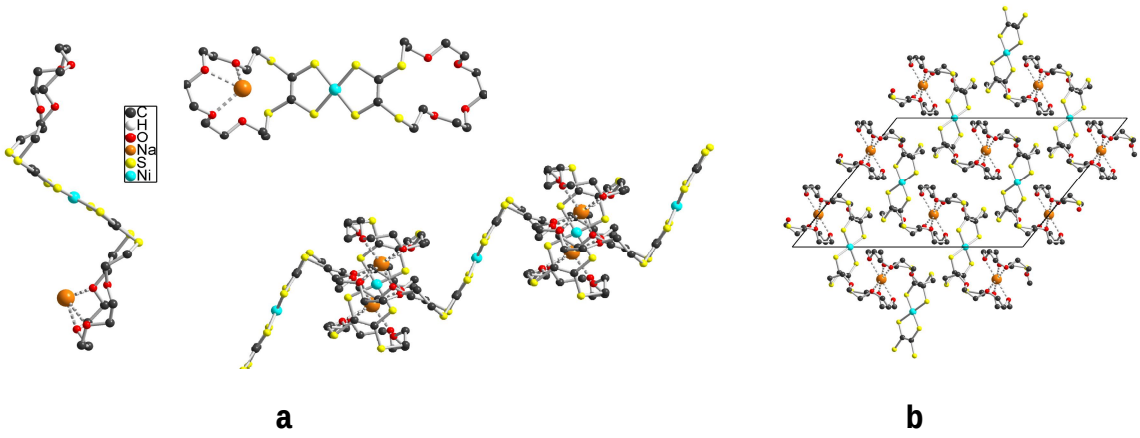


**Fig 4.12 a)** Dithiolene unity [Ni($C_{12}H_{20}S_4O_4$)$_2$Na] and **b)** polymetallic chains viewed along b axis

### *Electrochemical behaviour*

Cyclic voltammetry was performed on DMF solutions of [Ni($C_{12}H_{20}S_4O_4$)$_2$Na].

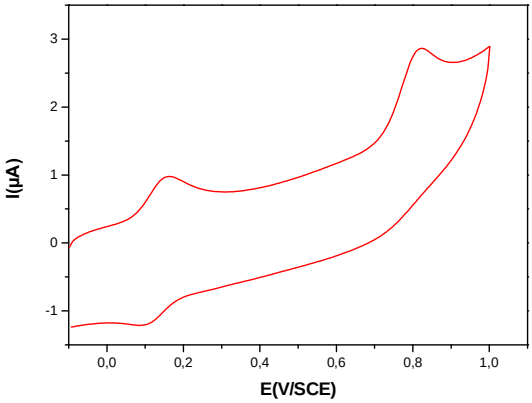


**Fig.4.13** Voltamograms of [Ni($C_{12}H_{20}S_4O_4$)$_2$Na], DMF, $Bu_4NPF_6$ , Pt vs SCE 0.2$Vs^{-1}$

Surprisingly, no waves were observed in the cathodic region, where the reduction to dianionic dithiolene $[Ni(C_{12}H_{20}S_4O_4)_2]^{\cdot-} \rightarrow [Ni(C_{12}H_{20}S_4O_4)_2]^{2-}$ is expected.

A first reversible oxidation wave is at 0.16 V while the second irreversible oxidation peak 0.82 V for $[Ni(C_{12}H_{20}S_4O_4)_2]^{\cdot-} \rightarrow [Ni(C_{12}H_{20}S_4O_4)_2]^{0}$ and $[Ni(C_{12}H_{20}S_4O_4)_2]^{0} \rightarrow [Ni(C_{12}H_{20}S_4O_4)_2]^{+}$**.**

***Magnetic properties***

Magnetic susceptibility of $[Ni(C_{12}H_{20}S_4O_4)_2Na]$ was measured as a function of the temperature in the 2-300K range.

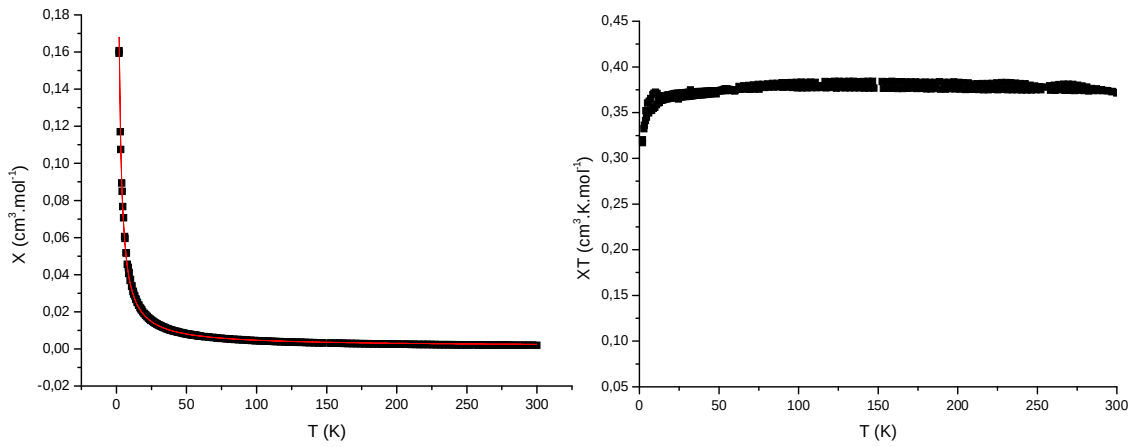


**Fig. 4.14** vs. T (fitting curve in red) en XT vs. T plot for $[Ni(C_{12}H_{20}S_4O_4)_2Na]$ at 5000 Oe.

The m agnetic susceptibility was fitted with the Curie law expression giving a Curie constant of 0.333 K $cm^3$ $mol^{-1}$ close to the one expected for S=1/2 with g value of 2. This behaviour is in good agreement with the crystal structure analysis that shows isolated dithiolene complexes.

### 4.2.2.3. Synthesis of {$[Ni(C_{12}H_{20}S_4O_4)_2]_2Ni,H2O$} (10)

The dithiocarbonate **2d** was treated with 2 equivalents of $Bu_4NOH$ in MeOH (scheme 4). Thereafter 0.5 eq. of nickel chloride hydrate were added to the solution and a brown

precipitate appears. Usually this reaction, using only 0.5 equivalent a $NiCl_2$ should give the monoanionic dithiolene complex with TBA+ as counter cation.

Crystallisation of the reaction production from DMF solution by slow diffusion of diethyl ether vapours afforded crystals after 1-2 days. Single crystal X-ray diffraction reveals us a surprising structure: $[Ni(C_{12}H_{20}S_4O_4)_2]^{-\cdot}$ does not crystallize with the $TBA^+$ cation as we expected, but with one $Ni^{2+}$ cation and one $H_2O$ molecule. This compound can be formulated as: $\{[Ni(C_{12}H_{20}S_4O_4)_2]_2Ni,H_2O\}$ (Scheme 4.13). Reaction carried out by adding 1.0 equivalents of $NiCl_2$ afforded compound $\{[Ni(C_{12}H_{20}S_4O_4)_2]_2Ni,H_2O\}$ in better yields (46%).

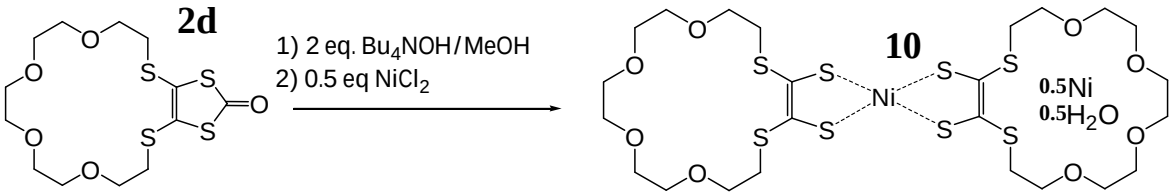


**Scheme 4.13**

### *Crystal structure*

$\{[Ni(C_{12}H_{20}S_4O_4)_2]_2Ni,H_2O\}$ crystallizes in the monoclinic system space group C 2/c. The asymmetric unit is shown in Fig 4.15 a, Ni of the dithiolene complex lies on an inversion center, Ni(II) shares with $H_2O$ the same site on a two fold axis. Occupation factors of both $Ni^{2+}$ and $H_2O$ molecule have been refined and then fixed to the converging value of 0.5.

Ni-$S_4$ core is planar (Fig 4.15 b) and Ni-S distances are 2.160 Å and 2.140 Å, consistent with a monoanionic dithiolene complex together with the C=C distance of 1.367 Å.

The $Ni^{2+}/H_2O$ site (noted NiO in the following discussion) is located in a cavity formed by two crown ether. NiO$^{\cdots}$O shortest distances are 2.977 Å, 2.855 Å, 2.898 Å, NiO$^{\cdots}$S distance are much longer 3.362 Å and 3.755 Å. Both NiO$^{\cdots}$O and NiO$^{\cdots}$S distances are much higher than those expected for a coordinated $Ni^{2+}$. As an exemple, Ni$^{\cdots}$S and Ni$^{\cdots}$O distances in $[Ni(C_6H_8S_4O)_2][Ni(Cl)(DMF)_4]$ are respectively 2.399 Å and 2.169Å. We have to note that

NiO····O distances observed in $\{Ni(C_{12}H_{20}S_4O_4)_2]_2Ni,H_2O\}$ are mean distances between $Ni^{2+}$····O and $H_2O$····O bonds.

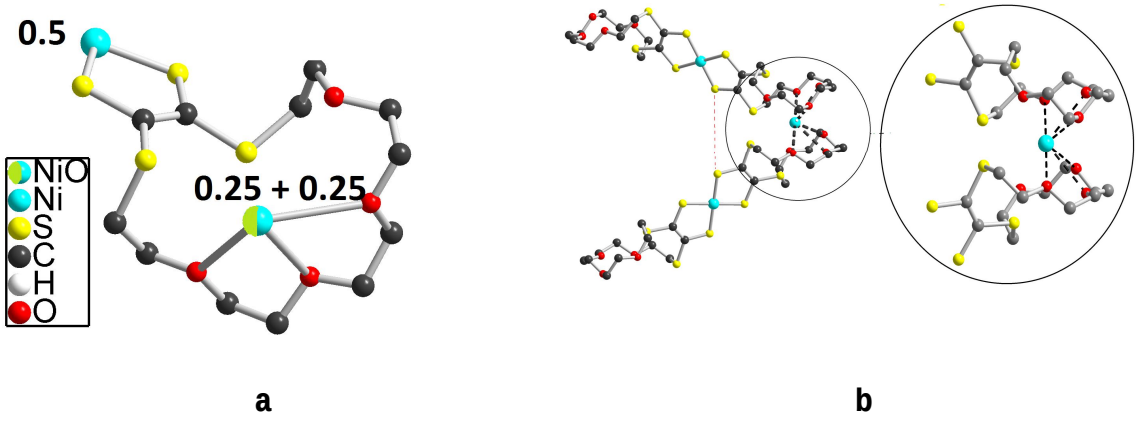


**Fig. 4.15: a)** Asymmetric unit for $\{[Ni(C_{12}H_{20}S_4O_4)_2]_2\ NiH_2O\}$ (occupancy of Ni and $H_2O$ is noticed) **b)** A trimer $\{[Ni(C_{12}H_{20}S_4O_4)_2]_2\ NiO\}$ and a view of the unusual coordination geometry of Ni(II).

The perspective view in Fig. 4.16 b shows the disposition of each array on the unit cell. Due to the Ni(II)-$H_2O$ site sharing, there is an intrinsic statistic disorder and coordination chains are formed upon coordination of Ni(II) or $H_2O$ by the crown-ether moiety of the dithiolene complexes.

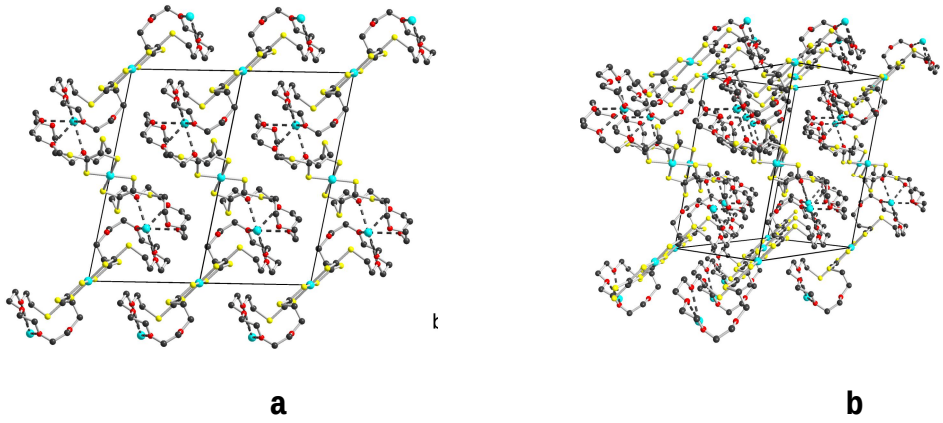


**Fig 4.16 a)** "Chains" developing along c and **b)** perspective view of "chains".

It has to be marked the unusual NiO coordination geometry of the six oxygen atoms of two different dithiolene molecules (Fig 4.15 b). It can be observed that NiO is "naked" on the side where two sulphur atoms of the dithiolene moiety are present. This is a rare example of such coordination geometry.

***Magnetic susceptibility measurement***

Magnetic susceptibility of {[Ni($C_{12}H_{20}S_4O_4$)$_2$]$_2$ $NiH_2O$} was measured as a function of temperature in the 2-300K. In Fig 4.17 χT is plotted against the temperature. Data for the magnetic susceptibilty χ have been fitted with a Curie Type law finding a Curie constant value of 1.142 K $cm^3$ $mol^{-1}$ with a Curie-Weiss Temperature θ=-0.91.

For a "naked" S=1 $Ni^{2+}$ and two S=1/2 dithiolene without any interaction the expected value of the Curie constant is 1.75 k.$cm^3$. The lower value measured for our sample strongly suggests strong magnetic interactions in the compound.

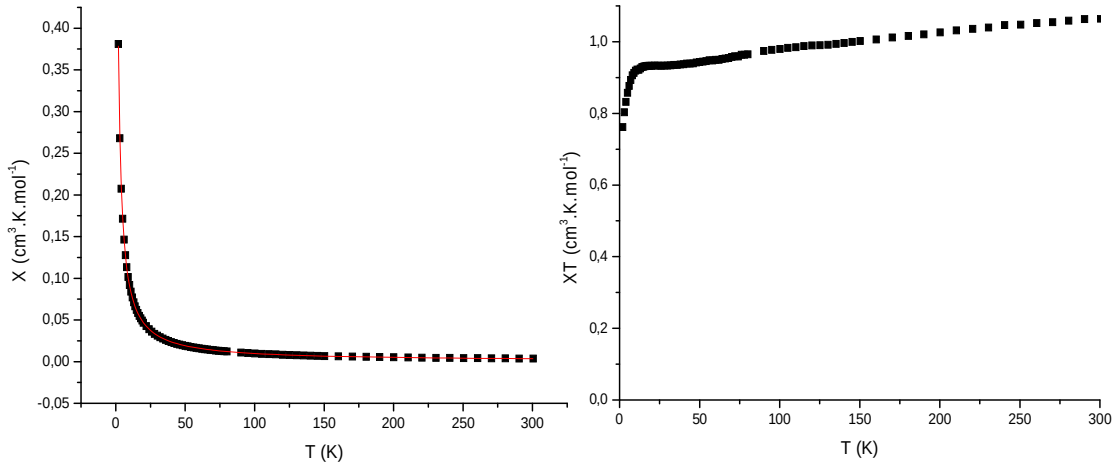


**Fig 4.17**: X vs T (fitting curve in red) and XT vs T plot for {[Ni($C_{12}H_{20}S_4O_4$)$_2$]$_2$ $NiH_2O$}

As mentioned above, no significantly short $Ni^{2+}\cdots O$ distances are observed, and we can reasonably consider the dithiolene and the $Ni^{2+}$ as isolated. To understand the lack of spin in the sample, we have to look more carefully the crystal structure of

{[Ni($C_{12}H_{20}S_4O_4$)$_2$]$_2$ $NiH_2O$. Analysis of the S....S short contacts does not reveal interchain interaction, but a short S····S distance of 3.332 Å is found between two external thioether sulphur (Fig. 4.18).

This very short distance repeated by symmetry along the chain allows the formation a 1/2 spin chain that can explain the lack of magnetic susceptibility.

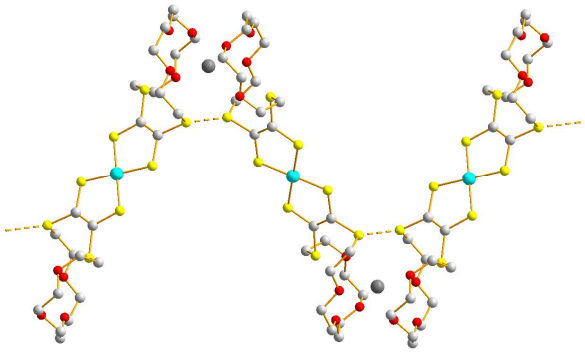

**Fig.4.18**: view of the intra-chain short contact between dithiolenes within the chain.

### *Electrochemical behaviour*

Redox behaviour of {[Ni($C_{12}H_{20}S_4O_4$)$_2$]$_2$ $NiH_2O$} has been studied by means of cyclic voltammetry on Pt electrode *vs* SCE in DMF with $NBu_4PF_6$.

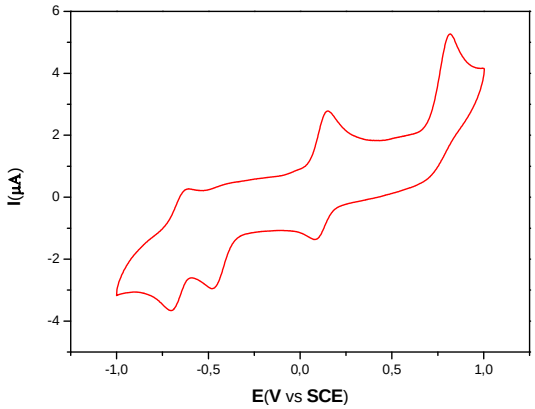


**Fig 4.19** Cyclic voltammetry for {[Ni($C_{12}H_{20}S_4O_4$)$_2$]$_2$ $NiH_2O$

In Fig 4.19 it is reported the cyclic voltammetry for {[Ni($C_{12}H_{20}S_4O_4)_2$]$_2$ $NiH_2O$}.

Three oxidation waves are present at -0.61 v (quasi reversible), at 0.145 V and at 0.810 V (irreversibile). The peak at 0.145 V is attributable to the oxidation process [Ni($C_{12}H_{20}S_4O_4)_2$]$^{-1}$→[Ni($C_{12}H_{20}S_4O_4)_2$]$^0$ it is reversible with a ΔV of 55 mV. The wave at 0.810 V corresponds to the second oxidation [Ni($C_{12}H_{20}S_4O_4)_2$]$^0$→ [Ni($C_{12}H_{20}S_4O_4)_2$]$^{+1}$. This process is irreversible probably due to the decomposition of cation [Ni($C_{12}H_{20}S_4O_4)_2$]$^{+1}$ to give organic radicals. The quasi reversible oxidation peak at -0.61 V is relative to the oxidation of the dianion [Ni($C_{12}H_{20}S_4O_4)_2$]$^{-2}$→[Ni($C_{12}H_{20}S_4O_4)_2$]$^{-}$ .

A reasonable comparison is with $Bu_4N$[Ni($C_6H_8S_4O)_2$],. The three oxidation waves for {[Ni($C_{12}H_{20}S_4O_4)_2$]$_2$ $NiH_2O$} are shifted toward less anodic potentials with respect to $Bu_4N$[Ni($C_6H_8S_4O)_2$].

The biggest shift concern [Ni($C_{12}H_{20}S_4O_4)_2$]$^0$→[Ni($C_{12}H_{20}S_4O_4)_2$]$^{+1}$of 440 mV, while oxidations [Ni($C_{12}H_{20}S_4O_4)_2$]$^{-2}$→[Ni($C_{12}H_{20}S_4O_4)_2$]$^{-}$ and [Ni($C_{12}H_{20}S_4O_4)_2$]$^{-,-}$ →[Ni($C_{12}H_{20}S_4O_4)_2$]$^0$ are shifted by 33mV and 68 mV respectively.

From these observations and also considering absorption spectra, complex {[Ni($C_{12}H_{20}S_4O_4)_2$]$_2$ $NiH_2O$}, which bears the biggest macrocyclic substituent, results more electron rich than $Bu_4N$[Ni($C_6H_8S_4O)_2$]. This could be due to the bigger electron donating ability of the dithia 18-crown 6 substituent chains with respect to the dithia 7-crown-3 macrocycle present in $Bu_4N$[Ni($C_6H_8S_4O)_2$]. This is in contrast with what has been found in the literature for [Ni(bddt)] $^-$ [Ni(pddt)] $^-$ and [Ni(dddt)] $^-$ where the oxidation potential decrease within the size of the macrocycle.

However, the four electronegative oxygen atoms on {[Ni($C_{12}H_{20}S_4O_4)_2$]$_2$ $NiH_2O$} macrocyclic chain should cause a shift toward more anodic oxidation potentials. Furthermore, the oxidation potential should be shifted to more positive values, due to the presence of a positive charged Ni(II) ion coordinated by the macrocycle, which decrease the electron density on the dithiolene complex.

To verify these qualitative considerations, cyclic voltammetry was performed on DMF solution containing {[Ni($C_{12}H_{20}S_4O_4)_2$]$_2$ $NiH_2O$} and exogenous $NiCl_2$, to check whether Ni(II) was complexes by a ion -free thio-ether moiety in {[Ni($C_{12}H_{20}S_4O_4)_2$]$_2$ $NiH_2O$}. The voltammograms are displayed in fig 4.19.

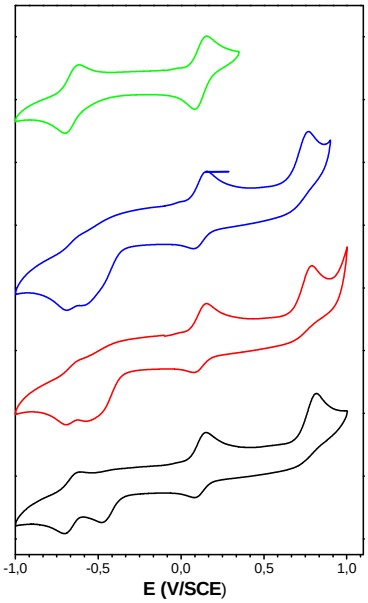


**Fig 4.19** black {[Ni($C_{12}H_{20}S_4O_4$)$_2$]$_2$ $NiH_2O$} in DMF, red {[Ni($C_{12}H_{20}S_4O_4$)$_2$]$_2$ $NiH_2O$} + 1 eq. $NiCl_2$, blue {[Ni($C_{12}H_{20}S_4O_4$)$_2$]$_2$ $NiH_2O$} + excess $NiCl_2$ , green {[Ni($C_{12}H_{20}S_4O_4$)$_2$]$_2$ $NiH_2O$} with scan limited to second oxidation wave.

After dissolution of 1 eq. of $NiCl_2$ the first reduction wave at -0.70 V becomes irreversible and the second reduction wave is at -0.58 V. The wave relative to [Ni($C_{12}H_{20}S_4O_4$)$_2$]$^{\cdot-}$ →[Ni($C_{12}H_{20}S_4O_4$)$_2$]$^0$ process remains unchanged at 0.145 V while the third irreversible oxidation wave is at 0.77 V. This shift toward negative potentials was unexpected, considering the complexation of Ni(II), and also a shift toward a more anodic potential is expected for the second oxidation wave. By adding an excess of Ni(II) (blue voltamogram), the same considerations are valid and further shifts of the potential are not observed. Another anomalous feature is that , by limiting the scan to 0.5 V, the irreversible cathodic wave at -0.58 V completely disappears, while the oxidation peaks at -0.60 V and 0.15 V are reversible.

For comparative purposes, it has been considered the electrochemical behaviour of Ni(II) complexed by di-aza 18-crown-6 ethers . Reduction potential for process Ni(II) → Ni(I) has been found at -0.835 V vs $Ag/Ag^+$ in $CH_3CN$. The reduction wave found for {[Ni($C_{12}H_{20}S_4O_4$)$_2$]$_2$ $NiH_2O$} could be attributed to the reduction to Ni(I). Its irreversibility is

due to the low stability of Ni(I) species. The fact that this wave disappears when the scan is limited only to 0.5 V remains unclear.

The electcrochemical behaviour has not been fully rationalized and further electrochemical experiments are on course on different batches of compound {[Ni($C_{12}H_{20}S_4O_4$)$_2$]$_2$ Ni$H_2$O}.

### 4.2.3 Further crown-ether substituted dithiolate ligands: 1,4,7 trioxa-10,13-dithiacycloheptadec-11- ene- 11,12-dithia-1,2-dithiolate and 1,4-dioxa-7-10-dithiacycloexadec-8-ene-8,9- dithia 1, 2-dithiolate

The two-and three oxygen macrocyclic **2d** and **3d** derivatives were also synthetized as proligands for the corresponding 1,2 dithiolate complexes.

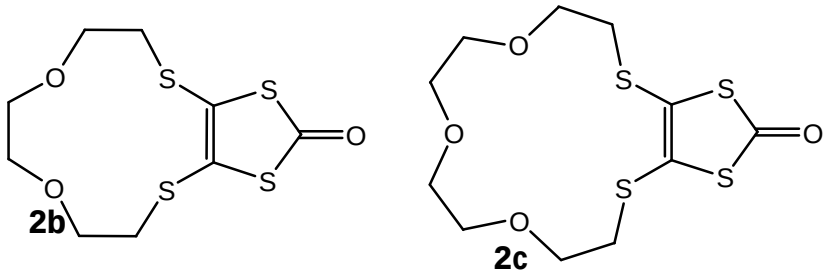


**Fig 4.20**

To date, any attempt to isolate their nickel complex by following the same synthetic way as for the analogue {[Ni($C_{12}H_{20}S_4O_4$)$_2$]$_2$Ni$H_2$O] and related compounds has led to brown-greenish precipitates soluble only in DMF which, upon recrystallization by slow diffusion of diethyl ethers vapours, afforded only non crystalline precipitates.

The elemental analyses of the precipitates are not satisfactory compared with those calculated by considering the dithiolene complex in its monoanionic and neutral form.

The investigation of compounds 2c and 2d is still in progress in order to isolate the corresponding radical Nickel complex.

### 4.2.4. Conclusion and perspectives: metallo-ligands toward Ln(III) and 3d metals.

As pointed out in the introductive part of this chapter, the complexes here described were synthetized in order to obtain radical metallo-ligands.

During this work, attempts to prepare polymetallic complexes starting from $[Bu_4N][Ni(C_6H_8S_4O)_2]$ and $\{[Ni(C_{12}H_{20}S_4O_4)_2]_2\ NiH_2O\}$ with $Gd(NO_3)_3$ or $GdCl_3$ in $CH_3CN$ or DMF solutions resulted in the recrystallization of the starting materials in the case of $[Bu_4N][Ni(C_6H_8S_4O)_2]$ and in the formation of the neutral $[Ni(C_{12}H_{20}S_4O_4)_2]$ complex in DMF solutions containing $\{[Ni(C_{12}H_{20}S_4O_4)_2]_2\ NiH_2O\}$ and $Gd(NO_3)_3$. In this last case, half of the crown-ether sites are occupied by Ni(II) anions and this could be the reason why the Gd(III) is not coordinated by the macrocycle.

However, it must be stressed that also the solubility and the crystal packing are very important factors that determine which product will be isolated in the solid state.

The charge of the hypothetical $\{[Ni(C_{12}H_{20}S_4O_4)_2][Ln(III)]\}^{+2}$ must be balanced by other counter anions, which could be $[Ni(C_{12}H_{20}S_4O_4)_2]^{\cdot-}$ radical anions or the counter ions introduced within the source of Ln(III) complex, in this case $NO_3^-$ or $Cl^-$. Also the formation of sandwhiched $[Ni(C_{12}H_{20}S_4O_4)_2Gd(III)Ni(C_{12}H_{20}S_4O_4)_2]^+$ is possible because of the tendency of Ln(III) ions to give sandwiched structures when macrocycle ligands or planar ligands are used. However, as discussed in this chapter, the formation $\{[Ni(C_{12}H_{20}S_4O_4)_2]_2\ NiH_2O\}$ is strongly favored and all attempts to obtain the simple $[R_4N][Ni(C_{12}H_{20}S_4O_4)_2]$ salt have failed. Probably, this is an obstacle to the formation of polymetallic complexes within $[Ni(C_{12}H_{20}S_4O_4)_2]^{\cdot-}$ complex as metallo-ligand.

To favours the formation of the Ln(III)-$[Ni(C_{12}H_{20}S_4O_4)_2]^{\cdot-}$ complex $GdCl_3$ was added after the nucleophilic opening of the dithiolone moiety, before $NiCl_2$. Also in this case $\{[Ni(C_{12}H_{20}S_4O_4)_2]_2\ NiH_2O\}$ was isolated. Any attempt to pre-coordinateGd(III) by the thione derivative 2d has failed.

By carrying out the Ni complexation reaction in DMF, in order to avoid the precipitation of $\{[Ni(C_{12}H_{20}S_4O_4)_2]_2\ NiH_2O\}$, and upon addition of an aqueous solution of $Dy(ClO_4)_3$,

another phase for neutral [Ni($C_{12}H_{20}S_4O_4$)$_2$] was obtained after recrystallization from DMF/diethyether.

From these observations, it can be concluded that complexation of Ln(III) ions is not trivial and the chemistry of such complexes, which is not straightforward, is still under investigation.

However, the important steps concerning synthesis and characterization of new dithiolene complexes have been performed and a lot of efforts have been spent to optimize the synthetic conditions and the re-crystallization processes. The characterization of metallo-ligands is a basic step that must be addressed prior to use them in the synthesis of polymetallic complexes.

**Bibliography**


Becher, J. J. *Org. Chem.* **1992**, 57, 6405

Becher, J. J. *Org. Chem.* **1992**, 33, 21, 3035

Becher, J. J. *Org. Chem.* **1993**

Bereman, *J. Coord. Chem.* **1994**, 52, 31

Moo-Lyong Seo *Bull. Kor. Chem. Soc.* **1991,** 12, 368

Cassouw et al.*Inorg. Chem.* **1996,** 35 ,3856

Echegoyen et al. *J. Org. Chem.* **2000,** 65, 3292

Green, M.L. et al *J. Chem. Soc. Dalton Trans.* **1990,** 3789

Soras, G. *Chem. Phys.* **2010,** 33, 372

Takahashi *J. Mater. Chem.* **1998,** 8, 309

Underhill, A.E. *Synth Metals* **1995,** 71, 1955

Vance, T.C. *Inorg. Chem.* **1985,** 24, 2909

Zuo, J.L., *Polyhedron* **1995,** 14, 483

Fourmigué, M.; Airligue, T.; Thierry, P.; Mathieu, R., Ephitrikhine, M. *Inorg. Chem.* **2005,** 44, 584

Galy, J. *Inorg. Chim. Acta* **1984**, 129

Green, *J. Chem. Soc. Dalton Trans* **1990**, 3789

Nishihara, S.; Akutagawa, T.; Hasegawa, T.; Nakamura, T. *Inorg. Chem.* **2003,** 42, 2480

Yong, *Dalton Trans.* **2008**, 2578

# Chapter 5

## Metal complexes with sulphur based ligands: the case of 2-mercaptonicotinic acid

In the present work, we switch to the mercapto-derivative 2-mercaptonicotinic acid to explore the possibility to achieve formation of mixed S-M-O bonds, with the aim of exploiting the sulphur species to tune the electronic properties of the complex. Adopting the same synthetic conditions for Zn(II) and Ni(II), in the first case we obtained a polymetallic Zn(II) chain with 2-mercaptonicotinic acid coordinating in a S,O chelating and O,O bridging fashion, while for Ni(II) no crystalline products were obtained. To date, a discrete monometallic Ni(II)-bis mercaptonicotinate complex has been obtained. The work on Ni(II) is still on progress because of the high number of reaction parameters that could be changed in a systematically, but not serendipitous way.

### 5.1 Thiol-carboxylate ligands and related complexes

Thiolate ligands are attractive candidates for the design and the synthesis of mono and polymetallic transition metal complexes with electronic, optical and magnetic properties. In particular, thiolate ligands allow a better metal/ligand orbital overlap because of the higher delocalization of the charge with respect to the oxygen analogous. Better matches of orbital energies lead to a greater concentration of spin density in the bridging atom with the possibility of exchange interactions between metal centers [Humphrey, 2005].
Moreover, photoactive materials, such as light emitters, require a certain overlap of the ligand orbitals and metal center orbitals because many photoluminescence processes observed for metal complexes involve LMCT, [YI Shang Song, 2005] ligand-metal charge transfer processes. As far as the functional molecular materials are concerned, the solid

state arrangement of such metal complexes is pivotal for the final properties of the material. In this last decade, a lot of efforts have been devoted to obtain metal complexes with different topologies. The number of polymetallic complexes arranged as chains developing along one direction or as discrete multi-metallic coordination compounds that have been obtained with sulphur polyfunctional ligands are limited with respect to the oxygen analogous [Gross, 2010].

In fact, due to their higher charge delocalization degree and to the presence of many stable oxidation states for the sulphur atom, thiolate-based ligands are more susceptible of oxidation with respect to the oxygen based ligands. For the design of functional materials, often redox active metals are employed and in most cases this leads to the oxydation of the thiol moiety to disulphide.

For example, Cu(II) thiolate complexes are very scarce because of the high tendency of Cu(II) to oxidize thiol groups, giving disulphides species and Cu(I) species.

In addition, most of the syntethic strategies allowing to obtain coordination polymers involves hydrothermal synthesis. Under such conditions, ligands bearing thiol groups are not generally stable, giving disulphides or other decomposition products.

Finally, a great number of coordination compounds synthetized to obtain molecular materials contains lanthanides ions which are very oxophylic, whereas coordination of a thiolate to a Ln(III) does not occur. All this factors explain the relatevely scarce literature on these compounds.

In general, for the formation of hetero-metallic complexes, polytopic rigid ligands such as thiol-carboxylate have been thought to overcome the problem of metal selectivity, because they contain both O and S- donor atoms, in principle selective for Ln(III) and 3d metal ions respectevely.

It has to be pointed out that the use of polytopic rigid ligands such as thiol-carboxylates makes however more difficult the prediction and the control of the resulting structure, since these ligands are prompt to originate different architectures, topologies and coordination fashion. However, the careful choice of the ligand molecule, and the evaluation of its coordination peculiarities and steric requirements allow, in some case, a certain degree of control on the structure of the resulting compound. In S,O polytopic ligands, the additional presence of nitrogen donor atoms further widens the coordination

possibilities, since different donor sites (S, O, N) compete in the coordination to the metal ion, and different coordination fashions can be observed, also according to the nature of the metal. This variability in terms of coordination modality is expected also to affect the electronic properties of the final complex [Gross, 2010].

Particularly interesting compounds such as $[Ni_9\text{-}(6\text{-mna})_8(\mu_3\text{-}O)_2(H_3O)_2(H_2O)_6]$, $[Cs_2Ni_{12}(6\text{-mna})_{12}(\mu_3\text{-}O)\text{–}(OH)_2(OH_2)_6]\cdot 8H_2O$ [Humphrey, 2005] were obtained using a (S, O, N) donor polytopic ligand, 6-mercaptonicotinic acid (6-mna).

As it can be seen on Fig 5.1, the mercaptonicotinate ligand coordinates the Ni(II) ion with the $-COO^-$ in a bidentate bridging fashion, with sulphur in a monodentate bridging fashion and finally with the pyridinic nitrogen atom in a monodentate fashion.

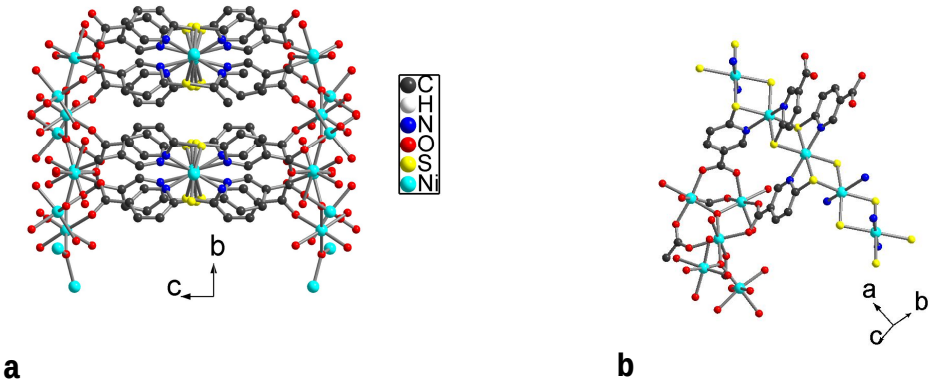


**Fig 5.1** $[Ni_9\text{-}(6\text{-mna})_8(\mu_3\text{-}O)_2(H_3O)_2(H_2O)_6]$: view of the crystal along a axis, b) extended asymmetric unit.

All these features, allowed by the polytopic nature of 6-mercaptonicotinic acid, lead to an interesting solid state arrangement where chains of octahedral Ni(II) linked via S monodentate bridges are connected to a pentanuclear Ni(II) cluster via bidentate bridging $COO^-$ groups in para position respect to thiolate group. The relative positions of functional coordinating group in 6-mercaptonicotinic acid determine the final topology of the complex. In the described example, the carboxylate moiety in para-position leads to a mixed chain- and cluster- topology which determines a spin canted system.

However, in literature examples of Ni(II) polymetallic complexes based on the isomer of 6-mercaptonicotinic acid, 2-mercaptonicotinic acid (2-mna), where –SH group is in ortho position with respect to the carboxylic function, are unknown to date. With Co(II) only a coordination compounds is reported [Humphrey, 2006], $[Co_4(2\text{-mna})_4(H_2O)]$ (Fig. 5.2).

In the asymmetric unity $[Co_4(2\text{-mna})_4(H2O)]$, each Co(II) ion is coordinated by the three S, O, and N donor atoms present in 2-mercaptonicotinate, that acts as a N,S,O tris chelating and O,O and S bridging ligand.

As it can be observed in Fig 5.2, a polymetallic chain is formed upon N,S,O chelation and S bridging coordination, while each chain is connected to the other via an O, O bridge.

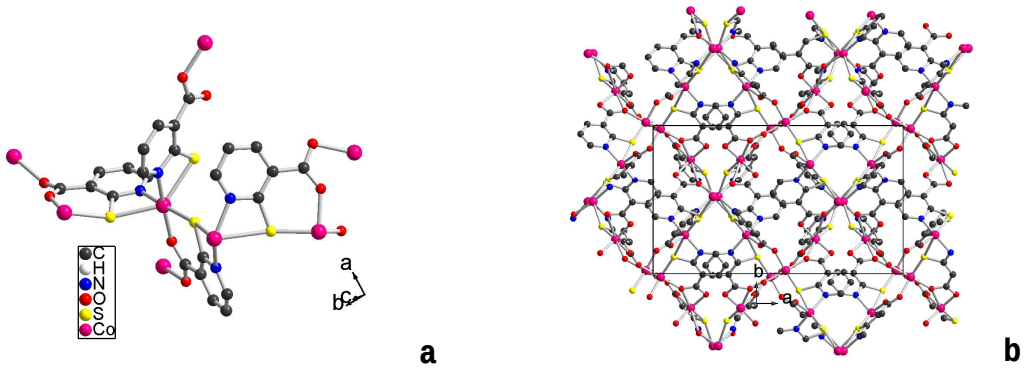


**Fig 5.2 a)**Extended asymmetric unity of $[Co_4(2\text{-mna})_4(H2O)]$ and **b)** of the crystal packing along c axis.

This leads to an interconnection between the chains in the three dimensions , as shown in Fig 5.2 b.

In this case, 2-mercaptonicotinate displayed a large variety of coordination modes and evidences a Co(II) affinity for all the three types of donor atoms.

Other examples featuring metals like Pt(II) and Pd(II) consist of trimeric species $[Pd_3$ (2-mna)3 $Cl_3$ ] and $[Pt_3$ (2-mna)3$Cl_3]$ [Polyhedron 1998 18 365 Marchal S et al], where the metal centers are coordinated in a S,N chelate fashion and the carboxylate groups remains uncoordinated.

This wide range of coordination modes displayed by 2-mercaptonicotinic acid are summarized in Scheme 5.1 [Gross, 2010]: (i) S, N donor chelate and carboxylic group

uncoordinated; (ii) S, N donor chelate and i) S, N donor chelate and carboxylic group uncoordinated; (ii) S, N donor chelate and carboxylic group in monodentate coordination mode; (iii) S, N donor chelate and carboxylic group in O,O-chelating mode; (iv) S-N donor chelate and S donor mode,non coordinated carboxylic group; (v) S, N donor chelate and carboxylic group in multidentate bridging coordination mode; (vi) S, O chelating mode and not coordinated nitrogen atom (vii) S, O bridging mode and non coordinated nitrogen atom.

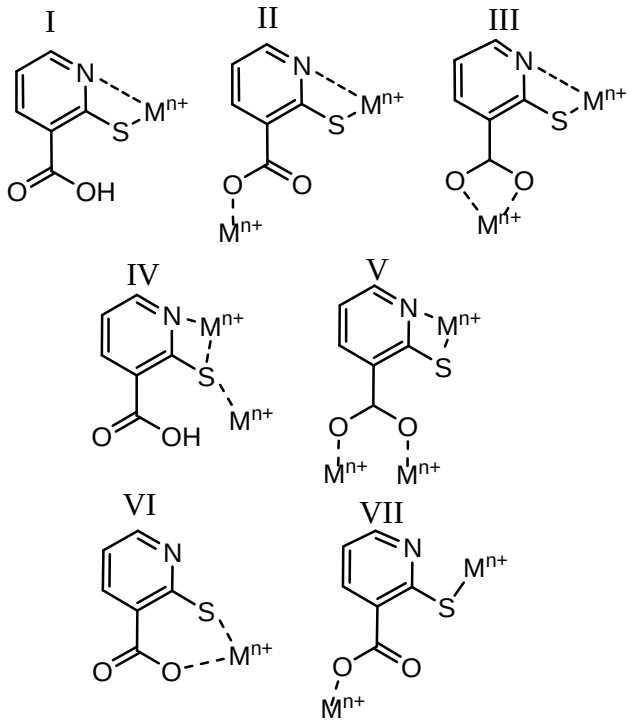


**Scheme 5.1** Coordination modes of 2 mercaptonicotinate ligand.

On account of these considerations, 2-mercaptonicotinic acid is an appealing possible ligand to build up metal complexes with 3d metals. The few examples reported in the literature with 2-mercaptonicotinic acid has prompted us to employ it to build up polymetallic complexes with Zn(II) and Ni(II) metals.

As far as the former metal is considered, several Zn(II)-based complexes and coordination polymers are known and characterised. Concerning this latter class of compounds, the $d^{10}$

metal ion $Zn^{2+}$ is particularly prone to form coordination polymers, since it can display coordination geometries different to the usual tetrahedral one, such as the octahederal, the trigonal-planar, the trigonal pyramidal, and the square pyramidal ones. Nicotinic acid has been already used as bi- and tridentate bridging units for the preparation of 3D Zn- and Cd based coordination polymers, whereas the formation of two isomorphous interpenetrating 2D frameworks of Cu and Zn by using a mixture of nicotinic and isonicotinic ligands has been reported.

Generally, Zn(II) based coordination polymers posses optical properties such as photoluminescence, displaying a blue emission at room temperature upon irradiation with UV light [inorg chem comm 2005 8 1165 YI Shang Song and related literature]. Coordination of such ligands to the $d^{10}$ metal ion Zn(II) makes this metal suitable for its exploitation in the synthesis of molecular functional materials. Furthermore, its redox stability and its versatility toward different coordination modes and toward different donor atoms make possible the design and the synthesis of polymetallic complexes without particular problems related to parassite redox reactions, for other metals (e.g. Cu(II)).

## 5.2 Synthesis and characterization of Zn(II) bis-mercaptonicotinate $[Zn(C_6H_4NO_2S)_2]$ and Zn(II) bis- hydroxynicotinate, $Zn(C_6H_4NO_3)_2(H_2O)_2$

The polymetallic Zn(II) complex $\{[Zn(C_6H_4NO_2S)_2]\}$ (named as Zn1) has been obtained via hydrothermal reaction of $[Zn(acac)_2]$ with 2-mercaptonicotinic acid in acqueous solution at 150°C (Scheme 5.2).

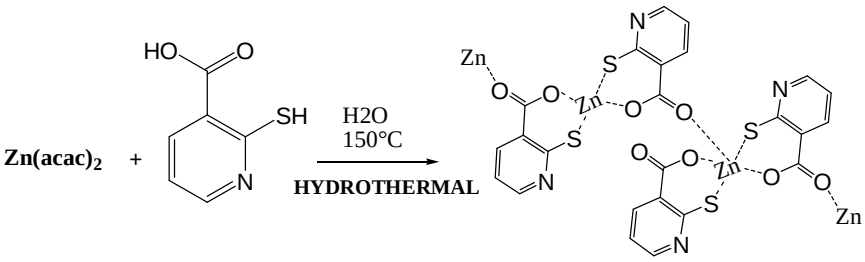


**Scheme 5.2**

Crystals of $[Zn(C_6H_4NO_2S)_2]$ were found after opening the reaction vessel together with a small amount of crystals of unreacted ligand 2-mercaptonicotinic acid.

**Zn1** is found to be insoluble in all solvents.

It should be highlighted that, a similar reaction performed by using the same amounts and molar ratios between the reactants by refluxing the suspension in water instead of using hydrothermal conditions, did not yield neither **Zn1** nor any other crystalline product. In fact, X-ray diffraction of the suspended solid reveals the presence of only unreacted ligand and $[Zn(acac)_2]$ while from the filtrate no crystaline products could be obtained.

This can be ascribed to the particular features of the hydrothermal synthesis, such as the possibility to achieve products which can be compositionally and structurally different from those obtained at room pressure. In fact, owing to the changes in the dielectric constant and viscosity of water, the increased temperature within a hydrothermal medium has a significant effect on the speciation, solubility, and transport of solids [ Hullinger, 1994; Byrappa, 2001; Sheets, 2006].

The use of other Zn(II) precursors within the same reaction conditions as for $[Zn(C_6H_4NO_2S)_2]$ led only to non crystalline powders. Increasing the reaction temperature up to 200-250°C in order to decrease the reaction time afforded only brown-black amorphous products which are indicative of the decomposition of the sulphur based ligand.

Furthemore, as mentioned in the introduction of this chapter, it should be also pointed out that similar reactions with redox active species such as Mn(II) and Cu(II) invariably

lead to the oxidation of the thiol group to give disulphide and, in the case of the reaction of $MnCl_2$ with the 2-mercaptonicotinic acid, the disulphide bridge formation was favoured over the formation of Mn-S bond [Humphrey, 2004].

In our study, the redox stability of Zn(II) was proved to play a key role in the formation of a coordination polymer where the ligand does not undergo oxidation and retains its integrity. This can be also partially be ascribed to the higher affinity of Zn for sulphur[Greenwood, 1990]: this "thiophilicity" can be invoked to explain the stability of the ligand in these conditions, since the thiolate is expected to be less susceptible of oxidation when coordinated to a transition metal.

For comparative purposes, the oxygen analog of 2-mercaptonicotinic acid, 2-hydroxynicotinic acid, was consider to investigate whether the same synthetic conditions used for $[Zn(C_6H_4NO_2S)_2]$, affords a similar coordination polymer.

Instead of the polymeric $[Zn(C_6H_4NO_2S)_2]$, the mononuclear complex $[Zn(C_6H_4NO_3)_2]$, named **Zn2** was obtained and identified by means of single crystal X-ray crystallography.

***Crystals structure of Zn1 and Zn2***

**Zn1** crystallizes in the monoclinic system, space group $P2_1/c$. Zn (II) cation and the two 2-mercaptonicotinate are in general positions. Zn(II) is coordinated by two ligand molecules in a O,S chelate fashion. Both ligands are roughly flat (angles between the aromatic ring and the carboxylate group are about 15° and 30°), and exhibit a protonated nitrogen atom, deprotonated oxygen and sulfur atoms. The coordination is completed by a carboxylic oxygen deriving from another $[Zn(C_6H_4NO_2S)_2]$ unity to give a distorted square pyramid coordination geometry, affording polymetallic chains along c axis (Fig 5.3).

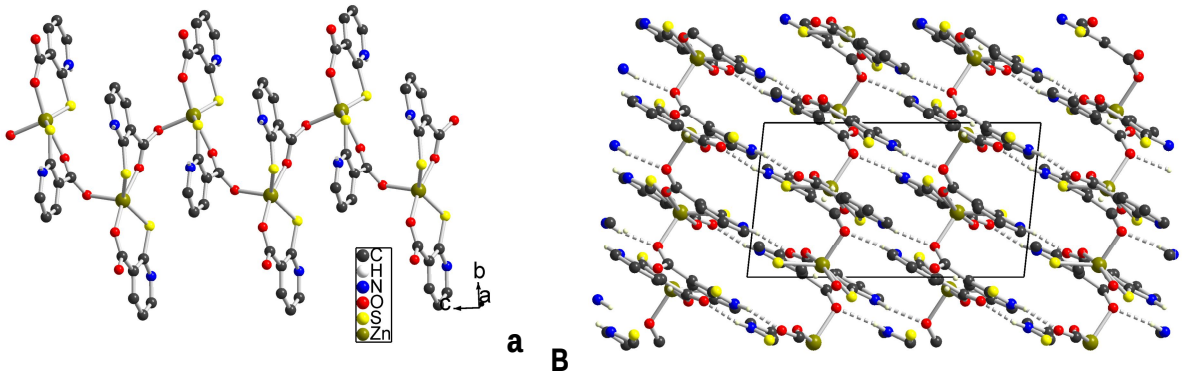


**Fig 5.3 a)**{[$Zn(C_6H_4NO_2S)_2$]}, a polymetallic chain
and **b)** view of the chains along b axis (dashed lines = hydrogen bondings)

These chains interact weakly through N-H···O hydrogen bonds (N···O = 2.845 and 2.730 Å, N-H···O = 152.4 and 154.1°), defining finally a three-dimensional hydrogen bonded network. In fig 5.4 hydrogen bonding within the chains are well visible.

Particularly, 6- membered rings of the type $ZnSOC_3$ are formed upon S,O chelation of 2 mercaptonicotinate to Zn(II) center. Within the chain, [$Zn(C_6H_4NO_2S)_2$] unities are staggered each other to give the zigzag array of the chain.

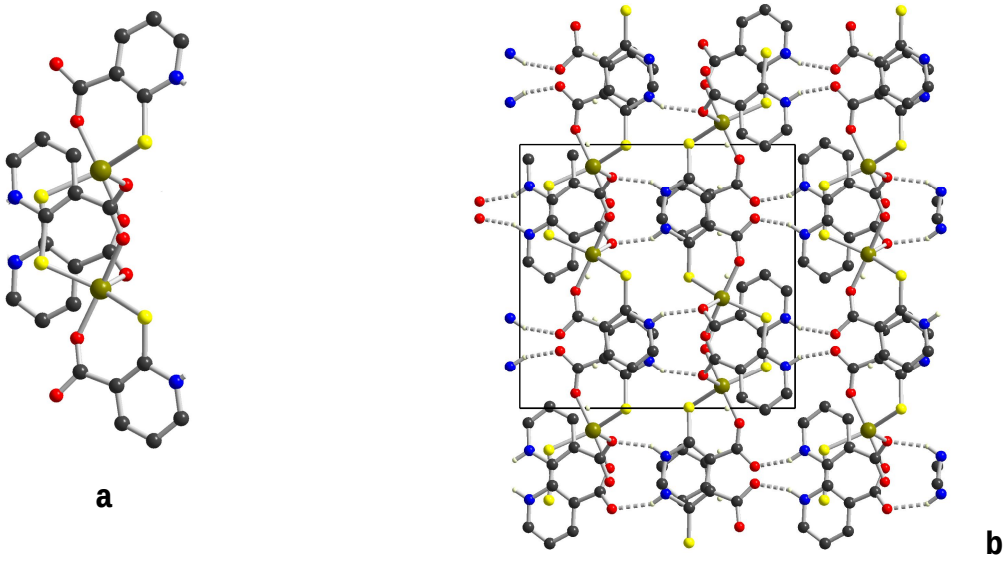


**Fig 5.4** view of {[$Zn(C_6H_4NO_2S)_2$]} chains along c axis: **a)** single chain and **b)** solid state arrangement of the chains by NH····H interactions.

It has to be mentioned that, by reacting Zn acetate with the 6-mercaptonicotinic acid, the ortho- isomer of 2-mercaptonicotinic acid, a completely different coordination fashion was achieved, characterized by the bifunctional ligand bridging two different zinc atoms with S,O donor atoms [Wang, 2008].

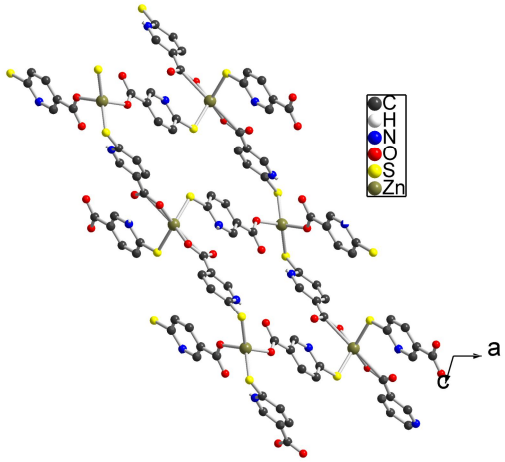


**Fig 5.5** Zn(II) bis-(6-mercaptonicotinate), a 3D coordination network.

In Fig 5.5, it can be observed that the by monoatomic bidentate bridging S¨Zn¨¨O a three dimensional coordination network is formed.

This indicates clearly that the two isomers, 2-mercaptonicotinic acid and 6-mercaptonicotinic acid lead to a different solid state arrangement because of the chelate- and monodentate coordination fashion of the first and the bidentate bridging of the second one. It has to be noted also that the nitrogen atom of the heterocycle is protonated in both cases.

The fact that no exhogenous base has been added to favor the deprotonation of the carboxylic group, together with the presence of the tautomeric equilibrium shifted to the thione form of 2-mercaptonicotinic acid has led to the structural features observed for Zn(II) bis-(2-mercaptonicotinate) and Zn(II) bis-(6-mercaptonicotinate). In principle, also the nitrogen atom of the aromatic ring of the ligand is coordinating, as it has been remarked in the introduction with the two examples of Co(II) and Ni(II) complexes with 2-mercapto- and 6-mercaptinicotinic acid.

The hydroxynicotinic complex **Zn2**, or Zn(II) bis-(hydroxynicotinate) is shown in Fig. 5.6.

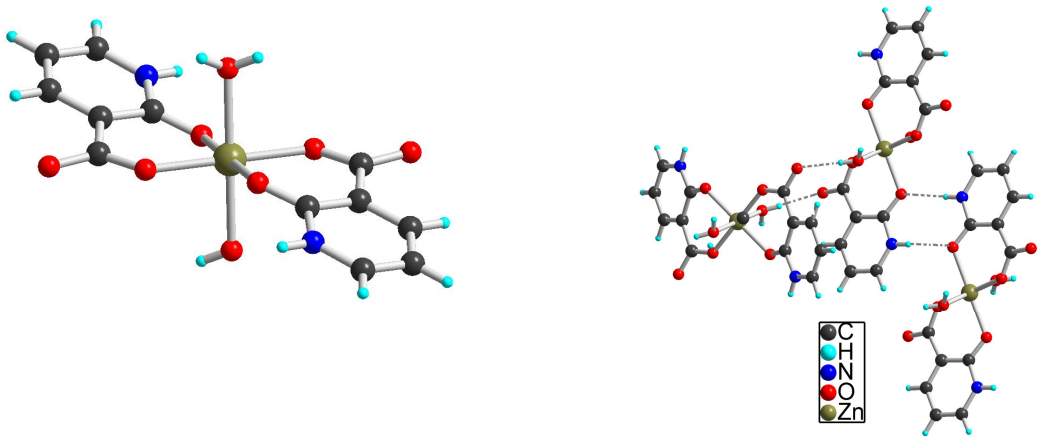


**a** **b**

**Fig 5.6 a**) $[Zn(C_6H_4NO_3)_2]$ and **b)** hydrogen interaction between three $[Zn(C_6H_4NO_3)_2]$

As can be observed in Fig 5.6 a), in this case a discrete monometallic Zn(II) complex was formed. $[Zn(C_6H_4NO_3)_2]$ crystallizes in the monoclinic system, space group P21/c. Zn(II) is located on an inversion center and the two hydroxynicotinate ligand are on general positions. Zn(II) shows an octahedral coordination geometry: the equatorial positions are occupied by two O,O chelating hydroxynicotinate ligands while two molecules of $H_2O$ complete the coordination in the apical positions. These 1:2 Zn : ligand complexes finally interact trough N-H···O (N···O = 2.893 Å, N-H···O = 162.7°) and O-H···O (O···O = 2.722 and 2.796 Å, O-H···O = 168.7 and 162.0°) hydrogen bonds along the *a* and *b*,*c* axes respectively, defining a three dimensional hydrogen bonded network (Fig 5.6b). This compound is isostructural with its known Ni, Co and Mn analogues. [Wagner L C 1975]

The Zn cation is 5-coordinated and lied out of the plane defined by the coordinating atoms of the ligands in $[Zn(C_6H_4NO_2S)_2]$, whereas it is 6-coordinated and lied in this plane in $[Zn(C_6H_4NO_3)_2]$; one-dimensional polymeric chains are present in $[Zn(C_6H_4NO_2S)_2]$, whereas only isolated molecular complexes form $[Zn(C_6H_4NO_3)_2]$. It is nevertheless difficult to conclude if these differences are related to the nature of the ligands, or are just serendipitous.

***XPS analysis of Zn1 and Zn2***

As already mentioned, the Zn atom in the compound **Zn1** is coordinated by both sulphur and oxygen atoms. X-ray data were then complemented with the outcomes of XPS measurements to get information about the chemical environment and the oxidation states of the different species (Zn, S, O, and N) in **Zn1** and **Zn2**. In Table 5.1, the binding energies (BE) of S2p, O1s, and N1s core levels in **Zn1 and Zn2** and in the free 2-mercaptonicotinic acid are reported together with the $Zn2p_{1/2}$ and $Zn2p_{3/2}$ BEs.

| **Sample** | **O1s (eV)** | **S2p (eV)** | **S2s (eV)** | **N1s (eV)** | **$Zn2p_{3/2}$ (eV)** |
|---|---|---|---|---|---|
| **2-mercaptonicotinic acid** | 532.2 | 161.8 | 226.0 | 400.2 | ----- |
| **Zn1** | 531.0 | 162.3 | 226.2 | 400.2 | 1021.1 |
| | 531.2 | - | - | 400.4 | 1021.9 |
| **Zn2** | 532.0 | | | | |
| | 532.5 | | | | |

**Tab.5.1** - BEs (corrected for charging effects) of the different elements.

Regarding the zinc atom, the BE of the $Zn2p_{3/2}$ region in **Zn1** has a BE of 1021.1 eV, which is lower than the BE reported for ZnS (1021.7-1022.0 eV)[NIST 2007] and more similar to those of ZnO (1021.1-1022.4 eV) [NIST 2007]. In Fig5 7, the Zn2p region of zinc in **Zn1** is shown, which displays the two component of the doublet due to the spin-orbit coupling. The Zn α parameter, determined as reported in literature,[Wagner L.C., 1975; Wagner L.C., 1975] resulted to be 2009.9 eV. This value is intermediate between those of Zn in ZnO (2009.5-2010.2 eV) and the values reported for ZnS (2010.3-2011.7 eV)[Wong J 2001] and in agreement with an "intermediate" state for the zinc atom, bonded to both oxgen and sulphur atoms.

Upon coordination of the zinc ion, both the S2s and S2p regions shift to higher BE with respect to the 2-mercaptonicotinic acid, passing from 226.0 to 226.2 eV and from 161.8 to 162.3 eV, respectively.

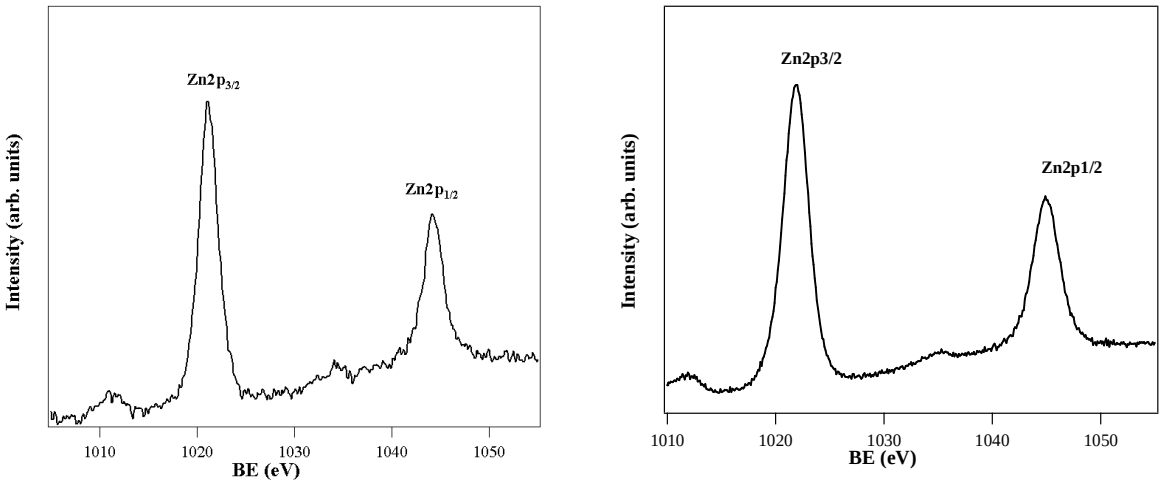


**Fig. 5.7.** Zn2p region of the complex **a) Zn1 b) Zn2** (BEs are corrected for charging effects)

The experimentally detected values are in good agreement with those reported for sulphur in ZnS (226.3 and 162.2-162.4 eV for S2s and S2p, respectively).

Conversely, the nitrogen N1s peak is not shifted, although the protonation observed in the crystal structure, and retains the same value of BE, i.e. 400.2 eV. This value, which is higher than the one reported for nitrogen in pyridine (399.0 – 399.3 eV),[Pietrzak, 2006; Lahaye, 1999] can be ascribed to the presence on the pyridinic ring of two carboxylic and thiol moieties, which could lead, the former to the formation of the zwitterionic form of the mercaptonicotinic acid, the latter to the protonation of the nitrogen by the thiol groups. Both events, causing the protonation of the nitrogen atom, would explain the higher BEs observed.

For complex **Zn2,** the $Zn2p_{3/2}$ is located at 1021.9 eV, a value very closed to the one reported for ZnO in literature.[Moulder J F 1992; NIST 2007] The Zn α parameter is 2009.0 eV and this value correspond to zinc in ZnO [Moulder J F 1992; NIST 2007] meaning that Zn(II) is coordinated by two oxygen atom and showing again the correlation between XPS analysis and single crystal diffraction measurment.

The **Zn2** O1s peak can be deconvolved in three different components at 531.2 eV, 532.0 eV and 532.5 eV (fig. 5.7b). The first two peaks at lower BEs are attribuable to the oxygen atoms of the ligand coordinated to the metal center. The one at higher BE derives from contaminants.

N1s is peaked at 400.4 eV, nearly the same value found for **Zn1**, because of the presence of protonated nitrogen in the heterocycle of the ligands, as unambigously observed by means of single crystal x ray diffraction.

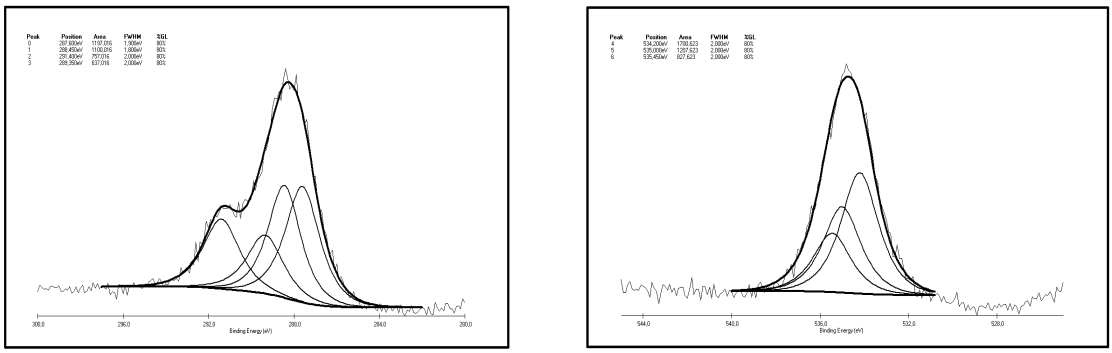

Fig 5.8**: a)** O1s and **b)**C1s deconvolved peak for **Zn2**

C1s region data was deconvolved in four components, 284.6 eV**,** 285.4 eV, 286.3 eV and 288.4 eV (Fig. 5.9b). Whereas the first one is adeventitious carbon, these last three values are attribuable to different carbon atoms present in the ligand in different chemical environments. On the basis of the different electronegativities of the heteroatoms in the ligand, peak at 288.4 eV corresponds to the carboxylic carbon, the α- and β- carbon are peaked at 286.3 while the three remaining carbons are at lower BE.

***Electronic properties of Zn1 and Zn2***

The electronic features correlated with S-Zn-O and O-Zn-O ligands were investigated by calculation of the electronic density of states with comparison with experimental XPS results [Gross, 2010]. The calculation have been done by A. Vittadini and M. Casarin from Padova UniversittIn Fig 8 DOS curves for Zn1 and Zn2 are reported

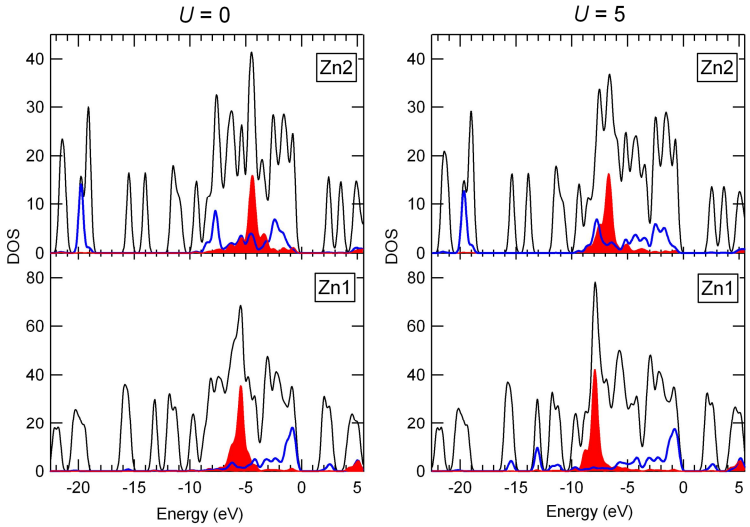


**Fig 5.9** DOS curves of **Zn2** and **Zn1** compounds. Relevant LDOS curves are also shown: red-filled regions are Zn states, while blue solid curves are sulphur and water LDOS in **Zn1** and **Zn2**, respectively. Electronic energies are referred to the valence band edge, so that only states with $E < 0$ are occupied. Left panel: GGA calculations; right panel: GGA+*U* calculations, with $U = 5$ eV.

The main difference between **Zn1** and **Zn2** is that in the former the top of the valence band is composed, as expected, by sulfur lone pairs, whereas in the case of **Zn2** it is composed by oxygen lone pairs. This has dramatic consequences on the band gap, which in the case of **Zn1** turns out to be narrower by ~0.5 eV. The bottom of the conduction band is essentially composed by ring $\pi^*$ combinations in both cases. A well known shortcoming of the application of currently available GGA (generalized gradient aproximation functionals to zinc compounds concerns the underestimation of the binding energy of the semicore Zn 3d levels. This gives rise to spurious interactions, and an artificial reduction of the band gap. A way to circumvent this problem is provided by the so-called GGA+*U* approach [Kharazanov, 2006] which consists in the application of a Hubbard *U* term [Anisimov, 1991]. The values of the *U* parameter are not only sensitive to the treated systems, but also to computational details, such as the adopted pseudopotentials, and should be determined from a self consistent procedure based on linear-response theory [Kulik, 2006]. In the present case, we simply used $U = 5$ eV, which is a typical value adopted in many GGA+*U* calculations, and seem to fit rather well the XPS experiments (Fig. 5.10 ). We emphasize that the effects of the GGA+*U* approach on the thermodynamical aspects discussed above is negligible. The GGA+*U* computed DOS

curves are shown in Figure 5.9, right: the main Zn 3d peaks of the **Zn1** and **Zn2** compounds are shifted towards higher binding energies by ~2.5 eV, and their shapes become more similar.

On the basis of the GGA+*U* results, *theoretical* valence band photoemission spectra were obtained by computing weighted density of states (WDOS) curves. This was made by weighting the GGA+*U* levels by the photo-ionization cross sections and using tabulated data for the atomic sub-shell cross sections [ Yeh. 1985]. A 0.7 eV Gaussian broadening has been adopted in order to match the resolution of the experiment.

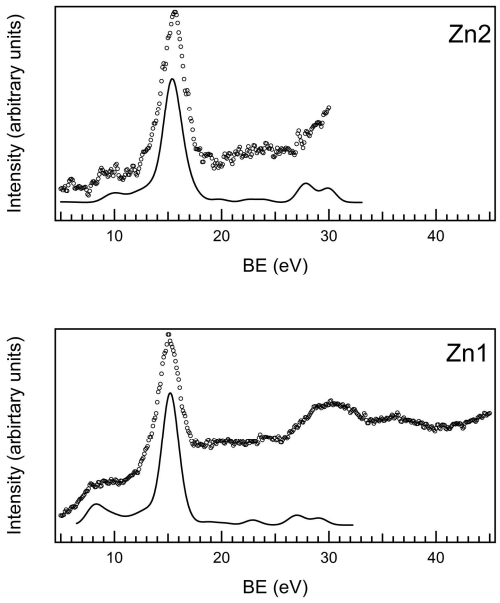


**Fig 5.10** Valence XPS regions (circles) compared with theoretical WDOS curves (see text, solid lines) for (top) **Zn2** and (bottom) **Zn1** compounds. The WDOS curves have been obtained from the GGA + *U* eigenvalues, applying a 0.7 eV Gaussian broadening. The energy scales of the WDOS curves have been shifted to align the maxima of the main peaks.

The WDOS curve and the Al K$\alpha$ XPS spectrum of **Zn1** are compared in Figure 5.10 (bottom). Both curves show a prominent peak, used to align the theoretical and the experimental curves, ascribed to the emission from the Zn 3d states on the basis of the Löwdin population analysis. Theoretical calculations also allow to assign the weak peak which marks the onset of the photoemission of **Zn1** at about 8 eV and absent in **Zn2**

(figure 5.10 top), to the ionization from the sulfur lone pair levels. Accordingly, the band gap is computed to be narrower on passing from **Zn2** to **Zn1** (2.50 eV vs. 2.19 eV).

***TGA and DSC analysis of Zn1 and Zn2***

The synthesis of complexes such $[Zn(C_6H_4NO_3)_2]$ and $[Zn(C_6H_4NO_2S)_2]$ is motivated not only by a systematic investigation of the possible topologies that a coordination compound can assume by changing the metal center and/or the ligand involved but the final (and most ambitious) aim is focused on the functional properties and the possibility of creating molecular-based materials or nano structured materials starting from such coordination compounds.

The thermal behaviors of Zn1 and Zn2 were investigated envisaging their possible exploitation as single source precursors for one step synthesis of nanostructured ZnO and $ZnO_xS_y$ materials by controlled calcination.

Particularly, TGA and DSC analysis were performed on both **Zn1** (air and $N_2$ atmosphere) and **Zn2** (air)**,** from 30°C to 800°C.

For **Zn1**, as it can be seen in Fig. 5.11a, the compound presents a clear decomposition pattern consisting of different steps.

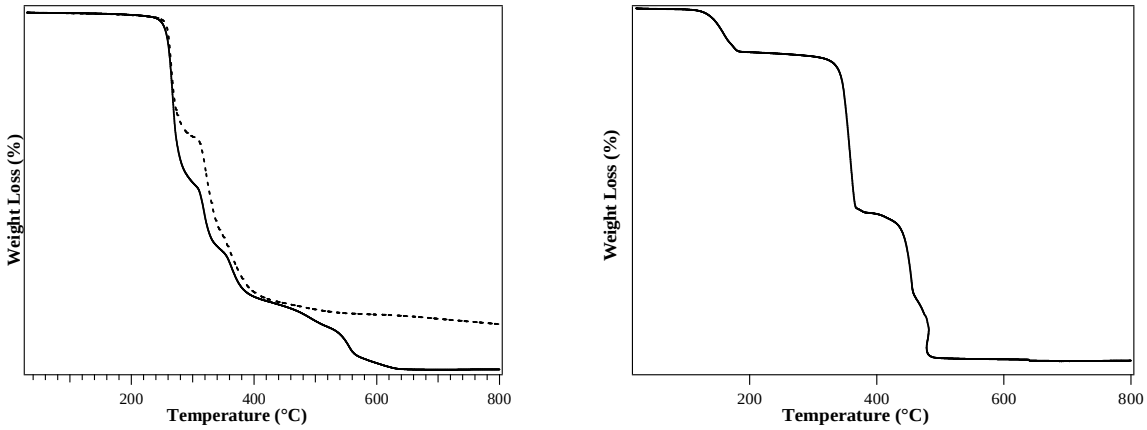


**Fig. 5.11** Thermo-gravimetric curves **a)** for **Zn1** in air (continuous line) and in $N_2$ atmosphere (dashed line), **b)** for **Zn2** in air.

Thermal decomposition in air starts, in the thermal range 200°C - 300°C and a weight loss of 41% was detected. From 300°C up to 423°C a further loss of 13% are detected. From 420°C to 605°C two further losses of 16% and 13% respectively, were observed. A last decomposition step was observed from 420°C up to 600°C. The polymeric nature of **Zn1** must be taken into account to justify the presence of multiple-weight losses. In fact, the simple complex $Zn(C_6H4NO_2S)_2$, obtained by precipitation from the zinc salt, decomposes to ZnO in a single [Yang, 2007; Chen, Gao, 2007].

In nitrogen atmosphere, the decomposition path is of course different and it occurs in three different thermal ranges:. 250°C-300°C, 300°C-350°C and 350°C-400°C. At 800°C the residual mass was 25.7 % in agreement with the formation of ZnS.

Complex **Zn2** exhibits a four steps decomposition path when treated in air. The first one occurs in the range between 100°C and 200°C and it corresponds to the loss of the water molecules present in the complex. A second loss appears in the range 200°C-400°C and it is attributable to thermolysis of the ligand. The other two steps are comprised between 400°C and 500°C with a remaining weight of 21.8%, corresponding to the final formation of ZnO.

The formation of ZnS and ZnO in the case of **Zn1** and **Zn2** respectively, proves that the two complexes can be used as single-source molecular precursors for the formation of nanostructured ZnS and ZnO upon changing the annealing conditions. Further investigations are in progress for what concerns the naostructured nature of ZnS and ZnO formed using this single-source precursors.

***DFT calculations: Structure and Stability***

The stability of the complexes was studied via periodic DFT calculations carried out by M. Casarin and A. Vittadini, University of Padova, not only on the $[Zn(C_6H_4NO_2S)_2]$ (**Zn1**) and $[Zn(C_6H_4NO_2S)_2]$ (**Zn2**) compounds, but also on their unknown analogues, i.e. the hydrated derivative of **Zn1,** isostructural with $[Zn(C_6H_4NO_2S)_2]$ and hereafter indicated **Zn1-hyd**, and the dehydrated derivative of **Zn2,** isostructural with **Zn1**, hereafter indicated as **Zn2-dry**). The theoretical constants fairly agree with the experimental ones, the largest (but still acceptable) deviations being found for c (-3% and -5% for **Zn1** and **Zn2**, respectively).

| | | *a* | *b* | *c* | *в* |
|---|---|---|---|---|---|
| **Zn1** | Theor | 13.100 (-2.3%) | 12.829 (+0.1%) | 7.278 (-3.0%) | 93.9 |
| | Exptl | 13.403 | 12.843 | 7.501 | 96.3 |
| **Zn1-hyd** | Theor | 8.615 | 12.466 | 7.268 | 103.0 |
| **Zn2** | Theor | 7.554 (+0.9%) | 12.224 (-0.8%) | 7.244 (-5.0%) | 102.3 |
| | Exptl | 7.485 | 12.332 | 7.626 | 100.6 |
| **Zn2-dry** | Theor | 12.495 | 12.393 | 7.476 | 93.5 |

**Table 5. 2** Theoretical unit cell parameters for the examined compounds (see text). deviations from experimental values are indicated in parentheses

Similar result has been already found previously [Bencini A 2009], and is due to the overestimation of the dispersion interaction obtained when the Grimme parameterization is used in solid systems. From a qualitative point of view, it is easy to explain why the hydrated form is preferred for the hydroxynicotinic complex, whereas the anhydrous form is preferred for the mercaptonicotinic complex. In fact, replacing the hydroxynicotinic ligands of **Zn2** by mercaptonicotinic ligands as in **Zn1-hyd** implies that the N-H···O hydrogen bonds are turned into the substantially weaker N-H···S interactions. In contrast to that, no significant differences can be found in the interactions occurring in the **Zn1-dry** and **Zn2-dry** compounds. In this regard, it could be interesting to consider the hydration/re-hydration process in which the **Zn1** is converted to **Zn1-hyd** and **Zn2** in **Zn2-dry.** This could be done by so-called atomistic thermodynamics, where the information derived by DFT total energies is employed to compute thermodynamic potential functions. [Reuter, 2005] In synthesis, we consider the process:

$$\mathbf{X}\,(s) + 2H_2O(g) \rightarrow \mathbf{X}(H_2O)_2\,(s) \qquad (1)$$

where **X** and **X**$(H_2O)_2$ are the anhydrous and hydrated form of the hydroxy-/meracpto-nicotinate complexes, respectively. At given (*T*,*p*) conditions, the equilibrium of (1) is fixed by the Gibbs energy, defined as:

$$\Delta G\ (T, p_{\mathrm{X(H_2O)_2}}, p_X, p_{\mathrm{H_2O}}) = g_{\mathrm{X(H_2O)_2}}(T, p_{\mathrm{X(H_2O)_2}}) - g_X(T, p_X) - 2\mu_{\mathrm{H_2O}}(T, p_{\mathrm{H_2O}}) \qquad (2)$$

For practical purposes, we can neglect the solid/gas equilibrium of the complexes, as well as the entropy differences between them. We note that the latter assumption implies that the entropic contribution by the vibrations of the lattice-included water molecules are negligible. This approximation is in general quite acceptable at RT [Law J. T. 1955]. Under the above enumerated assumptions, the molar free energies of the condensed phases can be replaced by the DFT total energies:

$$\Delta G\ (T, p_{\mathrm{H_2O}}) = E_{\mathrm{X(H_2O)_2}} - E_X - 2\mu_{\mathrm{H_2O}}(T, p_{\mathrm{H_2O}})\,. \qquad (3)$$

Furthermore, we estimate $\mu_{\mathrm{H_2O}}(T, p_{\mathrm{H_2O}})$ as follows:

$$\mu_{H_2O}(T, p_{\mathrm{H_2O}}) = E_{\mathrm{H_2O}} + \tilde{\mu}_{\mathrm{H_2O}}(T, p^0) + k_B T \ln\left(\frac{p_{\mathrm{O_2}}}{p^0}\right), \qquad (4)$$

where $E_{\mathrm{H_2O}}$ is the DFT total energy of a water molecule computed in a large supercell, while $\tilde{\mu}_{\mathrm{H_2O}}(T, p^0)$ includes contributions from rotations and vibrations of the molecules, as well the entropy of the ideal gas at $p^0$ = 1 atm, and it can be obtained from tabulated data.

On applying Eq. (3) at *T* = 300 K we compute that the hydrated form of the mercaptonicotinic complex is unfavored with respect to the dehydrated form **Zn1** even at a $p_{\mathrm{H_2O}}$ = 1 atm, whereas at the same temperature the hydroxynicotinic complex **Zn2** is stable against dehydration for water partial pressures as low as $10^{-6}$ atm. Even at 400 K, water partial pressures lower than $10^{-2}$ atm are needed to dehydrate **Zn2**.

These results are compatible with TGA measurments for **Zn2**, where the water loss is between 100°C and 200°C as it is described in the part of thermal behaviour.

## 5.3 Synthesis of a Ni(II) bis-mercaptonicotinate complex $[Et_4N]_2[Ni(C_6H_3NO_2S)_2]$

Prompted by the results obtained by reacting Zn(II) with 2-mercaptonicotinic acid, we have envisaged the possibility of building up also polymetallic Ni(II) chains by using 2-mercaptonicotinic acid as ligand.

To date, the investigated systems with 2-mercaptonicotinic acid as ligand involve metals such as manganese and cobalt [Humphrey, 2006; Humphrey, 2004 ], even if the presence of a redox active metal such as manganese leads to the formation of the disulphide. The same problem was verified with Cu(II), in principle another interesting paramagnetic metal able to assume many coordination geometries.

For these reasons, Ni(II) was choseen as a good candidate for the synthesis of complexes with magnetic properties. In the same reaction conditions as for $[Zn(C_6H_4NO_2S)_2]$, Ni(II) did not afford any crystalline product.

Analogously, further attempts carried out using different precursors ($Ni(OAc)_2$, $NiCl_2$) or a base to deprotonate the acid , did not afford neither crystalline products nor precipitates which could be redissolved. Different experimental conditions are summarized on Table 3

| **Ni(II) source** | **Solvent** | **Temperature** | **Time** |
|---|---|---|---|
| $NiCl_2 \cdot 6H_2O$ | $H_2O$ | 130°C solvothermal | 26 h |
| $NiCl_2 \cdot 6H_2O$ | $CH_3CN$ | 100°C solvothermal | 26 h |
| $NiClO_4 \cdot 6H_2O$ | $CH_3CN$ | 25°C | 24 h |
| $NiCl_2 \cdot 6H_2O$ | MeOH | 25°C | 22 h |
| $NiCl_2 \cdot 6H_2O$ | $H_2O$ | 25°C | 26 h |

**Table 5.3** Experimental conditions investigated with Ni(II) and 2-mercaptonicotinic acid

In all these cases, slow evaporation of the solvent led to a dark green oil soluble only in DMF. After several crystallization attempts using different co–solvents, prismatic deep-

red crystals appeared after 14 days upon slow diffusion of acetone vapors on DMF solutions or simple slow diffusion.

The crystals were characterized by means of X-ray single crystal diffraction and they were identified as compound $[Et_4N]_2Ni((C_6H_3NO_2S)_2]$(Fig 5.11).

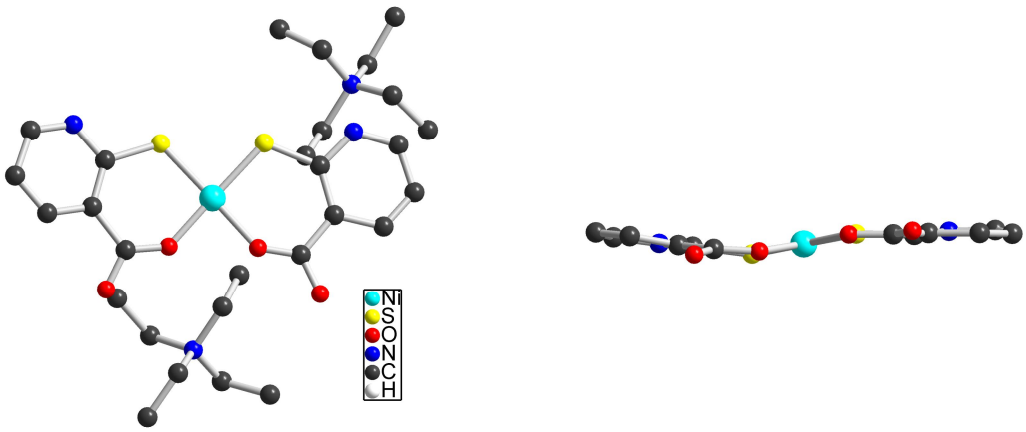


**Fig 5.11** Complex $[Et_4N]_2Ni((C_6H_3NO_2S)_2]$

However, this structure has been solved but not fully refined because of problems related to the twinning.

As it can be observed from fig 5.11,, the 2 mercaptonicotinate ligand coordinates Ni(II) in a S,O chelate fashion, as observed for $[Zn((C_6H_3NO_2S)_2]$ giving a square planar coordination geometry around the metal centre and, consequently, $[Ni((C_6H_3NO_2S)_2]^{2-}$ is diamagnetic. The N atoms of the heterocycles are deprotonated,and this justifies the presence of two $Et_4N^+$ cations balancing the charge.

Once red crystals are exposed to air, it was observed that after 2 days they become a greenish oil similar to the one obtained by slow evaporation of the solvent. This could be ascribed to possible hydration processes.

At the moment, further characterization such XPS analysis are in progress also to compare this system with $[Zn((C_6H_3NO_2S)_2]$.

As it can be verified in Table 5.11, $[Ni((C_6H_2NO_2S)_2]^{2-}$ forms already at room temperature, without need of hydro- or solvo-thermal conditions. Probably the solvo-thermal conditions chosen are not enough harsh to allow the formation of other Ni(II) 2-mercaptonicotinate complexes with different topologies. In fact, it has to be marked that by using the same conditions as for $[Zn((C_6H_3NO_2S)_2]$ no crystalline products were obtained.

This kind of synthesis required a systematic investigations and careful must be taken by the variation of the different parameters. In this case for example, the fact that pyridinic nitrogen was not protonated leads to the structure seen above. In $[Zn((C_6H_3NO_2S)_2]$, Zn(II) charge is already balanced by the two ligands, whereas $[Ni((C_6H_2NO_2S)_2]^{2-}$ needs two counter cations to be balanced. This factor is of great influence in the solid state arrangement favoring the co-crystallization of a single $[Ni((C_6H_2NO_2S)_2]^{2-}$ unity with two $Et_4N^+$ counter cations.

## 5.4 Conclusions

Two metal were investigated toward the coordination of 2-mercaptonicotinic acid.

This ligand posses three different donor atom: nitrogen, oxygen and sulphur.

The synthesized complex $[Zn((C_6H_3NO_2S)_2]$ is a coordination polymer where the Zn(II) centers are S,O chelated by 2-mercaptonicotinate and μ-O bridged by the other oxygen of 2-mercaptonicotinate acid. The complex $[Zn((C_6H_3NO_3)_2,$ obtained from 2-hydroxynicotinic acid is a monometallic complex, in contrast for the 2-mercaptonicotinic derivative.

Ni(II,) in the same synthetic conditions affords only non crystalline products. It is possible to obtain the mononuclear planar $[Et_4N]_2[Ni((C_6H_3NO_2S)_2]$ by changing the reaction conditions but, unfortunately, to date we are not able to refine the crystal structure.

The chemical environment was investigated by means of a combined spectroscopic and theoretical study for both $[Zn((C_6H_3NO_2S)_2]$ and $[Zn((C_6H_3NO_3)_2]$. The core level binding energies for the two different O-Zn-O and S-Zn-O coordination situations were measured by XPS and the values found are in very good agreement with the theoretical outcomes,

providing insight into the differences between [Zn(($C_6H_3NO_2S)_2$] and [Zn(($C_6H_3NO_3)_2$] including structures, stability and electronic properties.

**Bibliography**


Abu-Youssef, M. A. M. *Polyhedron* **2005**, *24*, 1829.

Barone, V.; Casarin, M.; Forrer, D.; Pavone, M.; Sambi, M.; Vittadini, A. *J. Comput. Chem*., **2009**, *30*, 934

Baroni, S.; Dal Corso, A.; de Gironcoli, S.; Giannozzi, P.; Cavazzoni, C.; Ballabio, G.; Scandolo, S.; Chiarotti, G.; Focher, P.; Pasquarello, A.; Laasonen, K.; Trave, A.; Car, R.; Marzari, N.; Kokalj, A. http://www.quantum-espresso.org/.

Batten, S. R.; Robson, R. *Angew. Chem. Int. Ed.* **1998**, *37*, 1460;

Bencini A.; Casarin, M.; Forrer, D.; Franco, L.; Garau, F.; Masciocchi, N.; Pandolfo, L.; Pettinari, C.; Ruzzi, M.; Vittadini, A. *Inorg. Chem.* **2009**, *48*, 4044.

Bernasconi, M.; Chiarotti, G. L.; Focher, P.; Scandolo, S.; Tosatti, E.; Parrinello, M. *J. Phys. Chem. Solids* **1995**, *56*, 501

Briggs, D.; Seah, M. P. *Practical Surface Analysis*, J. Wiley & Sons, **1990**.

Byrappa, K.; Haber, M. *Handbook of Hydrothermal Technology - Technology for Crystal Growth and Materials Processing*, William Andrews Puiblisjhing-Noyes, **2001**.

Chen, H-J. *Acta Cryst.* **2005**, *E61*, m616;

Chen, T-C.; Chin, Suslick, K. S. *Coord. Chem. Rev.* **1993**, *128*, 293.

Cindric, M.; Strukan, N.; Kajtez, T.; Kamenar, B.; Geister, G.; *Z.Anorg. Allg. Chem.***2001**, *627*, 2604;

Erxleben, A. *Coord. Chem. Rev.* **2003**, *246*, 203,

Goodman, D. C.; Farmer, P. J.; Darensbourg, M. Y.; H. J. Reibenspies *Inorg. Chem.* **1996**, *35*, 4989;

Grimme, S. J. Comput. Chem., **2006**, 27, 1787

Gross, S. *Inorg. Chem.* **2010**, 49, 4099

Holleman, A. F.; Wiberg, E. *Lerhrbuch der Anorganischen Chemie*, 101. Edition, **1995** W. De Gruyter, Berlin

Hong, M. *Crystal Growth & Design* **2007**, *7*, 10;

Hullinger, J., *Angew. Chemie* **1994**, *106*, 151;

Humphrey, S. M.; Mole, R. A.; Rawson, J. M.; Wood, P. T. *Dalton Trans.* **2004**, 1670;

Humphrey, M.S. et al *Inorg. Chem.* **2005**, 44, 5981

Humphrey, M.S. *Chem. Comm.* **2006,** 1607

Janiak, C. *Dalton Trans.* **2003**, 2781;

K. Reuter, C. Stampfl, and M. Scheffler, "Ab Initio Thermodynamics and Statistical Mechanics of Surface Properties and Functions". In: S. Yip (ed.), *Handbook of Materials Modeling, Part A. Methods*, Springer, Berlin (**2005**)

Khandwe, M.; Bajpai, A.; Bajpai, U. D. N. *Polymer Bull.* **1990**, *23*, 51.

Kitagawa, S.; Kitaura, R.; Noro, S. *Angew. Chem. Int. Ed.* **2004**, *43*, 2334;

Kitagawa, S.; Noro, S. *Comp. Coord. Chem. II* **2004**, *7*, 231;

Lahaye, J.; Nanse, G.; Bagreev, A.; Strelko, V. *Carbon* **1999**, *37*, 585.

Law, J. T. *J. Phys. Chem*. **1955**, *59*, 67

Li, F.; Wang, Y.; Li, G.; Sun, Y.; Gu, X.; Gao, E. *Inorg. Chem. Comm.* **2007**, *10*, 767.

Li, Y.-M. Che, Y.-X. , Zheng, J.-M. *Chin. J. Struct. Chem.* **2006**, *25*, 572.

Lin, W.; Evans, O. R.; Xiong, R-G.; Wang, Z. *J. Am. Chem. Soc.* **1998**, *120*, 13272;

Lu, J.; Zhao, K.; Fang, Q-R.; Xu, J-Q.; Yu, J-H.; Zhang, X.; Bie, H-Y.; Wang, T-G. *Cryst. Growth Design* **2005**, *5*, 1091;

Marchal, S. et al. *Polyhedron* **1998,** 18, 365

Maspoch, D.; Ruiz-Molina, D.; Veciana, J. *J. Mat. Chem.* **2004**, *14*, 2713;

Monkhorst, H.; Pack, J. *Phys. Rev. B* **1976**, *13*, 5188

Moulder, J. F.; Stickle, W. F.; Sobol, P. E.; Bomben, K. D. *Handbook of X-Ray Photoelectron Spectroscopy*, J. Chastain, Perkin-Elemer Corp. Eden Prairie, **1992**.

Na X., Wei, S., Dai-Zheng, L.*, Shi-Ping, Y., Peng, C. I*norg. Chem.* **2008**, 47, 8748–8756

Nakamoto, K. *Infrared Spectra of Inorganic and Coordination Compounds,*J. Wiley and Sons: New York **1997;**

NIST Standard Reference Database 20, Version 3.5, **2007**, http://srdata.nist.gov/xps***/***

NIST-JANAF Thermochemical Tables**,** Fourth edition, *Journal of Physical and Chemical Reference Data*, Monograph 9 (**1998**)

Perdew, J. P.; Burke, K.; Ernzerhof, M. *Phys. Rev. Lett.* **1996**, *77*, 3865

Pietrzak, R.; Wachowska, H.; Nowicki, P.; *Energy & Fuels* **2006**, *20*, 1275;

Quintal, S.M.O.; Nogueira, H.I.S.; Félix, V.; Drew M.G.B. *J. Chem. Soc. Dalton Trans.* **2002**, 4479-4487.

Robin, A. Y.; Fromm, K. M. *Coord. Chem. Rev.* **2006**, *250*, 2127;

Sheets W. C., Mugnier E., Barnabé A., Marks T.J., Kenneth R. Poeppelmeier K. R. Chem. Mater **2006**, 18, 7.

Shirley, A. *Phys. Rev. B* **1972**, *5*, 4709.

Socrates, G. *Infrared and Raman Characteristic Group Frequencies*; J Wiley and Sons Ltd:Chichester, **2001**

Toma, M.; Sanchez, A.; Garcia-T., Maria S.; Casas, J. S.; Sordo, J.; Castellano, E. E.; Ellena, J. *Central Europ. J. Chem.* **2004**, *2*, 534-552

Vanderbilt D. Phys. Rev. B **1990**, 41, 7892

Wagner, C. D. *Anal. Chem.* **1975**, *47*, 1201.

Wagner, C. D. *Faraday Discuss. Chem. Soc.* **1975**, *60*, 291;

Wang, Y.; Zhu, D-H.; Su, Z-M.; Shao, K-Z.; Zhao, Y-H. *Acta Crystall. C* **2008**, *C64,* m70;

Wen, D.C., Liu, S.-X., *Chin. J. Struct. Chem.* **2007**, *26*, 1281,

Wong, J. W. L.; Sun, W. D.; Ma, Z. H.; Sou, I. K. *J. Electr. Spectr. Relat Phenom.* **2001**, *113*, 215.

Yang, Q., Chen, S., Gao, S., *J. Therm Anal. Cal.* **2007**, *90*, 881-885

Zaworotko, M. J. *Chem. Commun.* **2001**, *37*, 1.

Zeng, M.-H., Wu, M.-C., Zhu, L.-H., Liang, H., Yang, X. W., *Chin. J. Chem.* **2007**, *25*, 16,

Zhou, Y.; Hong, M.; Wu, X. *Chem. Comm.* **2006**, 135;

Zyss, J. *Molecular Non-Linear Optics: Materials, Physics and Devices*, Academic Press, New York, **1993**

YI Shang Song *Inorg. Chem. Comm.* **2005**, 8, 1165

# General **Conclusions**

In this work, new transition metal complexes with thiolate and dithiolene ligands have been synthesized and characterized, exploring the versatility of these sulphur based ligands towards metal complexation.

"Classic" paramagnetic metal bis-dithiolene complexes such as $[Cu(mnt)_2]^{2-}$ , $[Cu(tfadt)]^{2-}$, $[Ni(dmid)_2]^{\cdot-}$ have been investigated as metallo-ligands towards the complexation of cationic Mn-based building characterized by a paramagnetic ground. In the case of $[Ni(dmid)_2]^{\cdot-}$ , dimerization processes allows to obtain trinuclear compounds of general formula $[Mn(TPP)(S)][Mn(TPP)(H_2O)][Ni_2(tto)(dmid)_2]$ and their magnetic behaviour correspond to two isolated spin S=3.

$[Cu(mnt)_2]^{2-}$ , $[Cu(tfadt)]^{2-}$ complexes were investigated with Mn(III)-salen derivatives, in order to build up polymetallic complexes of the type Cu—Mn---Cu through –CN—Mn(III) interactions. However, we have demonstrated by isolating mixed metal Mn/Cu salen complexes that $[Cu(mnt)_2]^{2-}$ can undergo ligand exchange reaction in the presence of the Mn(III) salen derivatives because of their quasi-planar coordination geometry. Only in the case of $[Mn_2\ (saltmen)_2]^{2+}$ the ligand exchange did not occur because of the relatively fast co-crystallization of $[Mn_2\ (saltmen)_2\ (CH_3CN)][Cu(mnt)_2]$. Taking into account this reactivity, we have switched to another Mn based complex characterized by the mixed valence Mn(II)Mn(III) cationic unity $[Mn_4hmp_6]^{4+}$ . By adding $[Cu(mnt)_2]^{2-}$ and $[Cu(tfadt)_2]^{2-}$ after the formation *in situ* of the cationic $[Mn_4hmp_6]^{4+}$ compounds $[Mn_7(hmp)_{12}][Cu(tfadt)]$ and $[Mn_7(hmp)_{12}][Cu(mnt)_2]$ have been isolated in the major crystalline products, indicating the presence of higher nuclearity Mn species in solution and showing the modest coordination ability of the –CN group of the dithiolene moiety. However, even if $Mn_7$ species with $hmp^-$ ligand are known, the $[Mn_7(hmp)_{12}]^{4+}$ has never been reported before in the literature. Further magnetic investigation are in progress in order to investigate the magnetic behaviour of this new complex.

These investigation prompted us to synthesized a new class of coordinating 1,2 dithiolato ligands and the related paramagnetic Ni complexes. These complexes are appealing for the synthesis of polynuclear complexes because they bear crown ether macrocycles as substituent groups. By varying their size it is also possible to modulate the metal

selectivity. Polymetallic chains have been synthetized with $Na^+$ ions and $Ni^{2+}$ ions, opening new perspectives in the field of metal bis-dithiolenes as metallo-ligands. Particularly, an anomalous magnetic behaviour has been observed for the $–Ni^{2+}$ based chains and we hypotized a strong antiferromagnetic interaction between spin S=1/2 dithiolene complexes. A bimetallic Ni complex has been obtained employing a smaller crown ether macrocycle. By varying the source of Ni(II) precursor, we can switch between the bimetallic Ni-Ni complexes and a simple co-crystallization product between $[Ni(dithiolene)]^{-}$and $Ni(S)_6$ cation, elucidating the chemistry associated with the formation of polynuclear compounds in order to improve new synthetic methods to obtain higher nuclearity complexes. Such systems are still under investigation because of their peculiar magnetic properties and of their structural features.

In the last chapter, the thiolate base-ligand 2-mercaptonicotini acid has been investigated toward coordination of Zn(II) and Ni(II) ions. For the former, a coordination polymer with an unusual square planar geometry on Zn(II) was obtained. The electronic properties correlated to the formation of the O-Zn-S bons have been investigated by theoretical calculations and experimental measruments. The coordination chemistry associated to 2-mercaptonicotinic acid was investigated with Ni(II) obtaining a discrete bis-mercaptonicotinato complex, even at hydrothermal conditions.

Attempts to obtain a Ni(II) based coordination polymer, appealing especially for the magnetic properties associated with an octahedral Ni(II) are on progress.

The chemistry of transition metal complexes with sulphur ligands continues to be an exciting research area. Even if many of them are already known and well characterized, their functional properties are still under investigation for what concerns molecular based materials, especially when properties related to electronic conduction are considered.

However, in the field of molecular magnetism, examples where discrete metal complexes or coordination polymers with sulphur based-ligands are still in low number with respect to the oxygen and nitrogen analogous. Even if the electronic features associated with sulphur, for instance the bigger polarizability and the presence of many stable oxidation states, make sulphur donor ligands suitable for the design and the synthesis of complexes for magnetic materials, their chemistry has not been fully explored.

## Experimental

$[Mn_7(hmp)_{12}][Cu(tfadt)_2]_2(CH_3CN)$

0.58 g (1.61 mmol) of $Mn(ClO_4)_2 \cdot 6\ H_2O$ were dissolved in 20 ml of $CH_3CN$. 0.45 g (4.08 mmol) of Hhmp were then added and the resulting solution was stirred for 5 minutes. 0.30 g (0.81 mmol) of $Me_4NOH$ (25% MeOH solution) were finally added to give a deep red-coloured solution. Stirring was maintained for two hours, then the solution was filtered.

0.6 ml of the solution so obtained were added to another solution prepared dissolving 23.0 mg (0.0024 mmol) of $[Bu_4N]_2[Cu(tfadt)_2]$ in 0.6 ml of $CH_3CN$. The solution was stirred for 10 minutes and then put in a glass tube 20 cm long with an internal diameter of 4.0 mm. $Et_2O$ was carefully added and after 10 days first dark brown prismatic crystals identified as $[Mn_7(hmp)_{12}][Cu(tfadt)_2]_2(CH_3CN)$ with single crystal XRD.

*FT-IR (KBr, $cm^{-1}$)*: 3059 (w, ν-CH aroma), 2840 (w), 2192 (s, ν -C=N ), 1605 (s, ν -C=C + ν-C=N), 1568 (m/s), 1467 (s, ν -C-O), 1449 (s), 1435(s), 1366(m), 1066 (m), 1046 (s), 1106(m), 1043 (s), 1017 (s), 862 (w), 754 (s)

$[Mn_4(hmp)_6(H_2O)_4](ClO_4)_4 \cdot 2H_2O$

This compound was synthetized following the procedure reported in [Clérac *et al* J. Am. Chem. Soc**. 2005**, 127, 17353] with small modifications.

0.51 g (1.42 mmol) of $Mn(ClO_4)_2 \cdot 6H_2O$ were dissolved in 20 ml di $CH_3CN$. 0.39 g (3.57 mmol) of Hhmp were added to this solution and stirring was maintained for 10 minutes. 0.55 g (0.73 mmol) of $Et_4NOH$ (20% in $H_2O$) were added. After stirring for 120 minutes, the solution was filtered and 10 ml of it were carefully layered on a 15 cm-long glass tube with a diameter of 1.5 cm containing 10 ml of toluene. After five days red-rose rhombus-shaped crystals of $[Mn_4(hmp)_6(H_2O)_4](ClO_4)_4 \cdot 2H_2O$ appeared (yeld 60% based on Mn(III).

*Elemental analysis*

% (Calc.): C 31.57 (31.46), H 3.37 (3.51), N 6.12 (6.11)

*FT-IR (KBr, $cm^{-1}$)*: 3370 (s, br ν -OH), 2890 (w), 2856 (w), 1606 (s, ν -C=V + ν-C=N), 1567 (m/s), 1484 (s, ν -C-O), 1284 (m), 1141 (s, ν Cl-O), 1106 (s, ν Cl-O), 1087(s, ν Cl-O), 1043 (s, ν Cl-O), 823 (w), 763 (m/s), 717 (m), 661 (m), 624 (s), 566 (w), 533 (w).

$[Mn_7(hmp)_{12}][Cu(mnt)_2]_2 \cdot xCH_3CN$

14.8 mg (0.011 mmol ) of preformed $[Mn_4(hmp)_6(H_2O)_4](ClO_4)_4 \cdot 2H_2O$ were dissolved in 0.6 ml of $CH_3CN$. 0.8 ml of a $CH_3CN$ solution containing 12.6 mg (0.021 mmol) of $[Et_4N]_2[Cu(mnt)_2]$ were then added and stirring was maintained for five minutes. The solution was filtered and layering with $Et_2O$ afforded needle-shaped crystals identified as $[Mn_7(hmp)_{12}][Cu(mnt)_2]_2\ xCH_3CN$ (yeld 50% based on $[Cu(mnt)_2]^{2-}$) after one week by single crystal XRD analysis.

*Elemental analysis % (calculated without $CH_3CN$.)*: C 44.21 (45.04), H 3.22 (3.28), N 11.02 (11.67), S 10.29 (10.69)

*FT-IR (KBr, $cm^{-1}$)*: 3059 (w, ν-CH aromatic), 2839 (w), 2193 (s, ν -C=N ), 1605 (s, ν -C=C + ν-C=N), 1578 (m/s), 1462 (s, ν -C-O), 1449 (s), 1435(s), 1366(m), 1067 (m), 1046 (s), 1106(m), 1046 (s), 1018 (s), 863 (w), 754 (s)

.

$[Mn_7(hmp)_{12}][Cu(mnt)_2]_2 \cdot (8+x)CH_3CN$

0.580 g (1.61 mmol) of $Mn(ClO_4)_2 \cdot 6H_2O$ were dissolved in 20 ml of $CH_3CN$. Thereafter, 0.51 g (4.67 mmol) of Hhmp and 1.06 ml (1.06 mmol) of $Me_4NOH$ (1M in $H_2O$) were added and the solution was stirred for 2 hours.

0.6 ml of this solution were added to 0.6 ml of a solution containing 14.4 mg (0.024 mmol) of $[Et_4N]_2[Cu(mnt)_2]$. Stirring was maintained for 5 minutes and then the solution was put in a 20 cm-long glass tube with an internal diameter of 4.0 mm and carefully

layered with $Et_2O$. After 10 days crystals identified with XRD analysis as $[Mn_7(hmp)_{12}][Cu(mnt)_2]_2 \cdot (8+x)CH_3CN$
Appears (yield 60%).

*Elemental analysis % (calculalted taking into account 2* $CH_3CN$*.)*: C 45.21 (45.48), H 3.54 (3.45), N 12.54 (12.42), S 10.29 (10.34)

*FT-IR (KBr, cm$^{-1}$)*: 3059 (w, ν-CH aromatic), 2829 (w), 2195 (s, ν -C=N ), 1603 (s, ν -C=C + ν-C=N), 1578 (m/s), 1468 (s, ν -C-O), 1455 (s), 1440(s), 1366(m), 1067 (m), 1046 (s), 1107(m), 1046 (s), 1020 (s), 868 (w), 754 (s)

Bis-(aquo)-(N,N' ethylen-bis salicylideneimminate)Mn(III) exafluorophosphate, $[Mn_2(salen)_2(H_2O)_2][PF_6]_2$

2.0 g (0.016 mol) of salycilic aldheide together with 0.47 g (0.0082 mol) of 1,2 ethyldiamine were dissolved in 40 ml of EtOH. 0.2 ml of $CH_3COOH$ were then added and the solution was heated at 70°C for two hours. After one day standing at RT, 2.0 g of yellow–needle-shaped crystals of $H_2$salen appear (yield 91%). 0.66 (2.5 mmol) of $H_2$salen were dissolved in 25 ml of MeOH. 0.58 g (2.5 mmol) of $Mn(AcO)_3 \cdot 2H_2O$ in 10 ml of MeOH were then added and the suspension was stirred and heated to reflux for 30 minutes. Then 0.46 g (2.5 mmol) of $KPF_6$ in 40 ml di $H_2O$ were added. After standing for 5 minutes at RT, the solution was filtered and after 5 days first prismatic brown crystals appeared by slow evaporation of the solvent.
0.80 g identified as $[Mn_2(salen)_2(H_2O)_2][PF_6]_2$ were obtained ( yield 67%)

*Elemental analysis*
% Sper. (Calc.): C 39.58 (39.69), H 3.43 (3.33), N 5.62 (5.79)
*FT-IR (KBr, cm$^{-1}$)* 1605 (s, 1603 s, ν -C=C + ν-C=N), 841 (m, ν P-F)

$[\{Mn(salen)(NCS)\}_2\{Cu(mnt)_2\}][Et_4N]_2$

12.0 mg (0.012 mmol) of $[Mn_2(salen)_2(H_2O)_2][PF_6]_2$ were dissolved in 0.6 ml of $CH_3CN$ and 13.0 mg (0.022 mmol) of $[Cu(mnt)_2][Et_4N]_2$ in 0.6 ml of $CH_2Cl_2$. The solution was stirred for 5 minutes and once filtered, it was put in a 8 cm long tube with internal diameter of 0.8 mm and $Et_2O$ was carefully layered. After 14 days prismatic crystals together with a brown powder appeared. Crystals were identified as $[\{Mn(salen)(NCS)\}_2\{Cu(mnt)_2\}][Et_4N]_2$ by means of single crystal X-ray diffraction. The powder was characterized by FT-IR.

FT-IR (KBr, $cm^{-1}$): 3548 (br,w), 3475 (br,w), 3413 (br,w), 3100 (w), 2921 (w), 2191 (s, ν CN dithiolene), 1638 (s), 1621 (s), 1600 (s, νC=N), 1542(m/s), 1390(m), 1328 (w), 1280 (m/s), 1199 (s), 904 (m), 866 (w), 800 (m), 754 (m), 633 (m), 597 (m)

[Mn(salen)Cu(salen)]$_2$[Cu(mnt)$_2$]

12.0 mg (0.012 mmol) of $[Mn_2(salen)_2(H_2O)_2][PF_6]_2$ and 13.0 mg (0.022 mmol) of $[Cu(mnt)_2][Et_4N]_2$ were dissolved in 2.0 ml of $CH_3CN$. The solution was filtered and after 10 days black prismatic crystals started to appear by slow evaporation of the solvent.
By means of single crystal XRD the compound was identified as $[Mn(salen)Cu(salen)][Cu(mnt)_2]_{0.5}$. Yield 50%.

*FT-IR (ATR, $cm^{-1}$)*: 3100 (w), 3000 (w), 2921 (w), 2193 (s, ν CN dithiolene), 1648 (s), 1620 (s), 1600 (s, νC=N), 1542(m/s), 1388(m), 1335 (m), 1286 (m/s), 1205 (s), 902 (m), 862 (w), 799 (m), 759 (m), 630 (m), 596 (m)

Bis-(aquo)(N,N'-Bis(salicylidene)-1,1,2,2-tetramethylethylendiamine)Mn(III)perchlorate, $[Mn_2(saltmen)_2(H_2O)_2][ClO_4]_2$

6.02 g (0.034 mmol) of $O_2N\text{-}C(CH_3)_2(CH_3)_2C\text{-}NO_2$ were put in 52 ml of HCl 37%. The suspension was heated to reflux (55 °C) and then metallic Sn (35 g, 0.3 mmol) was added during three hours. After cooling to RT, unreacted Sn was filtered-off and residual $O_2N\text{-}C(CH_3)_2(CH_3)_2C\text{-}NO_2$ was removed by washing three times the solution with 65 ml of $Et_2O$. 24.0 g (0.6 mol) of NaOH were carefully added keeping the solution at nearly 0°C. The suspension was filtered and the filtrate washed with 3 x 40 ml of $CH_2Cl_2$. The organic

phase was anidrified with $Mg(SO_4)$ and then the solvent removed by rotoevaporation giving a pale oil. After one night at 4°C, needle-like crystals of $H_2NC(CH_3)_2C(CH_3)_2NH_2$ , 2.88 g, yield 73% appeared.

2.88 g (0.025 mol) of $H_2NC(CH_3)_2C(CH_3)_2NH_2$ were put together with 6.15 g (0.05 mol) of salicili aldeide and 0.2 ml of $CH_3COOH$ in 45 ml of EtOH. Heating was mantained for 2 h at 70°C. The solution was filtered and after two days bright-yellow needle-shape crystals of $H_2$Saltmen were obtained by slow evaporation of the ethanolic solution.

To 1.95 g (5.01 mmol) of $H_2$saltmen in 50 ml di MeOH, 1.15 g (5.01 mmol) of $Mn(AcO)_3{\cdot}2H_2O$ in 20 ml di MeOH were added. After heating for 30 minutes at 50°C, 0.53 g (5.01 mmol) of $LiClO_4$ in 80 ml of $H_2O$ were added. After two weeks, 3.15 g of black needle-like crystals of $[Mn_2(saltmen)_2(H_2O)_2][ClO_4]_2$ were obtained, yield 63%.

*Elemental analysis*

% Sper. (Calc.): C 49.02 (48.55), H 5.04 (4.89), N 5.97 (5.66)

*FT-IR (KBr, $cm^{-1}$)* 1603 (s, νC=N), 1079, 1125, 1141 (m, ν Cl-O)

$[Mn_2(saltmen)_2(CH_3CN)_2][Cu(mnt)]$

12.5 mg (0.013 mmol) of $[Mn_2(saltmen)_2(H_2O)_2][ClO_4]_2$ were dissolved in 1.0 ml of $CH_3CN$ while 8.0 mg (0.013 mmol) of $[Et_4N]_2[Cu(mnt)_2]$ were dissolved in 1.0 ml di $CH_3CN$. $[Et_4N]_2[Cu(mnt)_2]$ was added to $[Mn_2(saltmen)_2(H_2O)_2][ClO_4]_2$ and stirring was mantained for 5 minutes. The solution was filtered and then put on a 5 cm-long tube with an internal diameter of 0.8 mm. After 4 days first needle-like crystals identified as $[Mn_2(saltmen)_2(CH_3CN)_2][Cu(mnt)_2]$ by single crystal XRD appeared.

Bis-(aquo)(N,N'R,R-bis-1,2diphenyl-salicylidene)Mn(III) tetrafluoroborate, $[Mn_2(RR\text{-}1,2diphenylsalen)_2(H_2O)_2][BF_4]_2$

0.25 g (1.18 mmol) of R,R-1,2 diphenyl-ethylendiammine and 0.29 g (2.36 mmol) of salicylic aldheide were dissolved in 18 ml di EtOH with 0.1 ml of $CH_3COOH$. The suspension was stirred

at 70°C for 2 h. After cooling and filtering, the yellow solid was washed with cold EtOH and dried by suction, 0.46g of R,R-1,2-diphenylsalen was obtained, yield 92%.

$[Mn_2(RR\text{-}1,2diphenylsalen)_2(H_2O)_2][BF_4]_2$ was synthesized following the procedure reported above for other Mn(III)salen analogous, with the following quantities: 0.25 g (0.6 mmol) of R,R-1,2-diphenylsalen, 0.15g (0.64 mmol) of $Mn(AcO)_3{\cdot}2H_2O$ in 13 ml di MeOH, 0.075 g (0.6 mmol) of $KBF_4$ in 10 ml of $H_2O$. After 5 days first prismatic crystals of $[Mn_2(RR\text{-}1,2difenilsalen)_2(H_2O)_2][BF_4]_2$appeared, yield 58 %.

*Elemental analysis*

% Sper. (Calc.): C 58.14 (58.16), H 4.62 (4.18), N 4.69 (4.84)

FT-IR (KBr, $cm^{-1}$) 1603 (s, νC=N), 1070 (m, ν B-F)

[Cu(N,N-R,R-1,2diphenyl-salen)]$CH_3CN$

30.4 mg (0.026 mmol) of $[Mn_2(N,N\text{-}R,R\text{-}1,2\ diphenyl\text{-}salen)_2(H2O)_2][BF_4]_2$ were dissolved in 1.5 ml of $CH_3CN$ while 26.6 mg (0.032 mmol) of $[Bu_4N]_2[Cu(mnt)_2]$ were dissolved in 1.5 ml of $CH_3CN$. $[Bu_4N]_2[Cu(mnt)_2]$ was added to $[Mn_2(N,N\text{-}R,R\text{-}1,2\ diphenyl\text{-}salen)_2(H2O)_2][BF_4]_2$ and the solution was stirred for 5 minutes and then filtered. The filtrate was put on a 5 cm-long tube wiht internal diameter of 0.8 cm and the solvent was left to slowly evaporate to give after 5 days prismatic crystals identified as [Cu(N,N-R,R-1,2diphenyl-salen)]$CH_3CN$ by means of single crystal XRD measurments.

$[Et_4N][Ni(dmid)_2]$

$[Et_4N][Ni(dmid)_2]$ was synthesized by reacting 1,3,4,6–tetrathiapentalene–2,5–dione (TPD) in distilled MeOH with 2 equivalent of NaOMe and then adding $NiCl_2{\bullet}6H_2O$ and $Et_4NBr$ as described in the literature.[1]Liu S.G *et al* Phosphorus, Sulfur, Silicon, Relat Elem 1994, 90,219].

$[Mn(TPP)(H2O)_2][BF_4]$

Free 5,10,15,20–*meso*–tetraphenylporphine ($H_2$TPP) was synthesised according to the Adler-Longo method, reacting pyrrole with benzaldehyde in refluxing propionic acid.

Under an argon atmosphere, $H_2$TPP (0.39 g, 0.64 mmol) was dissolved in previously degassed DMF (60 mL). 2,6–Lutidine (0.2 mL, 1.7 mmol) was then added followed by solid anhydrous $MnCl_2$ (1.19 g, 9.6 mmol).The green mixture was heated at 140 °C for 3 hours and the progress of the reaction followed by UV-Vis spectroscopy. After cooling, the solvent was removed under vacuum and the green solid was redissolved in $CH_2Cl_2$, filtered and concentrated to 8 mL. One drop of concentrated HCl was added in order to remove unreacted ligand. The solution was then chromatographied on $SiO_2$ column with pentane/$CH_2Cl_2$ 1/1 v/v as eluent, removing the pink spot corresponding to unreacted $H_2$TPP and then using MeOH/$CH_2Cl_2$ 1/7 v/v to collect the green spot of MnTPPCl. The solution was evaporated and the solid redissolved in a minimum amount of $CH_2Cl_2$ and layered with pentane, leading after 24 hours to green-black crystals of [Mn(TPP)]Cl (0.43 g, 92%). Under Ar atmosphere, [Mn(TPP)]Cl (0.33 g, 0.47 mmol) was added to $AgBF_4$ (0.23 g, 1.11 mmol) in distilled $CH_3CN$ (30 mL). The suspension was stirred for 3 h in the dark at room temperature, then filtered on Celite and the filtrate concentrated to ca 8 mL. The product was purified by column chromatography ($SiO_2$) using $CH_3CN$ as eluent collecting the first black fraction. Removal of the solvent and re-dissolution in $CH_2Cl_2$ followed by layering with *n*-hexane gave black needle–shaped crystals of [Mn(TPP)]$BF_4$•2$H_2O$ after 24 hours (0.35 g, 94%).

FT-IR ($cm^{-1}$, KBr) 3416 (br;ν -OH), 1622 (w), 1596 (w), 1487 (m;ν-C-C),1440 (m), 1340 (m; ν-C-C) [(*)], 1202 (m; δ-C-H) 1074 (s; ν- B-F), 1011 (s;), 806 (m/s), 755 (m) 702 (m) 661 (w) 523 (m; 1074 (s; ν- B-F) ) 454 (m)

[Mn(TPP)•THF][Mn(TPP)•$OH_2$][$Ni_2$(tto)(dmid)$_2$]•$(THF)_2$. [Mn(TPP)]$BF_4$•$(H_2O)_2$ (81.3 mg, 0.10 mmol) and [$Et_4N$][Ni(dmid)$_2$] (62.1 mg, 0.11 mmol) were dissolved separately in THF (6 mL). Both solutions were filtered and mixed together. The mixture was stirred for 15 mn, filtered and layered with *n*-hexane in a 20 cm long glass tube with internal diameter 8 mm to afford [Mn(TPP)•THF][Mn(TPP)•$OH_2$][$Ni_2$(tto)(dmid)$_2$]•$(THF)_2$ as black crystals (21.0 mg, 19.2 %) in the presence of a black powder.

FT-IR ($cm^{-1}$, KBr): 3434 (br; ν-OH ),1665 (s,ν-C=O), 1611 (s,ν-C=O), 1440 (m/s;ν-C=C), 1082 (m; δ-C-H+ ν-C-C, TPP), 1011 (vs; ν-C-C+ ν-N-C,TPP ), 890 (w; ν-C=S), 803 (m/s), 754 (m/s), 703 (m/s), 522 (w), 457 (w).

[Mn(TPP)•acetone][Mn(TPP)•$OH_2$][$Ni_2$(tto)(dmid)$_2$]•(acetone)

The same procedure as for [Mn(TPP)•THF][Mn(TPP)•$OH_2$][$Ni_2$(tto)(dmid)$_2$]•$(THF)_2$ was used with (81.0 mg,0.10 mmol) and [$Et_4N$][Ni(dmid)$_2$] (73.7 mg, 0.13 mmol) in acetone/$CH_2Cl_2$ 1/1 v/v. The mixture was then layered with diethylether to afford [Mn(TPP)•acetone][Mn(TPP)•$OH_2$][$Ni_2$(tto)(dmid)$_2$]•(acetone)
as dark crystals. (17.4 mg, 16.1 %) in the presence of a black powder.
FT-IR ($cm^{-1}$, KBr): 3437 (br; ν-OH ), 1710 (m,ν-C=O, acetone), 1660 (s,ν-C=O), 1604 (s,ν-C=O), 1440 (m/s;ν-C=C), 1083 (m; δ-C-H+ ν-C-C, TPP), 1012 (vs; ν-C-C+ ν-N-C,TPP ), 890 (m; ν-C=S), 802(m/s), 755 (m/s), 703 (m/s), 522 (w), 456 (w).

[Mn(TPP)•THF]$_2$[$Ni_2$(tto)(dmid)$_2$]

The same procedure as for [Mn(TPP)•THF][Mn(TPP)•$OH_2$][$Ni_2$(tto)(dmid)$_2$]•$(THF)_2$. was used with [Mn(TPP)] $BF_4$•$(H_2O)_2$ (10.2 mg, 0.013 mmol) and [$Et_4N$][Ni(dmid)$_2$] (7.8 mg, 0.014 mmol) in 1.2 ml of THF, with diethylether layering affording *[Mn(TPP)•THF]$_2$[$Ni_2$(tto)(dmid)$_2$]* (7.3 mg, 54 %).

FT-IR ($cm^{-1}$, KBr) 1657 (s; ν-C=O), 1603 (w; ν-C=O), 1439 (m/s;ν-C=C), 1071 (m ; δ-C-H+ ν-C-C TPP), 1012(vs; ν-C-C+ ν-N-C TPP ), 975 (m; ν-C=S), 802 (m/s), 736 (m) 702 (m) 520 (w) 456 (w)

1-oxo 4,7-dithiacyclopenta 5-ene 5,6-dithio 2-tione

Under Ar atmosphere, 0.47 ml (4.0 mmol) of 2-chloroethyl ether were put together with 1.44 g (2.0 mmol) of [Et4N]$_2$[Zn(dmid)$_2$] in 200 ml of cyclohexanone . This solution was heated to reflux for 24 hours. Evaporation of the solvent gave an oil that was dissolved in 120 ml of $CH_2Cl_2$ and washed with 3x 20 ml of H2O. The organic phase was anidrified on MgSO4 and after removal of the solvent a red solid was obtained. The crude was purified

by column chromatography on $SiO_2$ eluiting with $CH_2Cl_2$. The yellow fraction containing the product was concentrated and after 1 h yellow prismatic crystals appeared. They were washed quickly with a minimum amount of $CH_2Cl_2$ to eliminate their reddish liquor and then identified as 1-oxo 4,7-dithiacyclopenta 5-ene 5,6-dithio 2-thione by single crystal XRD analysis, $^1H$ NMR spectroscopy and FT-IR spectroscopy.
Yield 21%.

$^1H$ NMR ($CDCl_3$, ppm) 2.90 (t, 2H), 3.99 (t, 2H)
FT-IR (KBr, $cm^{-1}$) = 1066 (m, ν-C=S)

1-oxo 4,7-dithiacyclopenta 5-ene 5,6-dithio 2-thione was obtained also starting from 3.35 g (10.28 mmol) of 2-iodoethyl ether dissolved together with 3.59 g (5.0 mmol) of $[Et4N]_2[Zn(dmid)_2]$ in 500 ml of aceton. The mixture was heated to reflux for 15 hours then the solvent was removed and the solid residu dissolved in 300 ml of $CH_2Cl_2$ and washed with 3 x 150 ml of $H_2O$. The same purification procedure described above for the reaction with the dichlotoderivative was used. Yeld 26%.

$^1H$ NMR ($CDCl_3$, ppm) 2.91 (t, 2H), 3.99 (t, 2H)
FT-IR (KBr, $cm^{-1}$) = 1067 (m, ν-C=S)

The precursor 2-iodoethyl ether was synthetized starting from 8.20 g (0.057 mol) of 2-chloroethyl-ether and 21.13g (0.14 mol) of NaI dissolved in 150 ml of cyclohexanone. The white suspension was heated for 3 hours at 110-115 °C then filtered on Celite after cooling. The liquid was distilled under vacuum and the two fractions collected at 90-110 °C and 130-150 °C respectively were put together and re-distilled under vacuum. The fraction at 130 °C contained 2-iodoethyl ether.

<u>1-oxo 4,7-dithiacyclopenta 5-ene 5,6-dithio 2-one1oxo</u>
0.3130 g (1.16mmol) of 1-oxo 4,7-dithiacyclopenta 5-ene 5,6-dithio 2-thione and 0.8070 g (2.54 mmol) of $Hg(OAc)_2 \cdot nH_2O$ were suspended under Ar in 17.0 ml of $CH_3COOH/CHCl_3$= 3/1 (v/v).

The mixture was stirred for 2.5 hours at RT. Then the suspension was filtered on Cellite and the solvent and residual acetic acid were removed by rotoevaporation giving a white solid. This last was extracted with some portions of $CHCl_3$ and filtered on Celite The filtrate was concentrated and the day after crystals of 1-oxo 4,7-dithiacyclopenta 5-ene 5,6-dithio 2-one were obrtained (0.2447 g, yield 85%).

1H NMR t 4.05ppm 2H; t 2.98 ppm 2H

FT-IR ($cm^{-1}$, KBr) : νC=O 1658

1,4,7,10-tetraoxo-13,16-dithiacyclooctadec-14-ene- 14,15- dithia-2- thione,

**1,4,7,10-thione**

Under Ar atmosphere, 5.00 g of $[Zn(dmid)_2][Et_4N]_2$ (9.15 mmol) and 3.28 g of $TsO-(CH_2OCH_2)_5OTs$ were dissolve in 500 ml of acetone in a 1000 ml round bottom flask.

After degasing for 10 minutes, the solution was refluxed for seven days and then the solvent evaporated leaving a solid residu. This residu was dissolved in 300 ml of $CH_2Cl_2$,the solution filtered and washed with 3x 50 ml of $H_2O$.The organic phase was anhydrified with $MgSO_4$ and a red oil was obtained.

A first purification was performed on $SiO_2$ column chromatography collecting a fraction with $CH_2Cl_2$ then a second fraction with $CH_2Cl_2$ and 10 % of acetone. Each fraction was purified one or two times on $SiO_2$ column chromatography eluiting with petrol/acetone = 6/2 (v/v).

A yellow oil was obtained and after cooling at +4° for one night, needle shaped crystals were obtained with yield 20%.

$^1$H NMR (t) 3.05 ppm 4H, (s) 3.65 ppm 12H, (t)3.80 ppm 4H)

FT-IR (KBr, $cm^{-1}$) = (s 1065, ν-C=S)

Synthesis of 1,4,7,10-tetraoxo-13,16-dithiacyclooctadec-14-ene- 14,15- dithia-2- one.

**1,4,7,10-thiolone**

Under an Ar atmosphere, 0.2969 g (0.75 mmol) of **1,4,7,10-thione** where dissolved in 9.0 ml of a mixture $CH_3COOH/CH_3Cl$ 3/1 (v/v) together with 0.5169 g (1.60 mmol) of $Hg(OAc)_2$. The suspension was stirred at room temperature for two hours and then filtered on Cellite. The solvent was removed by rotoevaporation and the white solid was dissolved in $CH_2Cl_2$ and purified through $SiO_2$ column chromatography by eluiting with light petrol/acetone 6/2 v/v. A pale oil was obtained which yield needle shaped crystals of **1,4,7,10-thiolone** upon cooling at 4° (yield 78%).

$^1H$ NMR (t) 3.78 ppm 4H, (s) 3.69 ppm 12H, (t) 3.0 ppm 4H)
FT-IR (KBr, $cm^{-1}$) = (s 1667, ν-C=O)

$[(Ni(C_{12}H_{20}S_4O_4)_2)_2Ni]H_2O$

Under an Ar atmosphere, 100.0 mg (0.25 mmol) of **1,4,7,10-thiolone** were dissolved in 15 ml of distilled MeOH. Thereafter, 0.55 ml (0.55 mmol ) of $Bu_4NOH$ 1 M in MeOH were added. After stirring for one hour at RT, 30.1 mg (0.13 mmol)of $NiCl_2{\cdot}6H_2O$ were added.
The brown precipitate was stirred for ten minutes, then filtered and washed with MeOH and $CH_2Cl_2$. The solid was dried by suction and then redissolved in degased DMF Recrystallization under an Ar atmosphere upon diffusion of $Et_2O$ vapours led to needle crystals identified by XRD as$[(Ni(C_{12}H_{20}S_4O_4)_2)_2Ni]H_2O$ with yield 46%.

*Elemental analysis*
% Sper. (Calc.): C 33.46 (33.97), H 4.39 (4.99)

$[Ni(C_{12}H_{20}S_4O_4)_2Na]$

Under an Ar atmosphere, 0.4 g (1.04 mmol) of **1,4,7,10-thiolone** were dissolved in 10 ml of distilled MeOH. A solution prepared with 26.0 mg of Na (1.13 mmol ) in5 ml di MeOH was added and the mixture stirred for one hour at RT.
Thereafter, 110 mg (0.46 mmol) of $NiCl_2{\cdot}6H_2O$ were added. A brown precipitate appeared and the suspension was stirred for ten minutes. After filtering, the solid was washed with

MeOH e $CH_2Cl_2$ and then dissolved in degased DMF.Crystallization was carried out with slow diffusion of $Et_2O$ under Ar. After ten days first prismatic crystals identified by means of XRD as [$Ni(C_{12}H_{20}S_4O_4)_2$ Na] were obtained with 70% yield. The compound is soluble only on DMF.

*Elemental analysis*

% Sper. (Calc.): C 31.30 (31.27), H 5.07 (5.07)

[$(Ni(C_6H_{16}S_4O_1)_2$](DMF)[$Bu_4N$]

Under an Ar atmosphere, 0.1179 g (0.48 mmol) of **1-thiolone** were dissolved in 20 ml of distilled MeOH and then 1.05 ml (1.05 mmol) of $Bu_4NOH$ 1M. After one hour at RT, 55.6 mg (0.24 mmol) of $NiCl_2$ were added. The suspension was stirred for ten minutes and then tfiltrate. The brown solid was washed with MeOH and then dried by suction. The solid is soluble in $CH_3CN$, $CH_2Cl_2$ e DMF. Cristals of [$(Ni(C_6H_{16}S_4O_1)_2$](DMF)[$Bu_4N$] were obtained by diffusion of $Et_2O$ vapours in DMF solutions with yield 75%

*Elemental analysis*

% Sper. (Calc.): C 45.32 (45.92), H 7.18 (7.35) N 2.95 (3.35)

[$Ni(C_6H_{16}S_4O_1)_2Ni(DMF)_4(Cl)$]

10.0 mg (0.012 mmol) of [$(Ni(C_6H_{16}S_4O_1)_2$](DMF)[$Bu_4N$] were dissolved in 2.0 ml of $CH_3CN$. 10.5 mg (0.042 mmol) of $NiCl_2$· 6H2O were dissolved in 0.5 ml of MeOH. And then added to the solution of [$(Ni(C_6H_{16}S_4O_1)_2$](DMF)[$Bu_4N$] .The solution was filtered and after two days a black precipitate appeared on the bottom. The solid was redissolved in DMF and by slow diffusion of $Et_2O$ vapours prismatic crystals identified by means of XRD analysis as [$(Ni(C_6H_{16}S_4O_1)_2$]$Ni(DMF)_2(Cl)$ were obtained.

$[Ni(C_6H_{16}S_4O_1)_2]_2[Ni(DMF)_6]$

10.0 mg (0.012 mmol) of $[(Ni(C_6H_{16}S_4O_1)_2](DMF)[Bu_4N]$ were dissolved in 2.0 ml of $CH_3CN$. 31.3 mg of $Ni(ClO4)_2 \cdot 6H2O$ were dissolved in 2.0 ml of $CH_3CN$. After one day a black precipitate appeared.This was filtered and then washed with $CH_3CN$. The solid was dissolved in DMF and upon slow diffusion of $Et_2O$ vapours needle-shaped crystals were obtained after one night. They were identified by means of XRD analysis as $[Ni(C_6H_{16}S_4O_1)_2]_2[Ni(DMF)_6]$.

$[Zn(C_6H_4NO_2S)_2]$

$Zn(C_6H_4NO_2S)_2$ complex was hydrothermally synthesized (autogenous pressure) from a mixture of 0.15 g (0.57 mmol) of zinc acetylacetonate, (bis-2,4 pentanedionate zinc, $Zn(CH_3COCHCOCH_3)_2 \cdot xH_2O$and 5 equivalents (0.44 g, 2.84 mmol) of 2-mercaptonicotinic acid in 13 ml of water. The reactants were stirred a few minutes at RT before pouring the resulting suspension in a Teflon-liner which was introduced in a stainless steel autoclave and treated at 373 K for 96 h. Eventually, a further heating at 423 K for 5 h was carried out. The autoclave was left cooling at room temperature. The yellow solid was filtered and washed several times with ethanol, water and finally with acetone. Needle-shaped crystals were recovered which were suitable for X-ray single crystal analysis.

*Elemental Analysis (Calculated) for $Zn(C_6H_4NO_2S)_2$***.**

Found (Calc.): C: 37.80 (38.60), H: 2.13 (2.11), N: 7.44 (7.50), S:17.40 (17.10)

**FT-IR** (KBr, $cm^{-1}$). 3440 (broad, w; ν N-H) 3087 (w; δ C-H), 3074 (w; δ C-H), 1683 (vw), 1612 (m/s; $\nu_{as}$ C-O ), 1569 (s; δ N-H+ ν C=N ), 1488 (m/s); 1442 (m/w), 1421 (w); 1357 (m; $\nu_s$ C-O), 1311 (w, ν C=N+ ν C=S),), 1236 (s), 1139 (m, ν C=S), 1081 (w), 1058 (w; ν C=N+ ν C=S), 1006 (m/w) 919 (w), 850 (w), 821(w), 777 (m), 752 (w; δ C-H ), 709 (w; δ C-H), 642 (m; ν C=N+ ν C=S ), 563 (w), 545 (w), 499 (m), 485 (m), 408 (m; ν Zn-O).

$[Zn(C_6H_4NO_3)_2(H_2O)_2]$

$[Zn(C_6H_4NO_3)_2(H_2O)_2]$ was hydrothermally synthesized (autogenous pressure) in the same conditions used for $[Zn(C_6H_4NO_2S)_2]$, but using 2-hydroxynicotinic acid instead of 2-

mercaptonicotinic acid. [$Zn(C_6H_4NO_3)_2(H_2O)_2$] was identified by means of single crystal XRD.

*Elemental Analysis (Calculated):* C: 38.47 (38.34), H: 3.38 (3.22), N: 7.49 (7.46).

*FT-IR (KBr, $cm^{-1}$)*. 3370 (m/w; ν N-H) 3200-2917 (broad; δ C-H, ν-OH $H_2O$ ), 1635 (s; $\nu_{as}$ C-O), 1572 (m; δ N-H+ ν C=N), 1550 (m), 1489 (w); 1461 (w), 1421(m), 1378 (m; $\nu_s$ C-O), 1317 (w), 1234 (s), 1151 (m), 1123 (m; ν C-O ), 1089 (w),1078 (m/w) 989 (w), 950 (w), 902 (m/s), 835 (w), 781 (m/s; δ C-H), 742 (w) , 725 (w; δ C-H), 663 (w/m), 573 (m/s), 574 (m/s), 526 (m/s), 485 (m), 404 (m; ν Zn-O).

# Crystal data and structural refinement

Table 1. Crystal data and structure refinement for af90_1_26jan10.

| | | |
|---|---|---|
| Identification code | squeezed | |
| Empirical formula | C88 H72 Cu2 Mn7 N20 O12 S8 | |
| Formula weight | 2369.9 | |
| Temperature | 150(2) K | |
| Wavelength | 0.71073 Å | |
| Crystal system | Triclinic | |
| Space group | P-1 | |
| Unit cell dimensions | a = 14.1824(4) Å | α= 107.7620(10)°. |
| | b = 14.3911(4) Å | β= 96.2610(10)°. |
| | c = 15.3306(4) Å | γ = 92.5210(10)°. |
| Volume | 2952.17(14) $Å^3$ | |
| Z | 1 | |
| Density (calculated) | 1.333 $Mg/m^3$ | |
| Absorption coefficient | 1.273 $mm^{-1}$ | |
| F(000) | 1197 | |
| Crystal size | 0.2 x 0.1 x 0.06 $mm^3$ | |
| Theta range for data collection | 1.41 to 27.53°. | |
| Index ranges | -18<=h<=18, -18<=k<=18, -19<=l<=19 | |
| Reflections collected | 43820 | |
| Independent reflections | 13040 [R(int) = 0.0315] | |
| Completeness to theta = 27.53° | 95.8 % | |
| Absorption correction | Semi-empirical from equivalents | |
| Max. and min. transmission | 0.926 and 0.858 | |
| Refinement method | Full-matrix least-squares on $F^2$ | |
| Data / restraints / parameters | 13040 / 0 / 619 | |
| Goodness-of-fit on $F^2$ | 1.156 | |
| Final R indices [I>2sigma(I)] | R1 = 0.0454, wR2 = 0.1412 | |
| R indices (all data) | R1 = 0.0590, wR2 = 0.1505 | |
| Largest diff. peak and hole | 0.740 and -0.781 $e.Å^{-3}$ | |

Table 1. Crystal data and structure refinement for af90_100k_17sept_thf_iso_ordonne.

| | | |
|---|---|---|
| Identification code | import | |
| Empirical formula | C41.58 H44.75 F12 Mn2 N4 O11.42 P2 | |
| Formula weight | 1183.05 | |
| Temperature | 100(2) K | |
| Wavelength | 0.71073 Å | |
| Crystal system | Triclinic | |
| Space group | P1 | |
| Unit cell dimensions | a = 9.1410(3) Å | $\alpha$= 91.9520(10)°. |
| | b = 10.2569(3) Å | $\beta$= 93.3670(10)°. |
| | c = 13.3696(4) Å | $\gamma$ = 93.9690(10)°. |
| Volume | 1247.43(7) $Å^3$ | |
| Z | 1 | |
| Density (calculated) | 1.575 $Mg/m^3$ | |
| Absorption coefficient | 0.676 $mm^{-1}$ | |
| F(000) | 601.5 | |
| Crystal size | 0.23 x 0.16 x 0.11 $mm^3$ | |
| Theta range for data collection | 1.53 to 27.48°. | |
| Index ranges | -11<=h<=11, -13<=k<=13, -17<=l<=17 | |
| Reflections collected | 16335 | |
| Independent reflections | 9837 [R(int) = 0.0235] | |
| Completeness to theta = 27.48° | 99.4 % | |
| Absorption correction | Semi-empirical from equivalents | |
| Max. and min. transmission | 0.928 and 0.878 | |
| Refinement method | Full-matrix least-squares on $F^2$ | |
| Data / restraints / parameters | 9837 / 3 / 707 | |
| Goodness-of-fit on $F^2$ | 0.943 | |
| Final R indices [I>2sigma(I)] | R1 = 0.0347, wR2 = 0.1011 | |
| R indices (all data) | R1 = 0.0373, wR2 = 0.1128 | |
| Absolute structure parameter | 0.013(11) | |
| Largest diff. peak and hole | 0.903 and -0.468 $e.Å^{-3}$ | |

Table 1. Crystal data and structure refinement for af91_3_100k_31mar10_desord.

| | | |
|---|---|---|
| Identification code | import | |
| Empirical formula | C30 H25 Cu N3 O2 | |
| Formula weight | 523.08 | |
| Temperature | 100(2) K | |
| Wavelength | 0.71073 Å | |
| Crystal system | Monoclinic | |
| Space group | C2 | |
| Unit cell dimensions | a = 17.3482(6) Å | α= 90°. |
| | b = 18.5157(6) Å | β= 95.369(2)°. |
| | c = 7.7294(3) Å | γ = 90°. |
| Volume | 2471.90(15) $Å^3$ | |
| Z | 4 | |
| Density (calculated) | 1.406 $Mg/m^3$ | |
| Absorption coefficient | 0.917 $mm^{-1}$ | |
| F(000) | 1084 | |
| Crystal size | 0.15 x 0.08 x 0.06 $mm^3$ | |
| Theta range for data collection | 1.61 to 27.46°. | |
| Index ranges | -22<=h<=22, -23<=k<=22, -10<=l<=10 | |
| Reflections collected | 10647 | |
| Independent reflections | 5164 [R(int) = 0.0297] | |
| Completeness to theta = 27.46° | 99.0 % | |
| Absorption correction | Semi-empirical from equivalents | |
| Max. and min. transmission | 0.947 and 0.916 | |
| Refinement method | Full-matrix least-squares on $F^2$ | |
| Data / restraints / parameters | 5164 / 1 / 365 | |
| Goodness-of-fit on $F^2$ | 1.111 | |
| Final R indices [I>2sigma(I)] | R1 = 0.0334, wR2 = 0.0834 | |
| R indices (all data) | R1 = 0.0460, wR2 = 0.1153 | |
| Absolute structure parameter | -0.002(15) | |
| Largest diff. peak and hole | 0.522 and -0.811 $e.Å^{-3}$ | |

Table 1. Crystal data and structure refinement for af92_2_150k_25nov10.

| | | |
|---|---|---|
| Identification code | sqeezed | |
| Empirical formula | C104 H96 Cu2 Mn7 N28 O12 S8 | |
| Formula weight | 2698.33 | |
| Temperature | 150(2) K | |
| Wavelength | 0.71073 Å | |
| Crystal system | Triclinic | |
| Space group | P-1 | |
| Unit cell dimensions | a = 13.3724(4) Å | α= 96.567(2)°. |
| | b = 15.4677(6) Å | β= 104.259(2)°. |
| | c = 15.5742(6) Å | γ = 92.716(2)°. |
| Volume | 3092.08(19) $Å^3$ | |
| Z | 1 | |
| Density (calculated) | 1.449 $Mg/m^3$ | |
| Absorption coefficient | 1.227 $mm^{-1}$ | |
| F(000) | 1373 | |
| Crystal size | 0.41 x 0.12 x 0.06 $mm^3$ | |
| Theta range for data collection | 1.33 to 27.47°. | |
| Index ranges | -17<=h<=17, -20<=k<=20, -20<=l<=20 | |
| Reflections collected | 35896 | |
| Independent reflections | 14012 [R(int) = 0.0386] | |
| Completeness to theta = 27.47° | 99.0 % | |
| Absorption correction | Semi-empirical from equivalents | |
| Max. and min. transmission | 0.929 and 0.838 | |
| Refinement method | Full-matrix least-squares on $F^2$ | |
| Data / restraints / parameters | 14012 / 0 / 731 | |
| Goodness-of-fit on $F^2$ | 1.049 | |
| Final R indices [I>2sigma(I)] | R1 = 0.0470, wR2 = 0.1327 | |
| R indices (all data) | R1 = 0.0661, wR2 = 0.1428 | |
| Largest diff. peak and hole | 1.397 and -0.859 $e.Å^{-3}$ | |

Table 1. Crystal data and structure refinement for af94_150k_squeezed.

| | | |
|---|---|---|
| Identification code | AF94b_150K_24sept09_SQUEEZED | |
| Empirical formula | C102 H68 Mn2 N8 Ni2 O5 S12 | |
| Formula weight | 2097.74 | |
| Temperature | 150(2) K | |
| Wavelength | 0.71073 Å | |
| Crystal system | Triclinic | |
| Space group | P -1 | |
| Unit cell dimensions | a = 12.8290(6) Å | $\alpha$= 92.009(2)°. |
| | b = 19.6950(8) Å | $\beta$= 104.540(2)°. |
| | c = 20.6987(9) Å | $\gamma$ = 104.868(2)°. |
| Volume | 4865.2(4) $Å^3$ | |
| Z | 2 | |
| Density (calculated) | 1.432 $Mg/m^3$ | |
| Absorption coefficient | 0.952 $mm^{-1}$ | |
| F(000) | 2148 | |
| Crystal size | 0.3 x 0.2 x 0.1 $mm^3$ | |
| Theta range for data collection | 1.02 to 27.56°. | |
| Index ranges | -16<=h<=13, -21<=k<=25, -26<=l<=26 | |
| Reflections collected | 62530 | |
| Independent reflections | 22240 [R(int) = 0.0535] | |
| Completeness to theta = 27.56° | 98.9 % | |
| Absorption correction | Semi-empirical from equivalents | |
| Max. and min. transmission | 0.909 and 0.796 | |
| Refinement method | Full-matrix least-squares on $F^2$ | |
| Data / restraints / parameters | 22240 / 0 / 1182 | |
| Goodness-of-fit on $F^2$ | 1.064 | |
| Final R indices [I>2sigma(I)] | R1 = 0.0495, wR2 = 0.1424 | |
| R indices (all data) | R1 = 0.0736, wR2 = 0.1525 | |
| Largest diff. peak and hole | 0.747 and -0.651 $e.Å^{-3}$ | |

Table 1. Crystal data and structure refinement for af97_150k_13oct09.

| | | |
|---|---|---|
| Identification code | import | |
| Empirical formula | C116 H96 Mn2 N8 Ni2 O7 S12 | |
| Formula weight | 2326.11 | |
| Temperature | 150(2) K | |
| Wavelength | 0.71073 Å | |
| Crystal system | Triclinic | |
| Space group | P-1 | |
| Unit cell dimensions | a = 11.0004(9) Å | $\alpha$= 86.489(3)°. |
| | b = 13.6992(11) Å | $\beta$= 82.710(3)°. |
| | c = 18.1236(17) Å | $\gamma$ = 72.782(4)°. |
| Volume | 2586.9(4) $Å^3$ | |
| Z | 1 | |
| Density (calculated) | 1.493 $Mg/m^3$ | |
| Absorption coefficient | 0.902 $mm^{-1}$ | |
| F(000) | 1202 | |
| Crystal size | 0.4 x 0.2 x 0.1 $mm^3$ | |
| Theta range for data collection | 1.13 to 27.50°. | |
| Index ranges | -14<=h<=9, -17<=k<=15, -23<=l<=23 | |
| Reflections collected | 21541 | |
| Independent reflections | 11516 [R(int) = 0.0620] | |
| Completeness to theta = 27.50° | 97.0 % | |
| Absorption correction | Semi-empirical from equivalents | |
| Max. and min. transmission | 0.914 and 0.805 | |
| Refinement method | Full-matrix least-squares on $F^2$ | |
| Data / restraints / parameters | 11516 / 10 / 667 | |
| Goodness-of-fit on $F^2$ | 0.991 | |
| Final R indices [I>2sigma(I)] | R1 = 0.0766, wR2 = 0.1957 | |
| R indices (all data) | R1 = 0.1365, wR2 = 0.2443 | |
| Largest diff. peak and hole | 0.804 and -0.743 $e.Å^{-3}$ | |

Table 1. Crystal data and structure refinement for af99_2_150k_16fev10.

| | | |
|---|---|---|
| Identification code | AF99_2 | |
| Empirical formula | C54 H53 Cu Mn2 N11 O4 S4 | |
| Formula weight | 1221.73 | |
| Temperature | 150(2) K | |
| Wavelength | 0.71073 Å | |
| Crystal system | Monoclinic | |
| Space group | P21/c | |
| Unit cell dimensions | a = 13.7357(3) Å | $\alpha$= 90°. |
| | b = 15.8878(4) Å | $\beta$= 117.5300(10)°. |
| | c = 29.0178(7) Å | $\gamma$ = 90°. |
| Volume | 5615.5(2) $Å^3$ | |
| Z | 4 | |
| Density (calculated) | 1.445 $Mg/m^3$ | |
| Absorption coefficient | 1.022 $mm^{-1}$ | |
| F(000) | 2516 | |
| Crystal size | 0.1 x 0.05 x 0.02 $mm^3$ | |
| Theta range for data collection | 1.51 to 27.78°. | |
| Index ranges | -14<=h<=17, -20<=k<=20, -38<=l<=38 | |
| Reflections collected | 50098 | |
| Independent reflections | 12811 [R(int) = 0.0495] | |
| Completeness to theta = 27.78° | 96.6 % | |
| Absorption correction | Semi-empirical from equivalents | |
| Max. and min. transmission | 0.980 and 0.941 | |
| Refinement method | Full-matrix least-squares on $F^2$ | |
| Data / restraints / parameters | 12811 / 0 / 696 | |
| Goodness-of-fit on $F^2$ | 1.088 | |
| Final R indices [I>2sigma(I)] | R1 = 0.0370, wR2 = 0.0921 | |
| R indices (all data) | R1 = 0.0735, wR2 = 0.1276 | |
| Largest diff. peak and hole | 0.695 and -0.743 $e.Å^{-3}$ | |

Table 1. Crystal data and structure refinement for af124_2.

| | | |
|---|---|---|
| Identification code | import | |
| Empirical formula | $C_{10.50}H_{17.50}N_{1.50}Ni_{0.75}O_{2.50}S_4$ | |
| Formula weight | 377.03 | |
| Temperature | 293(2) K | |
| Wavelength | 0.71073 Å | |
| Crystal system | Triclinic | |
| Space group | P-1 | |
| Unit cell dimensions | a = 8.9808(2) Å | α= 83.5470(10)°. |
| | b = 13.5908(2) Å | β= 81.7430(10)°. |
| | c = 14.3025(3) Å | γ = 79.2450(10)°. |
| Volume | 1690.68(6) $Å^3$ | |
| Z | 4 | |
| Density (calculated) | 1.481 $Mg/m^3$ | |
| Absorption coefficient | 1.372 $mm^{-1}$ | |
| F(000) | 784 | |
| Crystal size | 0.42 x 0.12 x 0.1 $mm^3$ | |
| Theta range for data collection | 3.50 to 27.50°. | |
| Index ranges | -11<=h<=11, -17<=k<=17, -18<=l<=18 | |
| Reflections collected | 37140 | |
| Independent reflections | 7751 [R(int) = 0.0330] | |
| Completeness to theta = 27.50° | 99.7 % | |
| Absorption correction | Semi-empirical from equivalents | |
| Max. and min. transmission | 0.933 and 0.901 | |
| Refinement method | Full-matrix least-squares on $F^2$ | |
| Data / restraints / parameters | 7751 / 0 / 461 | |
| Goodness-of-fit on $F^2$ | 1.108 | |
| Final R indices [I>2sigma(I)] | R1 = 0.0364, wR2 = 0.0805 | |
| R indices (all data) | R1 = 0.0627, wR2 = 0.0993 | |
| Largest diff. peak and hole | 0.604 and -0.486 $e.Å^{-3}$ | |

Table 1. Crystal data and structure refinement for af128_100k_14avr10.

| | | |
|---|---|---|
| Identification code | import | |
| Empirical formula | C54 H53 Cu Mn2 N11 O4 S4 | |
| Formula weight | 1221.78 | |
| Temperature | 100(2) K | |
| Wavelength | 0.71073 Å | |
| Crystal system | Monoclinic | |
| Space group | P21/n | |
| Unit cell dimensions | a = 13.7340(4) Å | $\alpha$= 90°. |
| | b = 15.8397(5) Å | $\beta$= 90.718(2)°. |
| | c = 25.6549(8) Å | $\gamma$ = 90°. |
| Volume | 5580.6(3) $Å^3$ | |
| Z | 4 | |
| Density (calculated) | 1.454 $Mg/m^3$ | |
| Absorption coefficient | 1.028 $mm^{-1}$ | |
| F(000) | 2516 | |
| Crystal size | 0.34 x 0.23 x 0.11 $mm^3$ | |
| Theta range for data collection | 1.51 to 27.48°. | |
| Index ranges | -17<=h<=17, -20<=k<=16, -33<=l<=23 | |
| Reflections collected | 45832 | |
| Independent reflections | 12613 [R(int) = 0.0602] | |
| Completeness to theta = 27.48° | 98.6 % | |
| Absorption correction | Semi-empirical from equivalents | |
| Max. and min. transmission | 0.893 and 0.753 | |
| Refinement method | Full-matrix least-squares on $F^2$ | |
| Data / restraints / parameters | 12613 / 0 / 696 | |
| Goodness-of-fit on $F^2$ | 1.051 | |
| Final R indices [I>2sigma(I)] | R1 = 0.0525, wR2 = 0.1325 | |
| R indices (all data) | R1 = 0.1019, wR2 = 0.1722 | |
| Largest diff. peak and hole | 2.392 and -0.816 $e.Å^{-3}$ | |

Table 1. Crystal data and structure refinement for af141_4_b_150k_16juil10.

| | | |
|---|---|---|
| Identification code | import | |
| Empirical formula | C12 H20 Ni0.50 O4 S4 | |
| Formula weight | 385.88 | |
| Temperature | 150(2) K | |
| Wavelength | 0.71073 Å | |
| Crystal system | Triclinic | |
| Space group | P-1 | |
| Unit cell dimensions | a = 5.0317(2) Å | $\alpha$= 90.376(2)°. |
| | b = 8.9469(3) Å | $\beta$= 91.882(2)°. |
| | c = 18.6818(6) Å | $\gamma$ = 96.710(2)°. |
| Volume | 834.76(5) $Å^3$ | |
| Z | 2 | |
| Density (calculated) | 1.535 $Mg/m^3$ | |
| Absorption coefficient | 1.125 $mm^{-1}$ | |
| F(000) | 404 | |
| Crystal size | 0.32 x 0.07 x 0.05 $mm^3$ | |
| Theta range for data collection | 1.09 to 27.45°. | |
| Index ranges | -5<=h<=6, -11<=k<=11, -24<=l<=23 | |
| Reflections collected | 10315 | |
| Independent reflections | 3729 [R(int) = 0.0311] | |
| Completeness to theta = 27.45° | 97.3 % | |
| Absorption correction | Semi-empirical from equivalents | |
| Max. and min. transmission | 0.954 and 0.910 | |
| Refinement method | Full-matrix least-squares on $F^2$ | |
| Data / restraints / parameters | 3729 / 165 / 210 | |
| Goodness-of-fit on $F^2$ | 1.081 | |
| Final R indices [I>2sigma(I)] | R1 = 0.0709, wR2 = 0.1926 | |
| R indices (all data) | R1 = 0.0808, wR2 = 0.2125 | |
| Largest diff. peak and hole | 3.369 and -1.523 e.$Å^{-3}$ | |

Table 1. Crystal data and structure refinement for af172_150k_16juil10.

| | | |
|---|---|---|
| Identification code | import | |
| Empirical formula | C41.58 H44.75 F12 Mn2 N4 O11.42 P2 | |
| Formula weight | 1183.05 | |
| Temperature | 100(2) K | |
| Wavelength | 0.71073 Å | |
| Crystal system | Triclinic | |
| Space group | P1 | |
| Unit cell dimensions | a = 9.1410(3) Å | $\alpha$= 91.9520(10)°. |
| | b = 10.2569(3) Å | $\beta$= 93.3670(10)°. |
| | c = 13.3696(4) Å | $\gamma$ = 93.9690(10)°. |
| Volume | 1247.43(7) $Å^3$ | |
| Z | 1 | |
| Density (calculated) | 1.575 $Mg/m^3$ | |
| Absorption coefficient | 0.676 $mm^{-1}$ | |
| F(000) | 601.5 | |
| Crystal size | 0.23 x 0.16 x 0.11 $mm^3$ | |
| Theta range for data collection | 1.53 to 27.48°. | |
| Index ranges | -11<=h<=11, -13<=k<=13, -17<=l<=17 | |
| Reflections collected | 16335 | |
| Independent reflections | 9837 [R(int) = 0.0235] | |
| Completeness to theta = 27.48° | 99.4 % | |
| Absorption correction | Semi-empirical from equivalents | |
| Max. and min. transmission | 0.928 and 0.878 | |
| Refinement method | Full-matrix least-squares on $F^2$ | |
| Data / restraints / parameters | 9837 / 3 / 707 | |
| Goodness-of-fit on $F^2$ | 0.943 | |
| Final R indices [I>2sigma(I)] | R1 = 0.0347, wR2 = 0.1011 | |
| R indices (all data) | R1 = 0.0373, wR2 = 0.1128 | |
| Absolute structure parameter | 0.013(11) | |
| Largest diff. peak and hole | 0.903 and -0.468 e.$Å^{-3}$ | |

Table 1. Crystal data and structure refinement for af180_3_150k_16sept10_squeezed_iso.

| | | |
|---|---|---|
| Identification code | import | |
| Empirical formula | C41.58 H44.75 F12 Mn2 N4 O11.42 P2 | |
| Formula weight | 1183.05 | |
| Temperature | 100(2) K | |
| Wavelength | 0.71073 Å | |
| Crystal system | Triclinic | |
| Space group | P1 | |
| Unit cell dimensions | a = 9.1410(3) Å | $\alpha$= 91.9520(10)°. |
| | b = 10.2569(3) Å | $\beta$= 93.3670(10)°. |
| | c = 13.3696(4) Å | $\gamma$ = 93.9690(10)°. |
| Volume | 1247.43(7) $Å^3$ | |
| Z | 1 | |
| Density (calculated) | 1.575 $Mg/m^3$ | |
| Absorption coefficient | 0.676 $mm^{-1}$ | |
| F(000) | 601.5 | |
| Crystal size | 0.23 x 0.16 x 0.11 $mm^3$ | |
| Theta range for data collection | 1.53 to 27.48°. | |
| Index ranges | -11<=h<=11, -13<=k<=13, -17<=l<=17 | |
| Reflections collected | 16335 | |
| Independent reflections | 9837 [R(int) = 0.0235] | |
| Completeness to theta = 27.48° | 99.4 % | |
| Absorption correction | Semi-empirical from equivalents | |
| Max. and min. transmission | 0.928 and 0.878 | |
| Refinement method | Full-matrix least-squares on $F^2$ | |
| Data / restraints / parameters | 9837 / 3 / 707 | |
| Goodness-of-fit on $F^2$ | 0.943 | |
| Final R indices [I>2sigma(I)] | R1 = 0.0347, wR2 = 0.1011 | |
| R indices (all data) | R1 = 0.0373, wR2 = 0.1128 | |
| Absolute structure parameter | 0.013(11) | |
| Largest diff. peak and hole | 0.903 and -0.468 $e.Å^{-3}$ | |

Table 1. Crystal data and structure refinement for af_mn3cumnt_120k.

| | | |
|---|---|---|
| Identification code | import | |
| Empirical formula | C58 H68 Cu Mn2 N12 O4 S6 | |
| Formula weight | 1363.02 | |
| Temperature | 120(2) K | |
| Wavelength | 0.71073 Å | |
| Crystal system | Monoclinic | |
| Space group | P21/c | |
| Unit cell dimensions | a = 10.107 Å | $\alpha$= 90°. |
| | b = 29.051 Å | $\beta$= 102.15°. |
| | c = 10.853 Å | $\gamma$ = 90°. |
| Volume | 3115.4 $Å^3$ | |
| Z | 2 | |
| Density (calculated) | 1.453 $Mg/m^3$ | |
| Absorption coefficient | 0.994 $mm^{-1}$ | |
| F(000) | 1414 | |
| Crystal size | 0.3 x 0.2 x 0.1 $mm^3$ | |
| Theta range for data collection | 3.75 to 27.50°. | |
| Index ranges | -13<=h<=8, -37<=k<=25, -13<=l<=14 | |
| Reflections collected | 16659 | |
| Independent reflections | 7091 [R(int) = 0.0270] | |
| Completeness to theta = 27.50° | 99.2 % | |
| Absorption correction | Semi-empirical from equivalents | |
| Max. and min. transmission | 0.547599 and 0.362652 | |
| Refinement method | Full-matrix least-squares on $F^2$ | |
| Data / restraints / parameters | 7091 / 56 / 401 | |
| Goodness-of-fit on $F^2$ | 1.035 | |
| Final R indices [I>2sigma(I)] | R1 = 0.0451, wR2 = 0.1144 | |
| R indices (all data) | R1 = 0.0699, wR2 = 0.1246 | |
| Largest diff. peak and hole | 0.646 and -0.747 $e.Å^{-3}$ | |

Table 1. Crystal data and structure refinement for af_mntppbf4_2_100k_22juin09.

| | | |
|---|---|---|
| Identification code | import | |
| Empirical formula | C44 H28 B F4 Mn N4 O2 | |
| Formula weight | 786.45 | |
| Temperature | 100(2) K | |
| Wavelength | 0.71073 Å | |
| Crystal system | Monoclinic | |
| Space group | P21/n | |
| Unit cell dimensions | a = 10.3781(7) Å | $\alpha$= 90°. |
| | b = 8.0875(6) Å | $\beta$= 95.588(3)°. |
| | c = 21.1961(16) Å | $\gamma$ = 90°. |
| Volume | 1770.6(2) $Å^3$ | |
| Z | 2 | |
| Density (calculated) | 1.475 $Mg/m^3$ | |
| Absorption coefficient | 0.440 $mm^{-1}$ | |
| F(000) | 804 | |
| Crystal size | 0.4 x 0.1 x 0.05 $mm^3$ | |
| Theta range for data collection | 1.93 to 28.32°. | |
| Index ranges | -13<=h<=13, -10<=k<=10, -28<=l<=27 | |
| Reflections collected | 28550 | |
| Independent reflections | 4264 [R(int) = 0.0444] | |
| Completeness to theta = 28.32° | 96.5 % | |
| Absorption correction | Semi-empirical from equivalents | |
| Max. and min. transmission | 0.978 and 0.949 | |
| Refinement method | Full-matrix least-squares on $F^2$ | |
| Data / restraints / parameters | 4264 / 0 / 278 | |
| Goodness-of-fit on $F^2$ | 1.099 | |
| Final R indices [I>2sigma(I)] | R1 = 0.0616, wR2 = 0.1697 | |
| R indices (all data) | R1 = 0.0786, wR2 = 0.1921 | |
| Extinction coefficient | 0.035(4) | |
| Largest diff. peak and hole | 0.980 and -0.673 $e.Å^{-3}$ | |

Table 1. Crystal data and structure refinement for afmnh3_120k.

| | | |
|---|---|---|
| Identification code | import | |
| Empirical formula | C94 H81 Cu2 F12 Mn7 N19 O12 S8 | |
| Formula weight | 2665.02 | |
| Temperature | 100(2) K | |
| Wavelength | 0.71073 Å | |
| Crystal system | Triclinic | |
| Space group | P-1 | |
| Unit cell dimensions | a = 14.5545(4) Å | α= 62.0480(10)°. |
| | b = 14.8963(5) Å | β= 67.135(2)°. |
| | c = 15.2840(5) Å | γ = 80.554(2)°. |
| Volume | 2696.46(15) $Å^3$ | |
| Z | 1 | |
| Density (calculated) | 1.641 $Mg/m^3$ | |
| Absorption coefficient | 1.419 $mm^{-1}$ | |
| F(000) | 1343 | |
| Crystal size | 0.3 x 0.3 x 0.2 $mm^3$ | |
| Theta range for data collection | 3.56 to 27.50°. | |
| Index ranges | -18<=h<=17, -19<=k<=19, -19<=l<=19 | |
| Reflections collected | 111412 | |
| Independent reflections | 12320 [R(int) = 0.0345] | |
| Completeness to theta = 27.50° | 99.4 % | |
| Absorption correction | Semi-empirical from equivalents | |
| Max. and min. transmission | 0.753 and 0.660 | |
| Refinement method | Full-matrix least-squares on $F^2$ | |
| Data / restraints / parameters | 12320 / 0 / 748 | |
| Goodness-of-fit on $F^2$ | 1.224 | |
| Final R indices [I>2sigma(I)] | R1 = 0.0370, wR2 = 0.0739 | |
| R indices (all data) | R1 = 0.0681, wR2 = 0.0968 | |
| Largest diff. peak and hole | 0.735 and -0.657 $e.Å^{-3}$ | |

Table 1. Crystal data and structure refinement for oji109.

| | | |
|---|---|---|
| Identification code | import | |
| Empirical formula | C48 H80 Ni3 O17 S16 | |
| Formula weight | 1618.31 | |
| Temperature | 293(2) K | |
| Wavelength | 0.71073 Å | |
| Crystal system | Monoclinic | |
| Space group | C 2/c | |
| Unit cell dimensions | a = 13.4074(4) Å | α= 90°. |
| | b = 14.0031(4) Å | β= 104.5930(10)°. |
| | c = 19.1875(6) Å | γ = 90°. |
| Volume | 3486.15(18) $Å^3$ | |
| Z | 2 | |
| Density (calculated) | 1.542 $Mg/m^3$ | |
| Absorption coefficient | 1.341 $mm^{-1}$ | |
| F(000) | 1688 | |
| Crystal size | 0.3 x 0.1 x 0.08 $mm^3$ | |
| Theta range for data collection | 2.14 to 27.48°. | |
| Index ranges | -13<=h<=17, -18<=k<=18, -24<=l<=24 | |
| Reflections collected | 15378 | |
| Independent reflections | 3991 [R(int) = 0.0268] | |
| Completeness to theta = 27.48° | 99.4 % | |
| Absorption correction | Semi-empirical from equivalents | |
| Max. and min. transmission | 0.917 and 0.878 | |
| Refinement method | Full-matrix least-squares on $F^2$ | |
| Data / restraints / parameters | 3991 / 0 / 192 | |
| Goodness-of-fit on $F^2$ | 1.061 | |
| Final R indices [I>2sigma(I)] | R1 = 0.0528, wR2 = 0.1552 | |
| R indices (all data) | R1 = 0.0637, wR2 = 0.1811 | |
| Largest diff. peak and hole | 1.352 and -0.849 $e.Å^{-3}$ | |

Table 1. Crystal data and structure refinement for oji112_150k_08mar10.

| | | |
|---|---|---|
| Identification code | import_OJI112_150K_08mar10 | |
| Empirical formula | C24 H40 Na Ni O8 S8 | |
| Formula weight | 794.74 | |
| Temperature | 150(2) K | |
| Wavelength | 0.71073 Å | |
| Crystal system | Monoclinic | |
| Space group | C 2/c | |
| Unit cell dimensions | a = 23.6588(14) Å | $\alpha$= 90°. |
| | b = 10.1920(6) Å | $\beta$= 127.742(2)°. |
| | c = 17.5265(12) Å | $\gamma$ = 90°. |
| Volume | 3342.0(4) $Å^3$ | |
| Z | 4 | |
| Density (calculated) | 1.580 $Mg/m^3$ | |
| Absorption coefficient | 1.137 $mm^{-1}$ | |
| F(000) | 1660 | |
| Crystal size | 0.13 x 0.07 x 0.06 $mm^3$ | |
| Theta range for data collection | 2.18 to 27.49°. | |
| Index ranges | -26<=h<=30, -13<=k<=12, -22<=l<=22 | |
| Reflections collected | 12062 | |
| Independent reflections | 3800 [R(int) = 0.0563] | |
| Completeness to theta = 27.49° | 98.9 % | |
| Absorption correction | Semi-empirical from equivalents | |
| Max. and min. transmission | 0.934 and 0.909 | |
| Refinement method | Full-matrix least-squares on $F^2$ | |
| Data / restraints / parameters | 3800 / 0 / 192 | |
| Goodness-of-fit on $F^2$ | 1.044 | |
| Final R indices [I>2sigma(I)] | R1 = 0.0417, wR2 = 0.1053 | |
| R indices (all data) | R1 = 0.0829, wR2 = 0.1568 | |
| Largest diff. peak and hole | 0.523 and -0.617 $e.Å^{-3}$ | |